

THESIS  
3  
2002

This is to certify that the


dissertation entitled  
Use of mutagenesis, novel detergents and lipid analysis  
to optimize conditions for achieving high resolution  
3-dimensional crystal structure of Rhodobacter  
sphaeroides cytochrome c oxidase

presented by

Yasmin I. Hilmi

has been accepted towards fulfillment  
of the requirements for

Ph.D. degree in Food Science

  
Major professor

Date 8/28/02

LIBRARY  
Michigan State  
University

PLACE IN RETURN BOX to remove this checkout from your record.  
TO AVOID FINES return on or before date due.  
MAY BE RECALLED with earlier due date if requested.

DATE DUE	DATE DUE	DATE DUE
MAR 29 2004		
MAR 4 2005		
FEB 02 2007		

**USE OF MUTAGENESIS, NOVEL DETERGENTS, AND LIPID ANALYSIS  
TO OPTIMIZE CONDITIONS FOR ACHIEVING HIGH RESOLUTION  
3-DIMENSIONAL CRYSTAL STRUCTURE OF *RHODOBACTER*  
*SPHAEROIDES* CYTOCHROME C OXIDASE**

By  
Yasmin Hilmi

A DISSERTATION

Submitted to  
Michigan State University  
In partial fulfillment of the requirement  
For the degree of

DOCTOR OF PHILOSOPHY

Department of Food Science and Human Nutrition

2002



## ABSTRACT

### USE OF MUTAGENESIS, NOVEL DETERGENTS, AND LIPID ANALYSIS TO OPTIMIZE CONDITIONS FOR ACHIEVING HIGH RESOLUTION 3-DIMENSIONAL CRYSTAL STRUCTURE OF *RHODOBACTER* *SPHAEROIDES* CYTOCHROME C OXIDASE

By  
Yasmin Hilmi

Aerobic respiration is the most common means by which non-photosynthetic organisms convert carbohydrates, fats and proteins, into a biologically useful form of energy. In this process, electrons are released and passed through a series of enzymes known as the respiratory electron transport chain. This process is coupled to proton translocation from the mitochondrial matrix to the intermembrane space, leading to generation of a membrane potential, which can be used to drive the synthesis of ATP.

In mammalian systems the ability to produce heat, instead of ATP, and to respond to signals of too much stored energy, are important physiological functions. In the case of cytochrome *c* oxidase, knowing the proton and electron pathways and the mechanism of coupling may lead us to an understanding of how oxidase can be uncoupled, and thus contribute to the controlled production of heat instead of stored energy (fat). Understanding the mechanisms of electron transfer and proton pumping at a molecular level requires a structure at high resolution.

*Rhodobacter sphaeroides* cytochrome *c* oxidase was used as a good model for the mitochondrial enzyme, and many efforts were made to optimize conditions for achieving a high resolution structure. Different purification protocols were used, and the enzyme purified with Ni<sup>2+</sup>-NTA affinity chromatography followed by Mono Q ion-exchange chromatography was the most suitable for crystallization.

In order to standardize the crystallization conditions, associated membrane lipids were analyzed by thin layer chromatography, mass spectrometry and phosphate analysis. PE, PC, PG, sulfolipid and ornithine lipids were found in the membranes and at all purification steps. The two major lipid components in R.s. cells, PE and PC, were also found in the re-dissolved crystal. These results suggest the importance of these membrane lipids, and their retention, for getting a high resolution structure.

As another approach to improve the crystallization of cytochrome *c* oxidase, the protein was stabilized and the hydrophilic surface was increased by forming a covalently linked Cc/CcO complex. For this study R.s. cytochrome *c*<sub>2</sub> was engineered by putting in the missing lysine 13 that is found to be important for high affinity binding. This step improved the binding between cytochrome *c* and the oxidase significantly. Site-directed mutagenesis was used to form cysteine mutants on cytochrome *c* to cross-linked with cysteine mutants on subunit II of the oxidase. These mutations were made based on a computational model of the binding site between cytochrome *c* and cytochrome *c* oxidase. Purification and yield of cytochrome *c* mutants was improved significantly when we introduced a 5 histidine-tag at the C-terminus of cytochrome *c* and used Ni<sup>2+</sup>-NTA affinity chromatography as a purification system. All mutants have wild type characteristics and the formation of the complex was accomplished.

The results of these studies further our understanding of the nature of the C *c*/CcO complex and define the lipid content of the purified oxidase through to the crystal form. The lipid content of the purified enzyme is representative of the R.s. membranes, suggesting the importance of a number of different lipids in the native structure.

**Dedicated To**

**my husband, Galal,  
my son, Mohamad,  
My daughter, Monia  
& my family in the Sudan**

## ACKNOWLEDGMENT

I would like to express my deepest gratitude to my research advisor Dr. Ferguson-Miller for her guidance and continuous support. Her excellence and enthusiasm as a scientist and a teacher are a constant source of encouragement. I would like to sincerely thank my academic advisor Dr. Strasburg for his support and encouragement on all aspects, all through my graduate studies.

I am grateful to my committee members: Dr. Michael Garavito for his excellent suggestions in crystallization; and to Dr. John Linz and Dr. Maurice Bennink for their advice and support throughout my Ph. D. program.

It is a pleasure to thank all my present and past labmates: Dr. Carrie Hiser and Dr. Denise Mills for their continuous help with my research and reading through my thesis; Dr. Yuejun Zhen, Dr. Laurence Florens and Dr. Jie Qian for helping me start my project; Bryan Schmidt for his help with the computer puzzles; Ling Qin, Jun Yang, Namjoon Kim, Steve Kidd, Erica Westly and Nicole Webb for their help and friendship.

I am very grateful for Dr. Christoph Benning and Wayne Riekhof for their great help with thin layer chromatography. I thank Leslie Kuhn and Brandon Hespenheide for doing binding predictions for sulfhydryl group insertions.

I am also indebted to Dr. So Iwata and Margareta Svensson-Ek for letting me spend some time in their lab having a great experience in crystallizing membrane proteins. I am grateful to Dr. Timothy Donohue for providing the overexpressed strain for cytochrome  $c_2$ , and to Dr. John Allison and Ann Distler for the mass spectrometry

analysis. I would also like to thank Dr. Frank Millett's group for their effort in studying electron transfer in my mutants.

I am especially grateful to my husband for his love, patience and unconditional support. Many thanks to my kids, Mohamad and Monia, who make my life meaningful.

I thank my mother, my brother and my sisters: Ravi, Shiraz and Reham for their love and care, and I thank the Sudanese community in Michigan for their support.

Special thanks to my friends: Shahira, Manal, Amani, Hanan, Inaam and Nada for their support and encouragement.

## TABLE OF CONTENTS

LIST OF TABLES	-----	xiii
LIST OF FIGURES	-----	xiv
ABBREVIATIONS	-----	xviii

### CHAPTER I

LITURATURE REVIEW	-----	1
1. Background on Cytochrome <i>c</i> Oxidase: Electron Transfer and Proton Pumping Mechanisms	-----	4
1.1 Aerobic Respiration	-----	4
1.2 Regulation of efficiency by uncoupling mechanism	-----	7
1.3 Cytochrome <i>c</i> Oxidase	-----	10
1.3.1 Subunits of Cytochrome <i>c</i> Oxidase	-----	11
1.3.1.1 Subunit I	-----	12
1.3.1.2 Subunit II	-----	14
1.3.1.3 Subunit III	-----	14
1.3.1.4 Subunit IV	-----	15
1.3.2 Electron pathways and control of electron transfer	----	15
1.3.2.1 "Through-space" model	-----	17
1.3.2.2 "Through-bond" model	-----	18
1.3.3 Proton Pathway and control of pumping efficiency	----	18
1.3.3.1 Proton Pathways in <i>Rhodobacter sphaeroides</i>	-----	19
1.3.3.1.1 D-pathway	-----	22
1.3.3.1.2 K-Pathway	-----	23
1.3.3.1.3 H-Pathway	-----	24
1.3.3.2 Proton Pumping Models	-----	24
1.3.3.2.1 Direct Coupling Model	-----	25
1.3.3.2.2 Indirect Coupling Model	-----	26
1.3.3.3 Control of pumping efficiency	-----	27
2. Crystal Structures of Cytochrome <i>c</i> Oxidases from Different Species	----	29
2.1 Importance of the Crystal Structures	-----	29
2.2 Crystal Structure of <i>Paracoccus denitrificans</i> Cytochrome <i>c</i> Oxidase	-----	30
2.3 Crystal Structure of Bovine Heart Cytochrome <i>c</i> Oxidase	-----	32
2.4 Crystal Structure of <i>Rhodobacter sphaeroides</i> Cytochrome <i>c</i> Oxidase	-----	34
2.5 Importance of Available and Future Crystal Structures	-----	38

3. Substrate Docking on Cytochrome <i>c</i> Oxidase	39
3.1 Protein-Protein Interactions	39
3.2 Definition of the Interaction Domain for Cytochrome <i>c</i> on Cytochrome <i>c</i> Oxidase	41
4. Different <i>c</i> -Type Cytochromes : Which One is The Physiological Substrate For <i>aa</i> <sub>3</sub> Oxidase?	48
4.1 Background on Cytochrome <i>c</i>	48
4.2 Mitochondrial cytochromes <i>c</i>	50
4.3 Bacterial cytochrome <i>c</i>	54
4.3.1 Soluble cytochrome <i>c</i> of <i>Rhodobacter</i> <i>sphaeroides</i> and Related Bacteria	55
4.3.1.1 Cytochrome <i>c</i> <sub>554</sub>	55
4.3.1.2 Cytochrome <i>c</i> <sub>2</sub>	57
4.3.1.3 Isocytochrome <i>c</i> <sub>2</sub>	59
4.3.1.4 Cytochrome <i>c</i> '	59
4.3.1.5 A diheme cytochrome	60
4.3.1.6 Cytochrome <i>c</i> <sub>551</sub>	61
4.3.1.7 <i>Sphaeroides</i> heme proteins (SHP)	61
4.3.2 Membrane bound cytochromes <i>c</i> of <i>Rhodobacter sphaeroides</i> and Related Bacteria	62
4.3.2.1 Cytochrome <i>c</i> <sub>552</sub>	62
4.3.2.2 Cytochrome <i>c</i> <sub>y</sub>	64
4.4 Summary	65
5. Importance and Classification of Membrane Lipids	67
5.1 Importance of Membrane Lipids	67
5.1.1 Glycerophospholipids	68
5.1.2 Phosphosphingolipids	68
5.1.3 Glycosphingolipids	71
5.1.4 Glycoglycerolipids	71
5.1.5 Sterols	72
5.2 Membrane lipids in <i>Rhodobacter sphaeroides</i>	72
5.2.1 Phospholipids	73
5.2.2 Glycolipids	74
5.2.3 Other Polar Lipids	75
5.2.3.1 Ornithine Lipids	75
5.2.3.2 Betaine Lipids	75
5.2.3.3 Xenobiotic Lipids	75
5.2.4 Fatty Acids Composition in <i>Rhodobacter sphaeroides</i>	76

5.3 Factors Affecting Membrane Lipid Composition -----	76
6. Statement of problem -----	78
 <b>CHAPTER II</b>	
<b>PURIFICATION AND CRYSTALLIZATION OF</b>	
<b><i>RHODOBACTER SPHAEROIDES</i> CYTOCHROME C OXIDASE -----</b>	<b>80</b>
 Introduction -----	 81
Materials and Methods -----	82
Growth of <i>Rhodobacter sphaeroides</i> -----	82
Membrane preparation -----	82
Protein Purification -----	83
Protocol 1: -----	83
Ni <sup>2+</sup> -NTA affinity chromatography -----	83
FPLC-DEAE Ion Exchange Chromatography -----	84
Protocol 2: -----	84
Mono Q Anion Exchange Chromatography -----	84
Protein Assay -----	85
Visible spectra -----	85
SDS-PAGE -----	86
Activity measurement -----	86
pH-Dependence Assay -----	86
CO-binding Assay -----	87
Detergent Exchange by Gel Filtration -----	87
Spin column -----	88
Thin Layer Chromatography -----	88
Stability of cytochrome c oxidase in different detergents -----	89
Melting Temperature Assay -----	89
Crystallization -----	89
 Results -----	 93
Growth of <i>Rhodobacter sphaeroides</i> -----	93
Purification with Ni <sup>2+</sup> -NTA -----	93
DEAE anion exchange chromatography -----	96
Visible spectra -----	99
SDS-PAGE -----	99
Gel Filtration -----	104
Spin column chromatography -----	104
Activity assay -----	109
Stability of the enzyme in different detergents -----	109
Crystallization -----	116
 Discussion -----	 119



### CHAPTER III

#### USE OF THIN LAYER CHROMATOGRAPHY AND

#### MASS SPECTROMETRY TO ANALYZE

#### MEMBRANE LIPIDS FROM *RHODOBACTER SPHAEROIDE* -----124

#### Introduction -----125

#### Materials and Methods -----127

##### Growth of *Rhodobacter sphaeroides* -----127

##### Basic Lipid Extraction -----127

##### Acetone Extraction of Lipids -----127

##### Ammonia Extraction -----128

##### Thin Layer Chromatography (TLC) -----128

##### Fast Atom Bombardment Tandem Mass Spectrometry (FAB) -----130

##### Matrix-Assisted Laser Desorption ionization Mass Spectrometry -----130

##### Phosphate Analysis -----131

#### Results -----134

##### Lipids Extraction -----134

##### Thin Layer Chromatography -----135

##### Mass Spectrometry -----147

#### Discussion -----161

### CHAPTER IV

#### ENGINEERING OF *RHODOBACTER SPHAEROIDE*

#### CYTOCHROME $C_2$ TO TEST THE MODEL $Cc/CcO$ COMPLEX -----166

#### Introduction -----167

#### Materials and Methods -----176

##### Site-Directed Mutagenesis on Cytochrome $c_2$ -----176

##### Insertion of Histidine-Tag in Cytochrome $c_2$ gene -----176

##### Prediction of Positions for Cysteine Interactions -----183

##### Cell growth and Membrane Preparation -----183

##### Hydroxyapatite Column -----184

##### DEAE-Cellulose Column -----184

##### $Ni^{+2}$ -NTA Affinity Chromatography Column -----184

##### Visible Spectra -----185

##### Activity measurement -----185

##### Spin Column -----186

##### Gel-filtration Column -----186

SDS-PAGE .....	186
MALDI Mass Spectrometry .....	187
Results .....	188
Design of Mutants .....	188
Purification .....	191
Visible spectra and activity .....	193
Steady-State Kinetic Assay .....	193
Complex Formation .....	199
Discussion .....	213
SUMMARY AND CONCLUSION .....	217
1- Purification and crystallization of <i>Rhodod bacter sphaeroides</i> CcO .....	217
2- Use of thin layer chromatography, mass spectrometry and phosphate analysis to analyze lipid contents of <i>Rhodod bacter sphaeroides</i> CcO .....	218
3- Engineering of <i>Rhodod bacter sphaeroides</i> Cc <sub>2</sub> to test The model of the Cc/CcO complex .....	221
BIBLIOGRAPHY .....	223

## LIST OF TABLES

### CHAPTER I

Table 1.1	Bacterial cytochrome <i>c</i>	-----56
-----------	-------------------------------	---------

### CHAPTER III

Table 3.1	Molecular weights of major lipids in <i>Rhodobacter sphaeroides</i>	-----127
-----------	--	----------

### CHAPTER IV

Table 4.1	Characteristics of cytochrome <i>c</i> <sub>2</sub> mutants from <i>Rhodobacter sphaeroides</i>	-----185
-----------	--	----------

Table 4.2	Comparison between purification techniques	-----187
-----------	--	----------

## LIST OF FIGURES

### CHAPTER I

Figure 1.1	Respiratory chain complexes-----	4
Figure 1.2	The role of mitochondria in energy balance-----	9
Figure 1.3	Possible proton pumping pathways-----	21
Figure 1.4	Crystal structure of <i>Rhodobacter sphaeroides</i> cytochrome <i>c</i> oxidase and the associated lipids-----	36
Figure 1.5	Computational model for the docking site between cytochrome <i>c</i> and cytochrome <i>c</i> oxidase-----	45
Figure 1.6	Crystal structure of horse cytochrome <i>c</i> -----	53

### CHAPTER II

Figure 2.1	Comparison between the expression level of the wild type strain (CY91) and wild type overexpressed strain (YZ100).-----	91
Figure 2.2	Combination of Ni <sup>2+</sup> -NTA and FPLC columns as well as using relatively high salt wash (200 mM KCl) to improve the enzyme purity-----	94
Figure 2.3	Checking the native structure of the wild type and the mutant H333N by monitoring the absolute reduced spectra at the solet (444nm) and $\alpha$ (606) absorption regions for heme <i>a</i> and heme <i>a</i> <sub>3</sub> -----	97
Figure 2.4	Improving the homogeneity of the enzyme. -----	99
Figure 2.5	SDS-polyacrylamide gel electrophoresis (14% separating & 8% stacking) of oxidase purified with different columns-----	102
Figure 2.6	Measurement of detergent contents by thin layer chromatography (TLC)-----	104
Figure 2.7	Effect of pH on cytochrome <i>c</i> oxidase activity-----	107
Figure 2.8	Stability of the enzyme in different detergents-----	109

Figure 2.9	Melting temperature assay-----	111
Figure 2.10	Crystal of <i>Rhodobacter sphaeroides</i> wild type cytochrome <i>c</i> oxidase-----	114

### CHAPTER III

Figure 3.1	MALDI spectra (Matrix-Assisted laser Desorption Ionization Mass Spectrometry) showing the presence of cardiolipins with a molecular weight of 1458-----	132
Figure 3.2	Thin layer chromatography (TLC) of membrane and purified enzyme extracts-----	134
Figure 3.3	Diagnostic spray reagents for specific groups-----	137
Figure 3.4	Semi-quantitative analysis for membrane lipids by Thin Layer Chromatography-----	139
Figure 3.5	Comparison of lipid composition in membranes and after each stage of purification-----	141
Figure 3.6	Membrane lipid analysis by Fast Atom Bombardment Tandem Mass Spectrometry (FAB)-----	144
Figure 3.7	Fatty acid composition by Fast Atom Bombardment Tandem Mass Spectrometry (FAB)-----	146
Figure 3.8	The association between cardiolipins and subunit IV of <i>Rhodobacter sphaeroides</i> cytochrome <i>c</i> oxidase-----	149
Figure 3.9	Analysis of Ni <sup>2+</sup> -NTA purified cytochrome <i>c</i> oxidase by MALDI mass spectrometry-----	151
Figure 3.10	Combining Thin Layer Chromatography and MALDI mass spectrometry for lipid analysis-----	153
Figure 3.11	Lipid composition of a re-dissolved crystal analyzed with MALDI-----	155

### CHAPTER IV

Figure 4.1	Comparison of lysine residues on the front face of cytochromes <i>c</i> from horse, <i>Rhodobacter sphaeroides</i> and <i>Paracoccus denitrificans</i> -----	165
------------	--	-----

Figure 4.2	Crystal structure of horse cytochrome <i>c</i> -----	167
Figure 4.3	Cysteine mutants at the interface between cytochrome <i>c</i> and subunit II of the oxidase-----	170
Figure 4.4	Oligonucleotide sequences of wild type and mutants of <i>Rhodobacter sphaeroides</i> cytochrome <i>c</i> <sub>2</sub> -----	173
Figure 4.5	Wild type and histidine-tag insertion oligonucleotide sequences of <i>Rhodobacter sphaeroides</i> cytochrome <i>c</i> <sub>2</sub> -----	175
Figure 4.6	Steady-state kinetics of <i>Rhodobacter sphaeroides</i> <i>c</i> <sub>2</sub> wild type and mutants with <i>Rhodobacter sphaeroides</i> cytochrome <i>c</i> oxidase-----	183
Figure 4.7	Spectral analysis to test the efficiency of Ni <sup>2+</sup> -NTA method in comparison with other purification methods-----	189
Figure 4.8	Visible spectra for wild type and mutants of cytochrome <i>c</i> <sub>2</sub> from <i>Rhodobacter sphaeroides</i> -----	191
Figure 4.9	Elution profile for different fractions from gel-filtration column for cytochrome <i>c</i> cysteine mutant (N12C) with cytochrome <i>c</i> oxidase subunit II cystiene mutant (T159C)-----	194
Figure 4.10	Gel-filtration for cytochrome <i>c</i> cysteine mutant (N12C) with cytochrome <i>c</i> oxidase subunit II cystiene mutant (T159C)-----	196
Figure 4.11	Gel-filtration for cytochrome <i>c</i> cystiene mutant (K83C) with cytochrome <i>c</i> oxidase subunit II cystiene mutant (A213C)-----	198
Figure 4.12	Gel-filtration for horse cytochrome <i>c</i> with wild type <i>Rhodobacter sphaeroides</i> cytochrome <i>c</i> oxidase-----	200
Figure 4.13	Log molecular weights of the marker was plotted versus the position on the SDS gel (actual distance from the top of gel), to calculate the position of the complex between cytochrom <i>c</i> and subunit II of the oxidase-----	203
Figure 4.14	MALDI analysis to confirm the formation of the complex-----	205

## LIST OF ABBREVIATIONS

CMC	critical micelle concentration
DCCD	N,N'-dicyclohexylcarbodiimide
DEAE	diethylaminoethyl
DGD	digalactocyldiacylglycerol
DM	decyl maltoside
DTT	dithiothreitol
EDTA	ethylenediaminetetraacetic acid
FAB	fast atom bombardment mass spectrometry
FPLC	fast protein liquid chromatography
Im	imidazol
LM	lauryl maltoside
MALDI	matrix-assisted laser desorption ionization mass spectrometry
MGD	monogalactocyldiacylglycerol
Ni <sup>2+</sup> -NTA	Nickle-nitrilotriacetic acid
OL	ornithine lipid
PC	phosphatidylcholine
PCR	polymerase chain reaction
PE	phosphatidylethanolamine
PEG	polyethylene glycol
PG	phosphatidylglycerol
PI	phosphatidylinisitol
PS	phosphatidylserine
R.s.	<i>Rhodobacter sphaeroides</i>
SDS	sodium dodecyl sulfate
SL	sulfoquinovosyldiacylglycerol
TLC	thin layer chromatography
TMD	3,3',5,5'-tetramethylbenzidine
TMPD	N-N-N'N'-tetramethyl-p-phenylenediamine

**CHAPTER I**  
**LITURATURE REVIEW**



Mitochondria play an important role in energy transduction and energy balance. The synthesis of ATP, the major energy source for cells, occurs by oxidative phosphorylation in mitochondria. This process involves five mitochondrial inner membrane complexes: complex I (NADH: ubiquinone oxidoreductase), complex II (succinate dehydrogenase), complex III (cytochrome *bc<sub>1</sub>*), complex IV (cytochrome *c* oxidase) and complex V (ATP synthase) (Figure 1.1). Electrons produced from degradation of foodstuffs during glycolysis, fatty acid oxidation and the citric acid cycle are transferred from complex I and complex II through complex III to complex IV where molecular oxygen is reduced to water; therefore complexes I, II, III and IV are known as the electron transport chain or respiratory chain. Complexes I, III and IV also serve as proton pumps, using the energy of electron transfer to translocate protons from the matrix of the mitochondrion to the cytosol, to produce and sustain an electrochemical gradient across the inner membrane. Under normal physiological conditions, complex V uses the free energy released from the flow of protons back across the membrane in order to perform an endothermic reaction of producing ATP from ADP and inorganic phosphate. The processes of ATP production, utilization and energy storage as fat, are highly regulated to achieve energy balance by mechanisms yet to be elucidated.

In our lab we focus on studying electron transfer and proton pumping in *Rhodobacter sphaeroides* cytochrome *c* oxidase as an excellent model for mitochondrial cytochrome *c* oxidase, since these proteins are highly homologous. The goal of my doctoral studies was to optimize conditions for achieving high-resolution 3-dimensional crystal structures of the oxidase and the cytochrome *c*/ cytochrome *c* oxidase complex. One of the most critical steps in crystallizing membrane proteins is their solubilization

**Figure 1.1 Respiratory chain complexes.** The three-dimensional crystal structure of complexes II, III, IV, V and cytochrome *c* are shown. The blue boxes represent NADH: ubiquinone oxidoreductase or complex I because the crystal structure for it is not available yet. The figure was created by D. Mills using the computer program Rasmol and the coordinates from fumarate reductase or complex II (Iverson *et al*, 1999), bovine bc1 complex or complex III (Iwata *et al*, 1998), horse cytochrome *c* (Bushnell *et al*, 1990), *Rhodobacter sphaeroides* cytochrome *c* oxidase or complex IV (Svensson-Ek *et al*, 2002) and yeast ATP synthase or complex V (Stock *et al*, 1999).

## Respiratory Chain Complexes

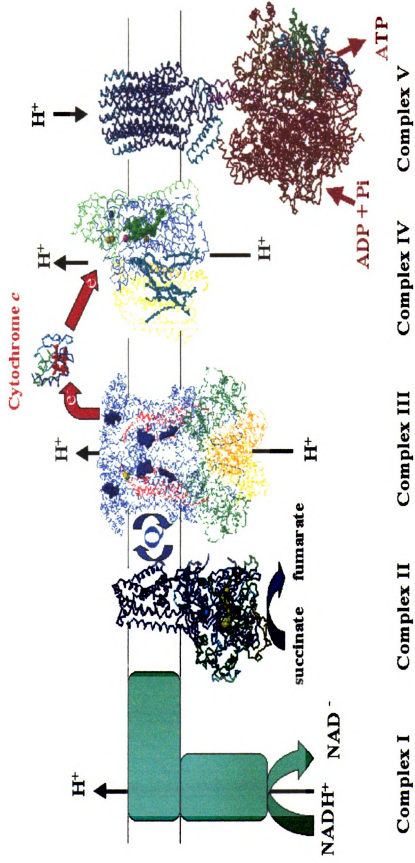


Figure 1.1



and isolation. In order to solubilize these proteins without affecting the stability and the nature of the enzyme and to get diffracting crystals, I used different detergents to exchange for the natural lipid bilayer that surrounds the membrane protein, and monitored the structural and functional characteristics of the protein under different conditions. Then I identified the lipids composition after protein isolation and after each step of purification to help determine at which level of detergent/lipid content the protein will give the best crystals.

My second approach was to use mutagenesis as a tool to test the predicted docking site of cytochrome *c* on the oxidase and produce a cross-linked complex with potential for crystallization. This involved changing residues of both cytochrome *c* and cytochrome *c* oxidase at the proposed binding site to form a disulfide bond between them.

In this chapter I will discuss some of the previous work that relates to my current projects in the following order:

- 1- Background on cytochrome *c* oxidase: electron transfer and proton pumping mechanisms.
- 2- Crystal structures of cytochrome *c* oxidase from different species.
- 3-Substrate docking on cytochrome *c* oxidase.
- 4-Different types of cytochromes *c* and which one is the physiological substrate for *aa<sub>3</sub>* cytochrome *c* oxidase.
- 5- Importance and classification of membrane lipids.
- 6- Statement of problem.

## **1. Background on Cytochrome *c* Oxidase: Electron Transfer and Proton Pumping Mechanisms**

### **1.1 Aerobic Respiration**

Aerobic respiration is the most common means by which non-photosynthetic organisms convert carbohydrates, fats and proteins derived from photosynthetic organisms into a biologically useful form of energy. In this process high-energy electrons are released and passed through a series of enzymes known as the respiratory electron transport chain. In eukaryotes, these enzymes are located within the inner membrane of mitochondria. In prokaryotes, they are located in the inner cytoplasmic membrane. The enzymes of the respiratory chain contain redox centers of increasingly positive reduction potential, and the final electron acceptor in aerobic respiration is dioxygen, which provides the driving force for the flow for electrons through the entire electron transport chain because of its high positive reduction potential.

Electrons are transferred from NADH or FADH<sub>2</sub>, which are formed in glycolysis, fatty acid oxidation and the citric acid cycle, to oxygen through four protein complexes in the respiratory chain (Stryer, 1995). Under normal physiological conditions, this process is coupled to proton translocation from the mitochondrial matrix to the intermembrane space, leading to generation of a membrane potential which can be used by ATP synthase to drive the synthesis of ATP from ADP and inorganic phosphate (Gennis and Ferguson-Miller, 1995).

## 1.2 Regulation of efficiency by uncoupling mechanism

In mammalian systems the ability to produce heat, instead of ATP, and to respond to signals of too much stored energy, are important physiological functions. One regulatory mechanism may involve less efficient proton pumping (uncoupling) to produce less stored energy and more heat. Uncoupling can be defined as **intrinsic uncoupling** (fewer proton pumped per electron transferred) or **extrinsic uncoupling**, in which there is an increase of the leakiness of the membrane (Figure 1.2).

The recent discovery of two new mammalian mitochondrial proteins with homology to the brown fat uncoupling protein suggests the involvement of mitochondria from tissues other than brown fat in regulation of body weight and energy balance.

It is now understood that adipose tissue secretes a peptide hormone, leptin, which is the product of the *ob* gene. Leptin circulates in the blood where its level may correlate with the level of stored fat. Leptin binds to receptors on the hypothalamus and is hypothesized to inhibit eating and activate the release of norepinephrin to the adipose tissues. When the latter binds to  $\beta_3$ -adrenergic receptors on fat cells, it stimulates uncoupling of mitochondria by mechanisms not yet understood, but likely both intrinsic and extrinsic processes. This burns fat and releases energy in the form of heat (Ezzell, 1995). In the case of cytochrome *c* oxidase, the final electron acceptor in the respiratory chain, knowing the proton and electron pathways and the mechanism of coupling may lead us to an understanding of how oxidase can be uncoupled, and thus contribute to the controlled production of heat instead of stored energy (fat).

**Figure 1.2 The role of mitochondria in energy balance.** The mitochondrial electron transport chain (green) transfers electrons from the degradation of food stuffs to the final electron acceptor (molecular oxygen) which is reduced to water. This process is accompanied by either coupling or uncoupling mechanisms where protons can be used by ATP synthase (blue) to produce ATP or by uncoupling proteins UCPs (red) to produce heat (“extrinsic” uncoupling), respectively. “Intrinsic” uncoupling due to uptake of protons from outside, will also produce heat (Ferguson-Miller and Babcock, 1996). Both are reactions that could be normally controlled by leptin. The figure was created by S. Ferguson-Miller using the computer program Canvas (Ferguson-Miller, S., 1999)



## Role of Mitochondria in Energy Balance

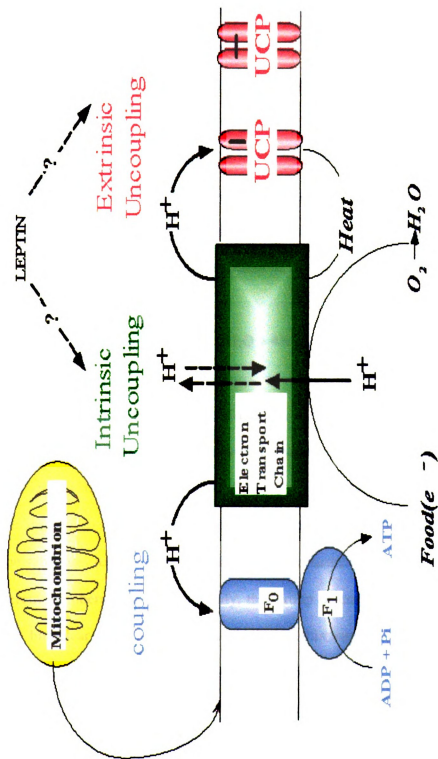


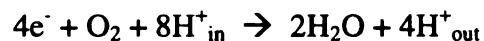
Figure 1.2



### 1.3 Cytochrome *c* Oxidase

Cytochrome *c* oxidase is a protein complex that is embedded in the inner mitochondrial membrane of eukaryotes and in the cytoplasmic membrane of many bacteria. It catalyzes the final step in the electron transfer chain to reduce molecular oxygen to water.

Four electrons are transferred from cytochrome *c* and four protons are taken up from the matrix to fully reduce oxygen to water. An additional four protons are translocated from the matrix to the cytosolic side of the membrane (Wikstrom, 1988). The overall reaction catalyzed by terminal oxidases is:



where electrons are donated by cytochrome *c* and  $H^+_{in}$  and  $H^+_{out}$  indicate that the protons are taken up and released on different sides with respect to the respiratory membrane (Ferguson-Miller and Babcock, 1996).

Cytochrome *c* oxidases are members of a superfamily of heme-copper oxidases. Although the substrates (cytochrome *c* or quinol) and the heme types (A, B, D or O) vary among different members of this superfamily, this group of enzymes has in common a heme-copper binuclear center that is diagnostic of this superfamily. The enzymes belonging to this superfamily are structurally homologous and share the same functional core (Calhoun *et al*, 1994).

### 1.3.1 Subunits of Cytochrome *c* Oxidase

Mammalian cytochrome *c* oxidase contains 13 subunits (Kadenbach *et al.*, 1983; Tsukihara and Yoshikawa, 1996). Ten subunits are encoded in the nuclear genome and three, which constitute the catalytic core of the enzyme, are encoded by mitochondria (Capaldi, 1990; Takamiya *et al.*, 1987). The enzyme contains four redox active metal centers: heme *a*, heme *a*<sub>3</sub>, Cu<sub>A</sub> and Cu<sub>B</sub> (Chan *et al.*, 1990; Brown *et al.*, 1993). Heme *a* is a low-spin six coordinate heme, while heme *a*<sub>3</sub> is a high-spin five coordinate heme with an open coordination site. This type of oxidase is known as an *aa*<sub>3</sub>-type cytochrome *c* oxidase, and it is found in mitochondria and some bacteria including *Rhodobacter sphaeroides*. In addition to *aa*<sub>3</sub>-type oxidase, some aerobic bacteria have other types of oxidases. Naming of these oxidases refers to the hemes that they contain. One of the well-described oxidases is cytochrome *bo*<sub>3</sub> from *E.coli*, which contains hemes *b* and *o* and transfers electrons directly from quinol to oxygen (Trumpower and Gennis, 1994).

In addition to the four redox centers, mammalian cytochrome *c* oxidase contains one atom of zinc and one atom of magnesium per molecule of enzyme, whereas bacterial oxidases have only Mg. In addition a new calcium-binding site was identified from the crystal structures of both bacterial and mammalian oxidases. The functional significance of these metals is not well understood yet.

Electron transfer into cytochrome *c* oxidase is initiated by binding of cytochrome *c* to subunit II on the external side of the membrane. Most studies on electron transfer indicate a linear sequence of events from cytochrome *c* through the metal centers:

Cytochrome *c* → Cu<sub>A</sub> → heme *a* → heme *a*<sub>3</sub> → Cu<sub>B</sub> → O<sub>2</sub> (Hill, 1993)

Heme *a*, heme *a*<sub>3</sub> and Cu<sub>B</sub> are located in subunit I while Cu<sub>A</sub> is located in subunit II.

Four genes for the *aa*<sub>3</sub>-type cytochrome *c* oxidase subunits from *Rhodobacter sphaeroides* genome have been cloned and sequenced (Shapleigh and Gennis, 1992; Cao *et al.*, 1992). Subunits I, II and III genes of the *aa*<sub>3</sub>-type cytochrome *c* oxidase show a high degree of homology to the equivalent mitochondrial genes and the subunit IV gene is only homologous to the *Paracoccus denitrificans* gene. The DNA-derived amino acid sequences of *Rhodobacter sphaeroides* subunits I, II and III show identity to bovine oxidase of 52% for subunit I, 39% for subunit II and 49% for subunit III. The *Rhodobacter sphaeroides* oxidase, like the mammalian enzyme, contains heme *a* and heme *a*<sub>3</sub>, Cu<sub>A</sub>, Cu<sub>B</sub> and Mg and Ca<sup>++</sup>, but it lacks zinc. This similarity and simplicity of *Rhodobacter sphaeroides* cytochrome *c* oxidase make it an excellent model of the mammalian cytochrome oxidase for studying energy transduction and proton translocation (Hosler *et al.*, 1992).

#### 1.3.1.1 Subunit I

Subunit I is the largest and most conserved subunit of cytochrome *c* oxidase. It has twelve transmembrane helices and plays a central role in reduction of oxygen to water at the binuclear center, heme *a*<sub>3</sub>- Cu<sub>B</sub> (Shapleigh and Gennis, 1992). Besides the binuclear center, subunit I contains both hemes, magnesium and the recently discovered calcium site. The Mg site is located at the interface between subunit I and subunit II with ligands from the two subunits. It lies at the bottom of a proposed water channel

Cytochrome *c* → Cu<sub>A</sub> → heme *a* → heme *a*<sub>3</sub> → Cu<sub>B</sub> → O<sub>2</sub> (Hill, 1993)

Heme *a*, heme *a*<sub>3</sub> and Cu<sub>B</sub> are located in subunit I while Cu<sub>A</sub> is located in subunit II.

Four genes for the *aa*<sub>3</sub>-type cytochrome *c* oxidase subunits from *Rhodobacter sphaeroides* genome have been cloned and sequenced (Shapleigh and Gennis, 1992; Cao *et al.*, 1992). Subunits I, II and III genes of the *aa*<sub>3</sub>-type cytochrome *c* oxidase show a high degree of homology to the equivalent mitochondrial genes and the subunit IV gene is only homologous to the *Paracoccus denitrificans* gene. The DNA-derived amino acid sequences of *Rhodobacter sphaeroides* subunits I, II and III show identity to bovine oxidase of 52% for subunit I, 39% for subunit II and 49% for subunit III. The *Rhodobacter sphaeroides* oxidase, like the mammalian enzyme, contains heme *a* and heme *a*<sub>3</sub>, Cu<sub>A</sub>, Cu<sub>B</sub> and Mg and Ca<sup>++</sup>, but it lacks zinc. This similarity and simplicity of *Rhodobacter sphaeroides* cytochrome *c* oxidase make it an excellent model of the mammalian cytochrome oxidase for studying energy transduction and proton translocation (Hosler *et al.*, 1992).

#### 1.3.1.1 Subunit I

Subunit I is the largest and most conserved subunit of cytochrome *c* oxidase. It has twelve transmembrane helices and plays a central role in reduction of oxygen to water at the binuclear center, heme *a*<sub>3</sub>- Cu<sub>B</sub> (Shapleigh and Gennis, 1992). Besides the binuclear center, subunit I contains both hemes, magnesium and the recently discovered calcium site. The Mg site is located at the interface between subunit I and subunit II with ligands from the two subunits. It lies at the bottom of a proposed water channel

(Tsukihara *et al.*, 1995; Florens *et al.*, 2001), 12 Å from the surface of the protein. The function of the magnesium site is not known but it is found to be important for stabilizing the overall structure. It is also possible that it is involved in proton/water exit (Ferguson-Miller and Babcock, 1996; Florens *et al.*, 2001).

The new Ca site was discovered when the high resolution crystal structures of bacterial and bovine oxidases were solved (Ostermeier *et al.*, 1997; Yoshikawa *et al.*, 1998), and was also detected by spectroscopic measurements (Saari *et al.*, 1989; Riistama *et al.*, 1999; Lee *et al.*, 2002). This metal is located at the periplasmic outside end of the first transmembrane helix of subunit I, with five oxygen atoms as direct ligands. It is close to the Cu<sub>A</sub> and heme *a* centers but its function is yet unknown.

Alignment of 75 subunit I sequences reveals six completely conserved histidine residues which were proposed to be ligands of the redox centers in subunit I (Saraste, 1990), subsequently confirmed by mutagenesis (Shapleigh *et al.*, 1992; Hosler *et al.*, 1993) and crystallography (Tsukihara *et al.*, 1995). His333 in *Rhodobacter sphaeroides* is one of the Cu<sub>B</sub> ligands that was suggested to have a role in a histidine shuttle model, a model of direct coupling of electron transfer and proton translocation (Morgan *et al.*, 1994; Iwata *et al.*, 1995).

Another ligand of Cu<sub>B</sub>, His284, has a covalent linkage with Tyr288. This tyrosine is also hydrogen-bonded through a water to the OH group of the farnesyl moiety of heme *a*<sub>3</sub>, and possibly to the bound O<sub>2</sub> at heme *a*<sub>3</sub>, suggesting it may be involved in the oxygen reduction mechanism (Yoshikawa *et al.*, 1998) possibly through formation of a radical (Proshlyakov *et al.*, 2000).

### 1.3.1.2 Subunit II

Subunit II from most heme-copper oxidases has two parts: an N-terminal hydrophobic transmembrane domain and a C-terminal soluble domain. Both N and C termini are on the outside of the cytoplasmic membrane (Chepuri and Gennis, 1990). There are two transmembrane helices near the N-terminus. In the C-terminal domain there are two conserved histidines, two cysteines, a methionine and a peptide carbonyl shown by crystallographic and mutational studies to be ligands of the two copper ions that make up the Cu<sub>A</sub> center.

The subunit II C-terminal domain has been suggested to be the substrate binding site (Steinrucke *et al.*, 1987), this is supported by chemical modification (Millett *et al.*, 1983) and mutational studies which indicated that some of the carboxyl residues are involved in cytochrome *c* binding (Witt *et al.*, 1995; Zhen *et al.*, 1999; Wang *et al.*, 1999), as well as computational modeling (Roberts and Pique, 1999).

Subunit II overlaps with subunit I and is bound to it in part by a shared magnesium ion, which has a carboxyl ligand from subunit I.

### 1.3.1.3 Subunit III

Subunit III of *aa*<sub>3</sub> cytochrome *c* oxidase contains seven transmembrane helices. A highly conserved residue Glu98 which resides in helix III has a high reactivity with N,N-dicyclohexyl carbodiimide (DCCD). Modification of the oxidase with DCCD leads to the loss of proton translocation activity. For this reason, subunit III was suggested to play a role in proton pumping (Casey, 1981; Prochaska *et al.*, 1981). However mutational



analysis of Glu98 in *Paracoccus denitrificans* showed retention of proton pumping (Haltia *et al.*, 1991). This conclusion was originally made on the basis of the observation that a subunit III depleted enzyme can still pump protons (Gregory and Ferguson-Miller, 1988). The role of subunit III is still unknown, but its cleft may be a docking site for other membrane proteins (Iwata *et al.*, 1995) or a storage site for oxygen. It is also suggested to maintain the functional integrity of the enzyme complex (Bratton *et al.*, 1999) and may form the entrance to a proposed oxygen channel (Riistama *et al.*, 1996). Evidence from a gene interruption experiment gives an alternative function for subunit III as an assembly factor (Haltia *et al.*, 1991).

#### **1.3.1.4 Subunit IV**

In *Rhodobacter sphaeroides* subunit IV was discovered recently because of its presence in a high-resolution crystal structure (Svensson-Ek *et al.*, 2002) but a homologue was already found in the *Paracoccus denitrificans* enzyme. It has no homology to the ten small subunits in the bovine oxidase, it has only one transmembrane helix, and its function is unknown. The deletion of this subunit from *Paracoccus denitrificans* has no obvious effect on the catalytic function of the enzyme (Witt and Ludwig, 1997).

#### **1.3.2 Electron pathways and control of electron transfer**

Electron transfer is central to biological organisms' ability to manage energy. In oxidative phosphorylation in mitochondria, a series of protein complexes catalyze electron transfer events, coupled to proton transfers that build up the chemiosmotic

gradient, which drives ATP synthesis. The way the amino acids and cofactors of these protein complexes control electron flow has been the subject of much theoretical and experimental work (Marcus and Sutin, 1985; Stuchebrukhov and Marcus, 1995)

Cytochrome *c* oxidase plays an important role in these processes. It catalyzes the final step in electron transfer, where oxygen is reduced to water at the active site of the enzyme. The entry of electrons from cytochrome *c* to cytochrome *c* oxidase appears to occur through the unique binuclear Cu<sub>A</sub> center located in subunit II close to the outside surface of the protein where cytochrome *c* must approach (Hill, 1991; Zhen *et al.*, 1999).

Some analyses suggest a pathway for electrons through Cu<sub>A</sub> to heme *a* and then to the heme *a*<sub>3</sub>-Cu<sub>B</sub> center, but the question of whether this electron transfer is facilitated by specific bonds, or alternatively is insensitive to the precise protein structure between metal centers, remains unsolved. Recently a number of mutants have been made in the vicinity of Cu<sub>A</sub> or the predicted pathway to heme *a* (Zhen *et al.*, 1999; Zhen *et al.*, 2002). The four surface carboxylate mutants (E157Q, D214N, D195N and E148Q) result in altered binding, as well as steady-state and time resolved kinetics with cytochrome *c*, indicating their involvement in the cytochrome *c* binding domain. The mutation of the direct ligands of Cu<sub>A</sub> (H260N and M263L) caused a severe inhibition of overall electron transfer rates. The crystal structure of the wild type oxidase indicates that H260 is hydrogen-bonded to a highly conserved pair of arginines in subunit I which is proposed to form part of a through-bond electron transfer pathway from Cu<sub>A</sub> to heme *a* (Iwata *et al.*, 1995; Ramirez *et al.*, 1995; Tsukihara *et al.*, 1996). Mutation of this residue (H260N) disrupts the hydrogen bonds and would be expected to give lower electron transfer rate, if the through-bond path is important. Indeed, a pathway to heme *a* is supported by the

much more inhibited intrinsic electron transfer rate from Cu<sub>A</sub> to heme *a* in H260N, compared to mutant, M263L, which is not in the path to heme *a* (Zhen *et al.*, 2002; Wang *et al.*, 2002). The results from these mutational studies support that Cu<sub>A</sub> is the input site for electrons from cytochrome *c* and its dinuclear character is important for rapid transfer to heme *a*.

In spite of all these efforts in studying the electron input site and electron pathway through cytochrome *c* oxidase, the mechanism of electron transfer from electron donor (D) to electron acceptor (A) has remained controversial. Several models have been proposed, including the “through-space” or distance dependent model (Hopfield, 1974; Moser *et al.*, 1992; Moser *et al.*, 1995) and “through-bond” or pathway model (Beratan *et al.*, 1992; Onuchic *et al.*, 1992; Curry *et al.*, 1995).

#### **1.3.2.1 “Through-space” model**

Electron transfer rates relative to the distance between electron donor and acceptor in the bacterial reaction center have been investigated (Moser *et al.*, 1992). A linear relationship between the distance and the logarithm of electron transfer rate was found. Based on these results, the investigators conclude that electron transfer rates are strongly dependent on distance, along with the difference in free energy between an electron donor and acceptor ( $-\Delta G^\circ$ ) and the reorganization energy ( $\lambda$ ), but that the chemical structure of the medium in-between is not a major determinant of the electron transfer rate. This theory implies that proteins present a relatively uniform barrier (or support) to electron tunneling, and that the specific amino acid bonding structure of the intervening protein does not affect the coupling between the redox centers. In summary,

this model indicated that there is no specific pathway involved in electron transfer between donors and acceptors. The directional specificity for an electron from donor to acceptor depends on the nuclear factors.

#### **1.3.2.2 “Through-bond” model**

Beratan and Onuchic have developed a tunneling-pathway model to describe electron coupling between redox sites (Beratan *et al.*, 1991). In this model there are three basic elements in the electron transfer pathway: covalent bonds, hydrogen bonds and through-space jumps. The through-covalent bonds tunneling is the most effective way, with lower tunneling barriers and smaller decay factors (electrons propagate faster and longer), while the through-space jumps have higher tunneling barriers and larger decay factors. A critical aspect of the pathway model is the important role of hydrogen bonds as tunneling mediators (Curry *et al.*, 1995). The hydrogen-bond interactions are reported as good tunneling mediators because they allow relatively small through-space gaps (Regan *et al.*, 1995). Considerable experimental evidence has been obtained to support a facilitating role for through-bond electron tunneling (Gray and Winkler, 1996)

#### **1.3.3 Proton Pathway and control of pumping efficiency**

For the function of cytochrome *c* oxidase, protons are required for two different purposes: chemical protons are consumed upon reduction of oxygen to water, and pumped protons are translocated from the matrix (or cytoplasm in bacteria) to the intermembrane space, but it is not known whether both types of protons move through the protein via the binuclear center (direct coupling mechanism) or whether the pumped

protons take a separate pathway (indirect coupling mechanism). At least three pathways for protons have been proposed; one pathway (D-pathway) involves residues in helices II, III and IV in subunit I ending at an internal carboxyl (E286) in helix VI; the second (H-pathway) is located mainly between helices XI and XII of subunit I ending at an external, but not conserved, carboxyl (D51), and the third one (K-pathway) involves helices VI and VIII of subunit I ending at the heme  $a_3$ -Cu<sub>B</sub> center. Neither the K nor the H proton pathways are clearly observed in the crystal structure of mammalian oxidase, but by proposing water linkages, all can be envisioned (Iwata *et al.*, 1995).

Tsukihara and colleagues recognize the possible proton channel (H) in the crystal structure that does not go to the  $a_3$ -Cu<sub>B</sub> center (Tsukihara *et al.*, 1996). This supports an indirect coupling mechanism. Other pathways, D and K, approach the active site supporting a direct coupling mechanism such as a ligand switching model (Rousseau *et al.*, 1993; Wikstrom *et al.*, 1994). The direct coupling mechanism makes use of the ligands to the metal centers as carriers for protons; with such a model it is harder to account for uncoupled activity (electron transfer without proton pumping). However, many studies have indicated that there are conditions under which the proton to electron ratio ( $H^+/e^-$ ) can differ from the normal 1:1 (Papa *et al.*, 1991; Frank and Kadenbach, 1996).

#### **1.3.3.1 Proton Pathways in *Rhodobacter sphaeroides***

Although proton pathways and the mechanism of proton pumping is still controversial, three proton pathways have been proposed in both mammalian and bacterial cytochrome *c* oxidase (Figure 1.3).

**Figure 1.3 Possible proton pumping pathways.** K-path and residues involved with it are shown in green, D-path and residues involved with it are shown in red and yellow represents the H-path and the residues involved with it. Yellow balls are used for Cu<sub>A</sub> and Cu<sub>B</sub>, a magenta ball for magnesium and red balls for heme irons. The figure was created by D. Mills using the computer program Rasmol (Mills *et al.*, 2002) with modification.

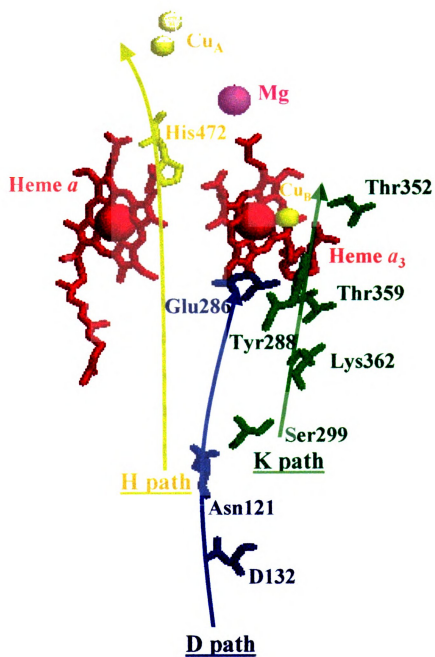
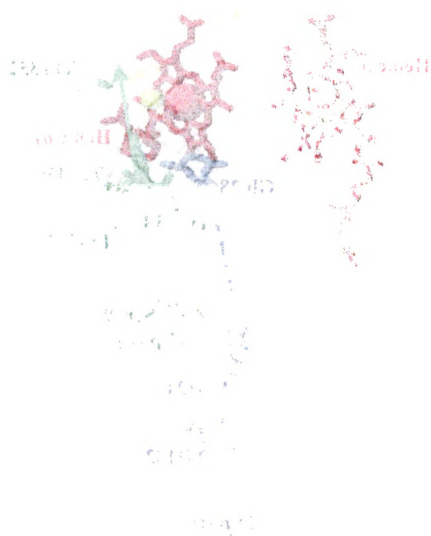


**Figure 1.3**



1 2 3



### 1.3.3.1.1 D-pathway

In *Rhodobacter sphaeroides* this proton channel involves an aspartate residue (D132) hence the name D-pathway. This aspartate is located near the inside surface of the protein between helix II/III of subunit I, close to the beginning of a hydrogen-bond network with numerous internal water molecules (resolved in the crystal structure) that leads to a glutamate residue (E286) which is about 10Å away from the heme-copper center. The proton pathway beyond E286 is not clear, but it is possible that both pumped as well as chemical protons are translocated through this channel to E286 (Gennis, 1998). Site-directed mutagenesis provides strong evidence that the D-channel is critical to delivery of protons for the oxygen chemistry following the binding of dioxygen and is critical for pumping protons (Lee *et al.*, 2000). Some mutants in this pathway have severely reduced enzymatic activity and the residual activity is decoupled from proton pumping (Thomas *et al.*, 1993; Fetter *et al.*, 1995). When D132 is mutated to any non-carboxylate residue such as alanine, the residual activity is only 5% of wild type. The activity of these mutants can be increased by increasing the membrane potential, positive on the outside of the membranes, leading to a phenomenon of “reverse” respiratory control; the normal wild type activity is dramatically decreased by a membrane potential. The normal pKa for the wild type is also not evident in the D132A mutant; the rate increases exponentially with decreasing pH on the outside of the vesicles, showing that availability of protons from the outside is rate-limiting in this mutant (Mills *et al.*, 2000). In the wild type enzyme, protons are rapidly supplied from the inside through the D-channel, but when this path is blocked, the external supply of protons becomes rate

limiting, presumably through reversal of the exit pathway. Regulation of reversibility of the proton exit path could be a normal regulatory mechanism and explain how “intrinsic uncoupling” or lowering of the normal proton to electron stoichiometry might occur under physiological conditions (Ferguson-Miller and Babcock, 1996).

Using a fully reduced enzyme in flow-flash transient absorption spectroscopy measurements, Brezinski's group found that the D-proton channel is required for kinetically competent complete turnover, perhaps because a proton transfer is needed for the movement of an electron from Cu<sub>A</sub> to heme *a* (Smirnova *et al.*, 1999).

#### **1.3.3.1.2 K-Pathway**

This pathway lies directly below the active site where oxygen is reduced to water, and contains a lysine (K362), two threonines (T359 and T352) above it, as well as a serine (S299) (Branden *et al.*, 2001) and a glutamate (E101) in subunit II, (Ma *et al.*, 1999) below it. These residues could connect via waters directly to tyrosine (Y288) that is covalently bound to a histidine ligand of Cu<sub>B</sub> (Buse *et al.*, 1999). This tyrosine is proposed to donate substrate protons; originally this pathway was designated as the substrate proton channel (Thomas *et al.*, 1994).

The very small residual activity of the K362 mutant (0.02% of the wild type activity) increases when the membrane potential is dissipated, both in steady-state measurements of oxygen consumption and in pre-steady-state stopped-flow measurements of cytochrome *c* oxidation (Mills *et al.*, 2000). This observation indicates that impaired proton uptake in the K-pathway cannot be overcome by protons supplied from the exterior, as is the case in the D-pathway. Thus the K-pathway does not appear to

lead to an externally accessible site, supporting its proposed role as a substrate proton channel.

#### **1.3.3.1.3 H-Pathway**

A third putative proton pathway was first suggested by the bovine crystal structure (Tsukihara *et al.*, 1995) and later was also identified in the *Paracoccus denitrificans* structure (Ostermeier *et al.*, 1997). A conserved histidine H472 in *Rhodobacter sphaeroides* (H456 in *Paracoccus denitrificans* and H429 in bovine oxidase) is found in this channel, hence the name H-pathway. This channel is proposed to be specifically for pumping protons in the mammalian oxidases, and does not lead to the heme-copper center but, instead comes in contact with heme *a*.

The functional importance of residues lining the putative H-channel was examined by site-directed mutagenesis (Lee *et al.*, 2000). Results from this study suggested that the H-channel is not functionally important in the prokaryotic oxidase, in agreement with the conclusion from previous work from *Paracoccus denitrificans* (Pfützner *et al.*, 1998).

#### **1.3.3.2 Proton Pumping Models**

Two mechanisms of coupling of electron transfer and proton translocation have been proposed: direct and indirect coupling models.

### 1.3.3.2.1 Direct Coupling Model

In the direct coupling model, the pumped proton channel would transfer protons to a metal center, where they would bind to metal ligands at stages during the redox chemistry and be released into a proton exit channel. (Ferguson-Miller and Babcock, 1996).

Most of the models proposed are based on this direct coupling mechanism. The first well-developed model, **ligand-exchange model**, was proposed by Chan and coworkers (Chan and Li, 1990). They suggested that a redox active metal could accomplish proton pumping by undergoing ligand exchange, dependent on the redox state of the metal. In this model the reduction of Cu<sub>A</sub> causes a conformational change in the Cu<sub>A</sub> site from planar to tetrahedral. This change draws in a nearby tyrosine residue to ligate Cu<sub>A</sub>, while one of its cysteine ligands is lost. This ligand exchange enables the tyrosine proton, which is from the inside of the membrane, to be transferred via the displaced cysteine residue to the outside of the membrane when the cysteine ligates back to Cu<sub>A</sub> site releasing a proton. In this model, each electron transfer step is coupled with one pumped proton.

Another model of a direct coupling mechanism was proposed by Wikstrom and colleagues (Wikstrom *et al.*, 1994). This model involves a histidine that is a Cu<sub>B</sub> ligand and hence the name **histidine-cycle model**. In this model, histidine was proposed to cycle between imidazolium (ImH<sub>2</sub><sup>+</sup>) and imidazolate (Im<sup>-</sup>), and two protons would be pumped in each cycle. Two separate proton uptake channels were proposed, a substrate proton channel and a pumped proton channel. At the beginning of the cycle, the histidine in the imidazolate form binds to Cu<sub>B</sub>. Then Cu<sub>B</sub> is reduced, and a negatively charged oxygen

intermediate binds to heme  $a_3$ . To balance the negative charge, two protons are taken up from the matrix, and the histidine is converted to the imidazolium state. It dissociates from  $\text{Cu}_B$  but retains some electrostatic interaction with the negatively charged oxygen intermediate. At this point, two substrate protons are taken up and a water molecule is formed. The electrostatic stabilization is no longer needed; therefore, two protons are released to the other side of the membrane, and the histidine returns to the imidazolate state and binds to  $\text{Cu}_B$  as a ligand and the cycle begins again.

Another model (Rousseau *et al.*, 1993) involved a tyrosine (Y422) which was proposed to substitute for the histidine legand of heme  $a_3$  (H419); in this case the histidine (H419) would act as the proton transfer element. This model was tested by mutation of the tyrosine (Y422) and was ruled out by Ferguson-Miller and coworkers (Mitchell *et al.*, 1996).

#### **1.3.3.2.2 Indirect Coupling Model**

In this model, electron transfer is proposed to be the driving force for proton movement by inducing a conformational change at a distance from the site where the redox changes occur. Yoshikawa and coworkers identified a conformational change in the reduced compared to the oxidized form of the bovine oxidase. In the basis of this change they have formulated an indirect coupling model involving the change of pK of D51 (not conserved in other oxidases) on the outside and its connection to the inside through a hydrogen-bonded path. (Yoshikawa *et al.*, 1998; Tsukihara *et al.*, 1996). They suggested that a proton conducting path may start at the aspartate (D132), as in the direct model, but not go through the glutamate (E286) and not access the heme  $a_3$ - $\text{Cu}_B$  site.

Instead two possible hydrogen-bonded networks involving residues in helices III and IV, or helices XI and XII, in subunit I were initially proposed to facilitate the proton translocation.

Hofacker and Schulten proposed that glutamate (E286), is the key residue in the coupling mechanism, as in the histidine cycle, but suggested that a proton is delivered directly to a heme  $a_3$  propionate group (Hofacker and Shulten, 1998), rather than a metal center ligand, to accomplish proton pumping. Alternatively, this glutamate can deliver a proton to the binuclear center or to the heme  $a_3$  propionate group by flipping itself, so this model is known as a **flipping model**. A proton is transferred from the D channel to the propionate group of heme  $a_3$  through flipping of the glutamate side chain. Two water molecules produced during the reduction of oxygen are suggest to form a hydrogen-bonded connection between the propionate group of heme  $a_3$  and glutamate (E286) stabilizing E286 in the flipped position. Uptake of a substrate proton from the K channel would drive the release of a proton from E286. This mechanism can transfer only one proton at a time.

#### 1.3.3.3 Control of pumping efficiency

The efficiency of energy transduction in mitochondria depends on protons pumped per electron transferred and on the “leakiness” of the membrane. Evidence from mutant bacterial oxidases suggests that inefficient (uncoupled) activity can be supported by reversal of the normal exit pathway for protons, even though this route for uptake of protons is only observed when the path from the interior is blocked (Fetter *et al.*, 1995). In mammalian oxidase, uncoupled electron transfer is observed in the presence of a high

ATP concentration (Kadenbach *et al.*, 1997). The crystal structure of cytochrome *c* oxidase shows a likely ATP binding site on subunit VIa, which directly interacts with residues that form a possible proton exit site. Thus an ATP-induced conformational change in this region could allow increased reversal of the proton exit channel. This provides a hypothesis for regulation of efficiency in cytochrome *c* oxidase (Ferguson-Miller and Babcock, 1996).

## **2. Crystal Structures of Cytochrome *c* Oxidases from Different Species**

### **2.1 Importance of the Crystal Structures**

As a prerequisite for understanding the molecular mechanism of oxygen reduction and its coupling to proton pumping by cytochrome *c* oxidase, the crystal structures at high resolution of many different states of the oxidase are required. The understanding of the energy transduction mechanism will lead to knowledge of the regulatory processes that govern cytochrome *c* oxidase activity and efficiency of energy production in eukaryotic cells.

Due to the difficulty in isolating many membrane proteins with the purity, stability and in the quantities demanded for structural analysis, besides the difficulty in overexpressing and crystallizing them, only a few families of membrane proteins have given 3D crystals of a quality allowing structure determination at atomic resolution. The structures of all the currently known polytopic membrane proteins from inner membranes of bacteria and mitochondria and from eukaryotic membranes; and from the outer membrane of gram negative and related bacteria have been reported at this web site (<http://www.mpibp.frankfurt.mpg.de/michel/public/memprotstruct.html>), along with monotopic membrane proteins (proteins that are inserted into, but not crossing the membrane).

Yoshikawa and coworkers successfully crystallized and analyzed the 3D structure of cytochrome oxidase from bovine heart initially at 2.8 Å, more recently at < 2.0 Å resolution, in a long-term effort that took twenty years (Tsukihara *et al.* 1995). In contrast to Yoshikawa's group who produced crystals by conventional methods, Michel's group introduced a novel approach in which a monoclonal antibody fragment is bound to the



membrane complex with the idea of extending the hydrophilic domain of the membrane protein and fixing a conformation. Their antibody recognizes a discontinuous epitope on the surface-exposed domain of cytochrome *c* oxidase, and it can be assumed to stabilize one conformation of the complex. Michel's group crystallized cytochrome oxidase from *Paracoccus denitrificans* (Iwata *et al.* 1995).

Recently the crystal structure of *Rhodobacter sphaeroides* cytochrome *c* oxidase has been solved to 2.3 Å resolution for a wild type and E286Q mutant at two different pH values: 6 and 10 (Svensson-Ek *et al.*, 2002).

## **2.2 Crystal Structure of *Paracoccus denitrificans* Cytochrome *c* Oxidase**

The crystal structure of cytochrome *c* oxidase from the soil bacterium *Paracoccus denitrificans* (Iwata *et al.*, 1995; Ostermeier *et al.*, 1997), provided new information and confirmed previous spectral and mutagenesis studies on protein structure including the protein subunits, metal centers and proton pathways.

The location of the redox active metal centers have been identified for *Paracoccus denitrificans*. The structure of the four subunit-enzyme was solved to 2.8 Å resolution (Iwata *et al.*, 1995), and the structure of the two subunit form (subunits I and II) was solved to 2.69 Å resolution in 1997 (Ostermeier *et al.*, 1997). The crystal structure indicated a high level of structural homology between the bacterial and mitochondrial oxidases in the regions of the redox active metal centers and confirmed the dinuclear nature of the Cu<sub>A</sub> center (Abramson *et al.*, 2001).

Two major domains are present in the crystal structure of *Paracoccus denitrificans* oxidase, a small extra-membrane domain and a large membrane-spanning

domain. The former domain is derived from subunit II, contains a binuclear Cu<sub>A</sub> center, and is the site at which cytochrome *c* interacts with the oxidase. Excluding subunit IV, the membrane-embedded core of cytochrome *c* oxidase consists of 21 transmembrane helices, four of which provide ligands for the three other metal centers: a low-spin heme *a*, a high spin heme *a*<sub>3</sub> and Cu<sub>B</sub>. These metal centers lie deep within the membrane-spanning regions of the enzyme. The path of electron transfer through the enzyme, as proposed by Hill (Hill, 1994) involves electrons entering via Cu<sub>A</sub>, which is in rapid equilibrium with cytochrome *c*, passing to heme *a* and then to the binuclear center heme *a*<sub>3</sub>-Cu<sub>B</sub> where dioxygen is reduced to water. This path is consistent with the observed structure.

Two possible proton transfer pathways are also observed in the protein structure. These show good agreement with the results of site-directed mutagenesis experiments for bacterial oxidases (Iwata *et al.*, 1998). One pathway, the K-channel, leads up the conserved polar face of the transmembrane helix VIII to the binuclear center. It also includes the hydroxyl group of the hydroxethyl farnesyl side chain of heme *a*<sub>3</sub>, a tyrosine residue and bound water molecules.

A second pathway, the D-channel, starts at the conserved aspartate located at the entrance of the pore formed by helices II-VI and leads into a polar cavity containing several water molecules. A conserved glutamate residue is found at the end of the cavity (E278 in *Paracoccus denitrificans* and E286 in *Rhodobacter sphaeroides*). Beyond this glutamate, the proton pathway is not clear, but various studies invoke transient water connections with the active site or the outside (Hofacker and Schulten, 1998).

### 2.3 Crystal Structure of Bovine Heart Cytochrome *c* Oxidase

The crystal structure of bovine heart mitochondrial cytochrome *c* oxidase was initially reported to a 2.8 Å resolution (Tsukihara *et al.*, 1995), and it has been greatly improved with the published structures of fully oxidized to 2.3 Å, fully reduced to 2.35 Å, azide bound to 2.9 Å and carbon monoxide bound to 2.8 Å resolution (Yoshikawa *et al.*, 1998), as well as an unpublished 2.0 Å structure, in which many waters have been defined (Yoshikawa, personal communication). The three core subunits with the redox active metal centers show remarkable, almost superimposable, similarity to the three major subunits of the bacterial enzyme.

In addition to the K-channel and D-channel, which are found in the *Paracoccus denitrificans* oxidase, a third proton pathway, the H-channel, is suggested in this higher resolution structure. This channel starts at an aspartate residue and involves seven polar side chains, several water molecules and one main chain peptide bond, as well as the low-spin heme *a*. The hydroxyl group of the farnesyl chain of heme *a* has hydrogen bonds to a serine residue and a water molecule with additional hydrogen bonds to serine and threonine residues. This hydrogen bond network and associated waters are part of the H-channel, which ends at an aspartate 51 (bovine) that is not conserved in any of the bacterial enzymes.

The crystal structure indicates that heme *a*<sub>3</sub> is facing heme *a* at an angle of 104° as in the *Paracoccus denitrificans* structure. Heme *a*<sub>3</sub> has the predicted histidine axial ligand; Cu<sub>B</sub> is coordinated by the three predicted histidine residues. The distance between heme *a*<sub>3</sub> and Cu<sub>B</sub> varies depending on the redox state and the presence of a bound ligand. According to Yoshikawa and his colleagues, the position of heme *a*<sub>3</sub> is always fixed but

the position of Cu<sub>B</sub> differs depending on either the oxidation state of the metal sites or the binding of a ligand (Yoshikawa *et al.*, 1998).

The Cu<sub>A</sub> site located in subunit II shows the identical structure, as found in the *Paracoccus denitrificans* oxidase and predicted from the sequence, liganded by two cysteines, two histidines, a methionine and a peptide carbonyl of a glutamate.

In addition to the redox-active centers, the enzyme also contains tightly bound nonredox-active metal centers: magnesium, sodium and zinc. The zinc ion is bound by a nuclear encoded subunit Vb on the matrix side of the membrane, whereas the other non-redox-active metals are bound within subunit I. The magnesium-binding site as in *Paracoccus denitrificans*, is observed at the interface between subunit I and II. Its ligands as defined by mutagenesis in *Rhodobacter sphaeroides* oxidase (Fetter, 1995) were identified as a histidine and aspartate in subunit I, a glutamate from subunit II (shared with Cu<sub>A</sub>) and three water molecules. The site could have a structural role for stabilization of the interface between these two subunits, and also could be important for proton pumping since it is located in the vicinity of a possible proton or water exit pathway.

A sodium (or calcium) binding site is not identical in its ligation to the bacterial version. It is formed by a loop between the transmembrane helices I and II on the outer side surface of subunit I. The function of this site is not known, but it could be also involved in the exit pathway of the pumped protons (Riistama *et al.*, 1999).

In the published bovine structure (Yoshikawa *et al.*, 1998) eight phospholipids, five phosphatidylethanolamines and three phosphatidylglycerols, were observed to be associated with each monomer of the oxidase. The lipids are oriented so that the

phosphorus atoms are located at the membrane surface, either the intermembrane space or matrix side, and the hydrocarbon tails are directed towards the inside of the transmembrane region. The resolved chain lengths of the lipid hydrocarbon tails range from 10-20. Two phosphatidylethanolamines and one phosphatidylglycerol form a lipid pool near subunit III. Three phosphatidylethanolamines and two phosphatidylglycerols surround the transmembrane surface of subunit I on the side opposite to subunit III. A higher resolution structure (Yoshikawa, personal communication) at 2.0 Å reveals 19 phospholipids per monomer, including cardiolipins binding at the interface between the two monomers in the dimer.

#### **2.4 Crystal Structure of *Rhodobacter sphaeroides* Cytochrome *c* Oxidase**

The structure of the *Rhodobacter sphaeroides* cytochrome *c* oxidase has been solved at 2.3 Å (Svensson-Ek *et al.*, 2002) (Figure 1.4). Although it is highly similar to the mammalian and *Paracoccus denitrificans* structures, this high-resolution structure reveals atomic details including water molecule positions and a potential oxygen pathway, which has not been reported in any other oxidase structures. The structure of the mutant enzyme, E286Q, is reported by the same group. Analysis of the latter structure indicated that structural rearrangement around E286 residue could be key in proton transfer in this enzyme.

The overall structures of subunits I, II and III are very similar to those of *Paracoccus denitrificans* and to the core subunits of the bovine heart enzyme (subunits I, II and III), except some differences at the C-termini and the N-termini and some inserted loops. Subunit IV, which had not been reported before in the literature for the

**Figure 1.4 Crystal structure of *Rhodobacter sphaeroides* cytochrome *c* oxidase and the associated lipids.** Helices of subunit I, II, III and IV are shown in yellow, blue, red and green, respectively. Green balls represent Cu<sub>A</sub> and Cu<sub>B</sub>, magenta ball for magnesium and red balls for heme irons. Associated lipids (phospholipids) are shown in black. The figure was created using the Rasmol program using coordinates from (Svensson-Ek *et al.*, 2002).

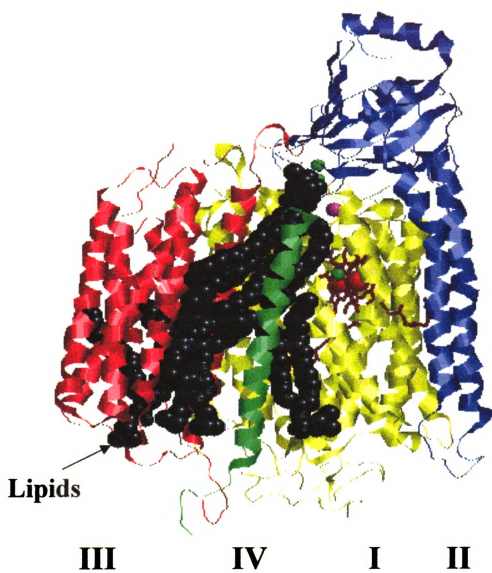


**Figure 1.4**





*Rhodobacter sphaeroides* enzyme, was found in the crystal structure. Isolation of its gene from *Rhodobacter sphaeroides* (Hiser, unpublished) shows it is similar (50% sequence identity) to subunit IV of *Paracoccus denitrificans* and its function is also unknown.

Four phosphatidylethanolamines are clearly identified in the structure. Two other phospholipids are also identified, but their electron densities are disordered and the type of lipids is not clear. Two of the six phospholipids are found in the cleft formed by the two-helix bundles of V-shaped subunit III; one of these lipids interacts with subunit I. The other four lipid molecules exist at the interface between subunit IV and subunits I/III, separating subunit IV almost entirely from the rest of the enzyme.

A total of 218 water molecules per monomer are resolved in the structure. The majority of the water molecules were found on the surfaces exposed to solvent, but many of them are also observed within the molecule in water channels such as the D-channel that are likely to be essential for proton translocation.

The crystal structure of *Rhodobacter sphaeroides* cytochrome *c* oxidase reveals a possible oxygen entry pathway for the first time. Two xenon molecules were identified in a hydrophobic cavity indicating a possible oxygen channel leading to the binuclear center. The entrance of the oxygen is suggested to be in the membrane-spanning region about 30 Å from the top surface of the protein, between helices II and III in subunit I. It had been previously suggested that the entrance to the oxygen channel was through subunit III (Hofacker and Schulten, 1998).

A comparative study of the structures at pHs 6 and 10 indicate that the side chain of E286, at the interior end of the D pathway, can adopt two different positions

depending on its protonation state. The connection of the D-pathway to the active site or to the external site of the membrane above E286 is still not clear.

## **2.5 Importance of Available and Future Crystal Structures**

A major advance in cytochrome *c* oxidase research was made with the X-ray structures of mitochondrial and bacterial enzymes. Analysis of these structures showed a high degree of similarity between the three functional subunits of the mitochondrial enzyme and subunits I, II and III from the bacterial enzyme (both *Paracoccus denitrificans* and *Rhodobacter sphaeroides*), indicating similarity of heme environments and the binuclear center where reduction of oxygen to water takes place. This confirmed the usefulness of the bacterial enzyme as model for the mammalian oxidase.

The magnesium and calcium sites were identified in the structure, and the similarities and differences could be recognized.

In spite of considerable insights gained from the structural studies, the proton pumping mechanism of the oxidase remains largely unsolved. Crystal structures of many forms and at higher resolution are needed to define water positions important in the pathways and mechanism of proton movement.

### **3. Substrate Docking on Cytochrome *c* Oxidase:**

#### **3.1 Protein-Protein Interactions**

Protein-protein interactions are found in biological systems for different reasons. One protein connects with another in order to pass along information, catalyze or inhibit a reaction, or to form a larger structure. These interactions occur with some affinity and specificity that can range from weak and non-specific to very tight and very specific. The affinity is most often expressed in terms of a binding constant (or dissociation constant), which reflects the change in free energy that occurs during the association. This free energy change is composed of underlying thermodynamic terms, enthalpy and entropy changes that largely depend upon the fit between the structures of the molecules involved.

Inter-protein electron transfer requires a specific type of protein-protein interaction that is important for energy transduction in biological systems. There are many examples of such protein-pairs including cytochrome *c* oxidase and its substrate cytochrome *c*.

The reaction between these two proteins is initiated by cytochrome *c* docking to the external surface of subunit II of cytochrome *c* oxidase. The docking interaction is primarily electrostatic and can be eliminated with increasing ionic strength.

Chemical modifications of horse cytochrome *c* showed that several lysine residues (Lys8, 13, 27, 72, 86 and 87) are involved in the interaction between cytochrome *c* and cytochrome *c* oxidase (Smith *et al.*, 1977; Ferguson-Miller *et al.*, 1978; Osheroff *et al.*, 1980). Consistent with these studies, crystallographic analysis reveals similar interaction sites for both yeast (Cc(Y)) and horse cytochromes *c* (Cc(H)) with

cytochrome *c* peroxidase (CcP) (Pelletier and Kraut, 1992). The crystal structures of CcP:Cc(H) and CcP:Cc(Y) were resolved under different conditions. They revealed the involvement of several lysines (Lys 8, 13, 72 and 87) of horse and yeast cytochromes *c* in hydrogen-bond interaction with CcP in the CcP:Cc complex.

In the case of cytochrome *c* oxidase, there is evidence for two cytochrome *c* binding sites, a low affinity site and a high affinity site, based on kinetics and binding studies (Ferguson-Miller *et al.*, 1976; Ferguson-Miller *et al.*, 1978); the biphasic kinetic plots yield Michaelis constant values of  $K_{m1} = 5 \times 10^{-8}$  and  $K_{m2} = 0.35$  to  $1 \times 10^{-6}$  M for horse cytochrome *c* with cytochrome *c* oxidase. Similarly, high and low affinity sites have been suggested for the 1:1 cytochrome *c* and cytochrome *c* peroxidase complex based upon crosslinking and kinetic experiments (Wang and Margoliash, 1995). For both these enzymes it is still not clear what the significance of a second interaction is.

Carboxylate groups on subunit II of cytochrome *c* oxidase were found by chemical modification to be involved in the interaction between cytochrome *c* and cytochrome *c* oxidase (Millett *et al.*, 1983). Recent mutagenesis studies have tested a series of carboxylic acid residues in the same region to determine their role in binding the positively charged lysine groups in cytochrome *c*. Mutants in both *Rhodobacter sphaeroides* and *Paracoccus denitrificans* have been generated at the cytochrome *c* binding site and Cu<sub>A</sub> site, and characterized by spectroscopy, electron paramagnetic resonance (EPR), resonance Raman analysis (RR), fast kinetics analysis and metal analysis (Zhen *et al.*, 1999; Wang *et al.*, 1999; Witt *et al.*, 1995). The results defined a set of these highly conserved carboxyls that are involved in cytochrome *c* binding.

### 3.2 Definition of the Interaction Domain for Cytochrome *c* on Cytochrome *c* Oxidase

Efficient electron transfer between cytochrome *c* and cytochrome *c* oxidase requires both rapid complex formation and rapid dissociation. Determination of the structure of the complex formed between the two proteins would reveal possible paths for intermolecular electron transfer. Intensive effort has been applied to define the interaction domain. Among these efforts is a computational search method based on static crystallographic structures (Roberts and Pique, 1999). Roberts and co-workers use the docking program DOT (Daughter of TURNIP) that provides a complete search of all orientations between two rigid molecules by systematically rotating and translating one molecule about the other. Using this program, an electron transfer complex between bovine cytochrome *c* oxidase and horse cytochrome *c* was predicted. Energies for over thirty six billion configurations were calculated, providing a free energy landscape showing guidance of positively charged cytochrome *c* to the negative region on the cytochrome *c* oxidase surface formed by subunit II. In a representative of the set of lowest energy configurations, the solvent-exposed cytochrome *c* heme edge is within 4 Å of the indole ring of Trp104 of subunit II (Trp 143, *Rhodobacter sphaeroides* numbering), indicating a likely electron transfer path. These two groups are surrounded by a small, hydrophobic contact region, which is surrounded by electrostatically complementary hydrophilic interactions. Cytochrome *c*-cytochrome *c* oxidase interactions of Lys13 with Asp119 (Glu157 in *Rhodobacter sphaeroides*), Lys72 with Gln103 (Gln142 in *Rhodobacter sphaeroides*) and Asp158 (Asp214 in *Rhodobacter sphaeroides*), Lys86 with Glu109 (Glu148 in *Rhodobacter sphaeroides*) and Lys8 with

Asp139 (Asp195 in *Rhodobacter*), are the most critical interactions due to their charge/charge proximity to the hydrophobic region and exclusion from bulk solvent (Figure 1.5a & 1.5b). The predicted complex matches previous mutagenesis, binding and time-resolved kinetic studies that implicate Trp104 (Trp143) in electron transfer and show the importance of specific charged residues to protein affinity (Wang *et al.*, 1999; Zhen *et al.*, 1999).

In *Rhodobacter sphaeroides*, a number of conserved carboxyl residues in subunit two were mutated to neutral forms (Zhen *et al.*, 1999). A highly conserved tryptophan, Trp143 (Trp104 in bovine cytochrome *c* oxidase) was also mutated to phenylalanine and alanine. Spectroscopic and metal analysis of the surface carboxyl mutants revealed no overall structural changes. The double mutants D188Q/E189N and D151/E152N *Rhodobacter sphaeroides* oxidase exhibit similar steady-state kinetic behavior as wild-type *Rhodobacter sphaeroides* oxidase with horse cytochrome *c* showing that these residues are not involved in cytochrome *c* binding. The single mutants E148Q, E157Q, D195N and D214N have decreased activities and increased  $K_m$  values, indicating they contribute to the cytochrome *c*:cytochrome *c* oxidase interface. However, their reactions with horse and *Rhodobacter sphaeroides* cytochromes *c* are different, as expected from the different distribution of surface lysines on these cytochromes *c*. Mutation of Trp143 severely inhibits activity without changing the  $K_m$  for cytochrome *c* or disturbing the adjacent  $Cu_A$  center. These data provide important information about cytochrome *c* binding area on cytochrome *c* oxidase with Trp143 and Asp214 close to the site of electron transfer and Glu148, Glu157 and Asp195 providing electrostatic guidance. The

results are completely consistent with time-resolved kinetic measurements (Wang *et al.*, 1999) and with the prediction by Roberts and Pique (Roberts and Pique, 1999).

**Figure 1.5 Model for the docking site of cytochrome *c* and cytochrome *c* oxidase.** The computational model for the binding site between horse cytochrome *c* (blue) and *Rhodobacter sphaeroides* cytochrome *c* oxidase (subunit I is green, subunit II is magenta, subunit III is yellow and subunit IV is red) was made by (Roberts and Pique, 1999). The lysine residues on cytochrome *c* that involved in the binding (Ferguson-Miller *et al.*, 1978) are shown in yellow and the carboxylate residues on subunit II of the oxidase that are found to be important for the binding (Zhen *et al.*, 1999) are shown in black. The tryptophan that is involved in the electron transfer between cytochrome *c* and the oxidase (Zhen *et al.*, 1999) is shown in black. Coppers are cyan balls. The figure was made with Rasmol. Figure 1.5a shows the whole structure, whereas figure 1.5b shows only the binding site between cytochrome *c* and subunit II of the oxidase.





**Figure 1.5a**

1892



1892

1892

1892

1892

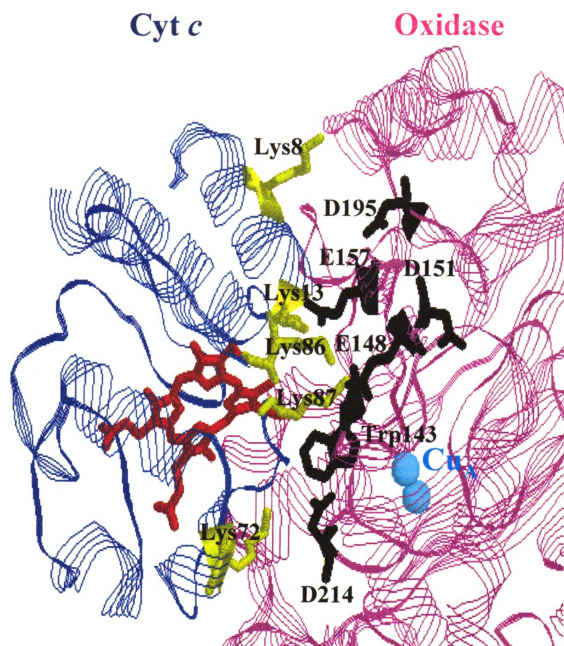
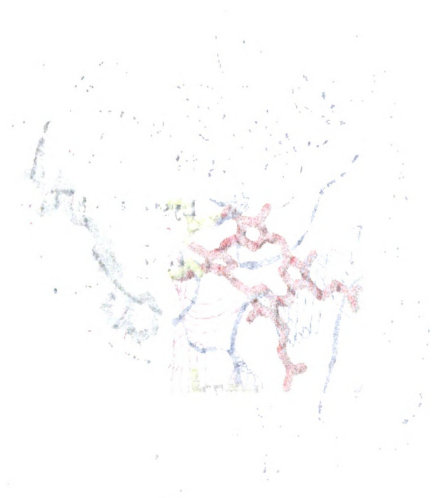


**Figure 1.5b**

100



100

Millett's group studied the reaction between cytochrome *c* and the above mutants of cytochrome *c* oxidase of *Rhodobacter sphaeroides* using a horse cytochrome *c* derivative labeled with ruthenium trisbipyridine at lysine 55 (Ru-55-Cc) (Wang *et al.*, 1999). The effects of cytochrome *c* oxidase mutations on the kinetics follow the order D214N > E157Q > E148Q > D195N > D151N/E152Q  $\approx$  D188N/E189Q  $\approx$  Wild type, indicating that the acidic residues Asp214, Glu157, Glu148 and Asp195 on subunit II interact electrostatically with lysines surrounding the heme crevice of cytochrome *c*. Mutating the highly conserved tryptophan residue, Trp143, to phenylalanine or alanine decreased the intracomplex electron transfer rate constant by 450 and 1200 fold respectively, without affecting the dissociation constant,  $K_D$ . It therefore appears that the indole ring of Trp143 somehow mediates electron transfer from the heme group of cytochrome *c* to Cu<sub>A</sub>, consistent with its predicted van der Waals contact with the edge of cytochrome *c* heme (Roberts and Pique, 1999).

## **4. Different *c*-Type Cytochromes : Which One is The Physiological Substrate For *aa*<sub>3</sub> Oxidase?**

### **4.1 Background on Cytochrome *c***

Cytochromes are central figures in the process of electron transfer during energy metabolism. These heme-containing proteins are so ubiquitous that the name, “cytochrome”, which means cellular pigment, was given when Keilin found them in every organism he tested including bacteria, yeast, higher plants, insects, amphibians, birds and mammals (Keilin, D. 1925). Cytochromes comprise a diverse group of proteins with respect to structure and function, but the presence of a heme group, a redox-active iron-containing porphyrin, is common to all. The heme group is, in fact, what gives these proteins their characteristic absorbance spectrum, and as Keilin noted, their visible color. The heme iron serves as an electron transfer center by changing its valence state from +3 to +2 as it accepts an electron from another redox center. The iron atom returns to the ferric state when the cytochrome is oxidized and the electron is donated to an acceptor molecule. In a particular electron transfer chain the redox midpoint of the components will often indicate the direction of electron flow. Among these cytochromes, several *c*-type cytochromes have been found to be important in shuttling electrons between membrane-bound complexes (Meyer and Cusanovich, 1985).

Typically cytochrome *c* is a small, basic, heme-containing protein with a single iron porphyrin covalently attached through two cysteine amino acids. The iron is coordinated to four nitrogen atoms in the porphyrin ring. The axial positions are coordinated by the sulfur of methionine and a nitrogen of one histidine. Eukaryotic cytochromes *c* are commonly composed of 103-113 amino acids (molecular weight of

12,000 g mol<sup>-1</sup>) with redox potentials around 260 mV, and overall charge of +7 at pH 7.0 (Pelletier and Kraut, 1992). They are essential components of the terminal segment of the mitochondrial respiratory chain. Mitochondrial cytochrome *c* is a highly charged, water-soluble protein of the mitochondrial intermembrane space. Its major function is to transfer electrons from cytochrome *c* reductase (cytochrome *bc<sub>1</sub>* complex) to cytochrome *c* oxidase. The implication is that the function of cytochrome *c* is critically dependent on its relatively high mobility, which allows it to shuttle electrons between these two relatively immobile membrane protein complexes (Gupte and Hackenbrock, 1988). Studies have shown that at the high ionic strength of the mitochondrial intermembrane space, cytochrome *c* has rapid three-dimensional mobility compared to its membrane bound redox partners. The high mobility of cytochrome *c*, and its high concentration in this enclosed space, shows an increased rate of electron transfer between the cytochrome *bc<sub>1</sub>* complex and cytochrome *c* oxidase compared to low ionic strength conditions under which the movement of cytochrome *c* is confined to two dimensions (Gupte and Hackenbrock, 1988). An alternative view is that cytochrome *c* functions in the respiratory chain most efficiently when its mobility is restricted to two-dimensions (Ferguson-Miller *et al.*, 1986; Craig and Wallace, 1993). Cytochrome *c* also functions as an electron transfer carrier for other reductases that are not part of the inner membrane; for this function, three-dimensional mobility of cytochrome *c* is required (Pettigrew and Moore, 1987). This mobility of cytochrome *c* is in contrast to some prokaryotic cytochromes *c*, such as *Bacillus subtilis* cytochrome *c*, which are integral membrane proteins. Indeed, in *Paraccocus denitrificans* an active complex between *bc<sub>1</sub>* complex, *c<sub>552</sub>* and *aa<sub>3</sub>* oxidase has been isolated (Berry & Trumpower, 1985). The existence of a similar membrane-

bound cytochrome *c*<sub>y</sub> in *Rhodobacter sphaeroides* raises the question of functional aggregates in the system.

Other mobility studies in mammalian mitochondria have led to the concept of a “dynamic aggregate model” of the electron transfer chain (Hockman *et al.*, 1985; Ferguson-Miller *et al.*, 1986) which suggests a combination of two dimensional, three dimensional and “solid-state” electron transfer in the respiratory chain under different conditions.

The amino acid sequences of cytochrome *c* from over 100 eukaryotic species have been determined (Moore & Pettigrew, 1990), and the atomic resolution 3D structures of the proteins from many species have been determined by x-ray crystallography (Tanaka *et al.*, 1975; Swanson *et al.*, 1977; Takano & Dickerson, 1981; Ochi *et al.*, 1983; Louie *et al.*, 1988; Louie & Brayer, 1990; Bushnell *et al.*, 1990; Sanishvili *et al.*, 1995).

#### **4.2 Mitochondrial cytochromes *c***

The crystal structures of the proteins from horse (Sanishvili *et al.*, 1995), tuna (Takano and Dickerson, 1981), bonito (Matsuura *et al.*, 1979), rice (Ochi *et al.*, 1983) and yeast iso-1 (Louie and Brayer, 1990) have been determined revealing that the “cytochrome *c* fold” remains the same for all. The crystal structures showed that the heme location and the polypeptide chain conformation are identical for both horse and rat cytochrome *c*. Also comparison of the reduced and oxidized forms of tuna cytochrome *c* (Takano and Dickerson, 1981) showed that the redox-linked conformation change is small.



The typical cytochrome *c* fold has the polypeptide chain organized into a series of  $\alpha$ -helices and fairly extended loop structures (Sanishvili *et al.*, 1995). The polypeptide is folded in such a way that the heme is sandwiched between the “right side” and the “left side”, leaving the heme edge exposed to solvent, thus defining the front surface of the molecule. The majority of the heme prosthetic group is buried within a hydrophobic pocket formed by the polypeptide chain. The vinyl side chains of pyrrole rings I and II of the heme group are covalently attached to the polypeptide chain via two thioether bonds to the side chains of two cysteine residues. This covalent bond attachment is suggested to be an important factor in establishing the heme conformation, which is distorted into a saddle shape with the front and rear edges of the heme deviating toward the right, and the top and bottom edges toward the left of the molecule. The two heme propionate groups are buried within the protein matrix and form a number of hydrogen bonds with nearby polar groups. The posterior heme propionate carboxyl atom also forms a charge interaction with the guanidinium group of an arginine residue as in cytochrome *c* oxidase; this interaction is mediated by one or two of the internal water molecules. Thus, while internally positioned, these propionate groups occupy a local environment that is clearly hydrophilic in character. The heme ion is held in the center of the heme by six coordinate ligands. The fifth and sixth ligands are provided by the imidazole nitrogen of a histidine residue on the right and the sulfur atom of a methionine residue on the left side of the molecule, respectively, while the other four are from the heme itself (Figure 1.6).

**Figure 1.6 Crystal structure of horse cytochrome *c*.** The heme (red) and heme ligands, methionine (yellow), two cysteines (magenta) and histidine (green) are shown. The lysines residues that are involved in binding with cytochrome *c* oxidase are shown in black.

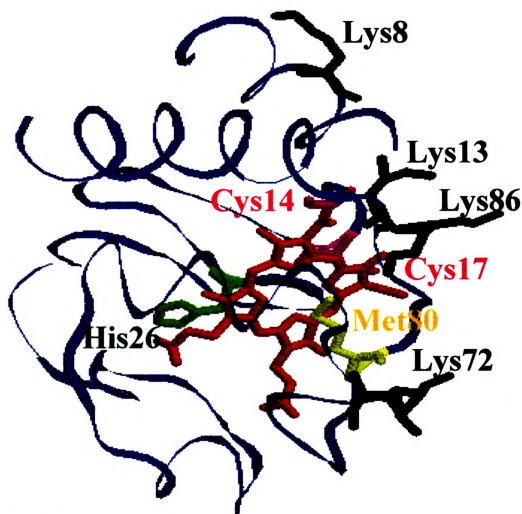
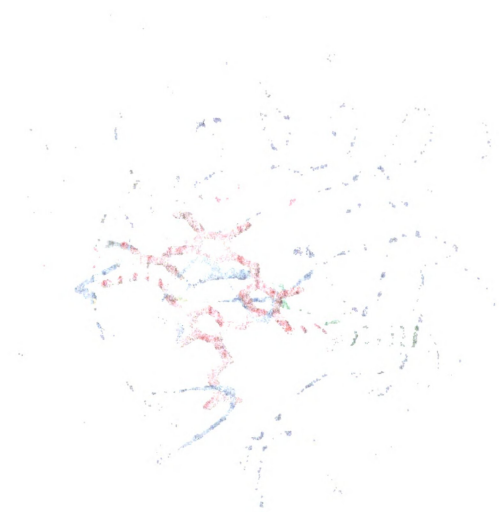


Figure 1.6



### 4.3 Bacterial cytochrome *c*

In the mitochondria of higher eukaryotes a single cytochrome *c* species mediates the electron transfer between cytochrome *c* reductase (complex III) and cytochrome *c* oxidase (complex IV). In bacteria due to the branching of the electron transport chain, many cytochromes are found. They appear to be involved in different electron transfer processes.

Many of the crystallized bacterial cytochromes *c* are globular structures with more than 40%  $\alpha$ -helical content, which is similar to that seen in mitochondrial cytochromes *c*, but the greater diversity in the structure of bacterial cytochrome *c* reflects the diverse composition of bacterial respiratory systems. Bacterial respiratory systems are more complex than the mitochondrial system, some containing more than one terminal oxidase, which differ from the mitochondrial type and may utilize a terminal electron acceptor other than oxygen (Thony-Meyer, 1997).

*Rhodobacter sphaeroides*, as many other bacteria, contains more than one *c*-type cytochromes that serve as either electron donors or acceptors in different electron transfer chains. The *aa<sub>3</sub>*-type oxidase that is the experimental system in our laboratory, accepts electrons from cytochrome *c*, but which cytochrome *c* is its physiological substrate has been a debated issue for a long time. The *aa<sub>3</sub>*-type oxidase is present at higher levels when the cells are grown aerobically. To qualify for the physiological substrate of oxidase, the *c*-type cytochrome should be present at higher levels under the same conditions. However, more than one cytochrome *c* show high expression levels during aerobic growth and mutagenesis studies of some of these cytochromes *c* that argue

against this importance for the function of the *aa*<sub>3</sub>-type cytochrome *c* oxidase, as will be discussed later in this section.

The solubility, stability, ease of purification and manipulation, spectral characteristics and relative abundance of cytochrome *c* have caused it to be one of the most studied proteins. In the next section I will discuss different *c*-types cytochromes in the purple, non-sulfur photosynthetic bacterium, *Rhodobacter sphaeroides* and which one is likely to be the physiological substrate for *aa*<sub>3</sub>-type oxidase. (Table 1.1) summarizes the different *Rhodobacter sphaeroides* *c*-type cytochromes and their characteristics.

#### **4.3.1 Soluble cytochrome *c* of *Rhodobacter sphaeroides* and Related Bacteria**

Most of the known soluble cytochromes in *Rhodobacter sphaeroides* are *c*-type cytochromes, those with propionate side chains on the tetrapyrrole ring and two covalent attachments sites to the polypeptide. The physical properties of many of these soluble *c*-type cytochromes from *Rhodobacter sphaeroides* have been examined.

##### **4.3.1.1 Cytochrome *c*<sub>554</sub>**

Cytochrome *c*<sub>554</sub> is the major soluble *c*-type of *Rhodobacter sphaeroides* under aerobic conditions. When reduced, this protein exhibits an  $\alpha$ -maximum at approximately 554 nm. The redox potential of cytochrome *c*<sub>554</sub> is 203 mV at pH 7. This type of cytochrome is found to be located to the periplasm (Flory and Donohue, 1995). It has a low spin heme, with a methionine residue as the distal ligand near the N-terminus (Meyer and Cusanovich, 1985).

**Table 1.1 Bacterial cytochromes *c***

<b>C-type cytochrome</b>	<b><math>\alpha</math>-peak (nm)</b>	<b>M.wt. (kDa)</b>	<b>Present in R.s.</b>	<b>Possible physiological role</b>
<i>C</i> <sub>554</sub> (Soluble)	554	14	+	It has high expression level during aerobic respiration, but has no similarity with mitochondrial cytochrome <i>c</i> in arrangement of charge residues, which makes its function unclear.
<i>C</i> <sub>2</sub> (Soluble)	550	14	+	Shuttles electrons between <i>bc</i> <sub>1</sub> complex and <i>cbb</i> <sub>3</sub> oxidase, and transfers electrons from <i>bc</i> <sub>1</sub> to the photosynthetic reaction center.
Iso <i>C</i> <sub>2</sub> (Soluble)	552	14		Substitute for cytochrome <i>c</i> <sub>2</sub> in transferring electrons from <i>bc</i> <sub>1</sub> to the photosynthetic reaction center.
Diheme (Soluble)	551	26		Unknown
<i>C</i> <sub>551</sub> (Soluble)	551	16		Unknown
SHP (Soluble)	548	?		Unknown
<i>C</i> <sub>552</sub> (membrane bound)	552	22		Involved in electron transfer from <i>bc</i> <sub>1</sub> to <i>aa</i> <sub>3</sub> oxidase in <i>Paracoccus denitrificans</i> .
<i>C</i> <sub>y</sub> (membrane bound)	552	24	+	Transfers electrons from <i>bc</i> <sub>1</sub> to <i>cbb</i> <sub>3</sub> and <i>aa</i> <sub>3</sub> oxidases in <i>Rhodobacter sphaeroides</i> .
<i>C</i> ' (Soluble)	552	14		Unknown

Results of amino acid sequence analysis of cytochrome  $c_{554}$ , indicated that the protein is 14 kDa (Bartsch *et al.*, 1989), whereas Meyer and Cusanovich found that this cytochrome  $c$  had a molecular weight of 44 kDa, suggesting that the protein is present as a trimer (Meyer and Cusanovich, 1985).

When the abundance of the protein was estimated by the available methods, it appeared that cytochrome  $c_{554}$  was most abundant at high oxygen tensions, with low levels under anaerobic conditions. The first reported preparation containing cytochrome  $c_{554}$  was made from cells grown photosynthetically under semiaerobic conditions (Orlando and Horio, 1961). Orlando followed this study with another one, and he found that cytochrome  $c_{554}$  is at approximately four-fold higher levels in cells grown by aerobic respiration than by photosynthesis (Orlando, 1962); therefore he suggested that it may play a role in the aerobic respiratory pathway. Meyer and coworkers were able to purify enough cytochrome  $c_{554}$  from photosynthetic cultures to perform amino acid sequencing (Meyer and Cusanovich, 1985). Beside its relatively high expression level during photosynthetic growth, the protein sequence analysis indicated that there is no similarity between cytochrome  $c_{554}$  and the mammalian cytochrome  $c$ , therefore it may not be the substrate for the  $aa_3$  oxidase.

#### **4.3.1.2 Cytochrome $c_2$**

Cytochrome  $c_2$  is a well-studied cytochrome that is a bacterial homologue of mitochondrial cytochrome  $c$  (Rios-Velazquez *et al.*, 2001). It is a soluble component of photosynthetic and aerobic respiratory electron transfer in *Rhodobacter sphaeroides*; it functions as a mobile periplasmic redox carrier (Prince *et al.*, 1975). In cells grown



chemoheterotrophically with high oxygen tensions, cytochrome  $c_2$  has been thought to transfer electrons from the membrane-bound cytochrome  $bc_1$  complex to a terminal cytochrome  $aa_3$  oxidase (Gennis *et al.*, 1982). Under photoheterotrophic conditions, cytochrome  $c_2$  has been considered to complete the cyclic photosynthetic chain by transferring electrons from the cytochrome  $bc_1$  complex to the oxidized reaction center (Prince *et al.*, 1974). It has an absorption maxima of 550 nm, so it is also known as cytochrome  $c_{550}$ .

The crystal structure of cytochrome  $c_2$  shows that a number of lysine side chains are found on the front face of the protein close to the heme edge. These lysine residues corresponding to Lys 8, 13, 72, 73, 86 and 87 of horse cytochrome  $c$  that are found to be important for interacting with its electron transfer partners (Smith *et al.*, 1977; Ferguson-Miller *et al.*, 1978): the *Rhodobacter sphaeroides* cytochrome  $c_2$  does not have the counterparts of the most critical lysines, Lys 13 and Lys 72 (Figure 1.6). Although *Rhodobacter sphaeroides* cytochrome  $c_2$  is acidic overall, the protein itself is a dipole, with most of the positively charged residues located at the front surface (Koppenol *et al.*, 1978), where the heme edge is exposed. Cytochrome  $c_2$  has been found to use this positively charged face to interact with its physiological partners (Long *et al.*, 1989).

The expression levels of *Rhodobacter sphaeroides* cytochrome  $c_2$  have been found to be approximately four to seven fold higher under phototrophic growth conditions than aerobic growth (Brandner *et al.*, 1989) suggesting a more important role in photosynthetic electron transfer. In a recent study Daldal and coworkers demonstrated that cytochrome  $c_2$  is able to carry electrons efficiently from the  $bc_1$  complex to either the cytochrome  $cbb_3$  oxidase or the cytochrome  $aa_3$  oxidase during respiratory growth of

*Rhodobacter sphaeroides* (Daldal *et al.*, 2001), but an earlier study involving deletion of the cytochrome  $c_2$  gene showed no obvious effect on the cell's aerobic growth (Donohue *et al.*, 1988; Rott and Donohue, 1990). This evidence argues against the physiological involvement of cytochrome  $c_2$  in mediating electron transfer to the  $aa_3$  oxidase.

#### **4.3.1.3 Isocytochrome $c_2$**

Isocytochrome  $c_2$  is another periplasmic redox carrier. It is about 14 kDa and highly homologous to cytochrome  $c_2$ . It has a redox potential of 294 mV. Despite an extensive analysis of photosynthetic membrane function in *Rhodobacter sphaeroides*, the potential for isocytochrome  $c_2$  to serve as an alternative electron donor to reaction center complexes was not uncovered until a cytochrome  $c_2$  deficient mutant was made. This mutation showed an increase in isocytochrome  $c_2$  in the absence of cytochrome  $c_2$  (Rott and Donohue, 1990). Although there is no evidence that isocytochrome  $c_2$  is involved in electron transfer to the  $aa_3$  oxidase, being structurally related to bovine cytochrome  $c$  and having a high redox potential that is close to the mitochondrial one make it a possible electron donor to the  $aa_3$  oxidase. However, it too lacks the most critical lysines for that function.

#### **4.3.1.4 Cytochrome $c'$**

Cytochromes  $c'$  are predominantly high-spin cytochromes (Maltempo *et al.*, 1974) with heme covalently bound to the peptide chain, as in all other  $c$ -type cytochromes. Most cytochromes  $c'$  have been isolated in a dimeric form, with molecular weights in the range of 28-30 kilodaltons (Cusanovich, 1971).

A number of cytochromes *c'* have been crystallized from several strains (Weber *et al.*, 1980; Yasui *et al.*, 1992), including *Rhodobacter capsulatus* (Tahirov *et al.*, 1996), a strain closely related to *Rhodobacter sphaeroides*. Although cytochrome *c'* from different bacteria show very little sequence similarity, X-ray crystallography indicates that the tertiary structure is conserved in all the known structures. Despite widespread occurrence and the fact that the structure is conserved, the functional roles of cytochrome *c'* remain unknown.

The redox potential of cytochrome *c'* is about 30 mV at pH 7.0, much lower than that of mitochondrial cytochrome *c* (Meyer and Cusanovich, 1985). The redox potential and the fact that the expression levels of cytochrome *c'* during the aerobic growth are very low suggest that it is not the substrate for the *aa*<sub>3</sub>-type oxidase.

#### 4.3.1.5 A diheme cytochrome

These proteins have not received as much attention as have high-potential cytochromes and no sequences had been reported until recently (Devereese *et al.*, 2000). These low-redox potential cytochromes have been reported in a number of purple phototrophic bacteria. In *Rhodobacter sphaeroides* these cytochromes have two heme-binding sites per 126 residues (Vandenberghe *et al.*, 1998). One of the heme-binding sites is located near the N-terminus and the other one more distinctly near the C-terminus separated by 101 residues, and the conserved histidines and methionines are located between the two hemes.

In *Rhodobacter sphaeroides* this type of cytochrome *c* is encoded by gene *cycG* and located in the same operon as cytochrome *c*<sub>554</sub> and is transcriptionally linked to it;

and even the discovery of this diheme cytochrome occurred during the process of cloning cytochrome *c*<sub>554</sub> (Flory and Donohue, 1995). This protein has not been purified and its spectroscopic, structural and functional properties are unknown.

#### **4.3.1.6 Cytochrome *c*<sub>551</sub>**

*Rhodobacter sphaeroides* cytochrome *c*<sub>551</sub> is a 16 kDa protein, which contains two hemes (Meyer and Cusanovich, 1985). One heme is near the N-terminus and the other is near the C-terminus. It consists of 138 residues and it has a high redox potential (254 mV), and has two histidines ligands for each heme. This type of cytochrome has not been found in any other species so far, and the sequence shows that it is not related to any known cytochrome (Van Beeumen, 1991). It is found in small amounts in *Rhodobacter sphaeroides* and its function is not known, and it is unlikely to be the physiological substrate for the *aa*<sub>3</sub> oxidase.

#### **4.3.1.7 *Sphaeroides* heme proteins (SHP)**

*Rhodobacter sphaeroides* produces a heme protein (SHP), which is an unusual green *c*-type cytochrome capable of transiently binding oxygen during autooxidation. The absorption maxima for the reduced form are at 548 nm for the  $\alpha$  peak and 429 for the Soret peak. The absorption peak changes in different buffers, reflecting the binding of small ligands to the high spin heme (Meyer and Cusanovich, 1985).

The three-dimensional structures of SHP in the oxidized state at 1.82 Å, the reduced state at 2.1 Å, the oxidized molecule liganded with cyanide at 1.9 Å and the reduced molecule liganded with nitric oxide at 2.2 Å resolution have been solved (Leys *et*

*al.*, 2000). The SHP structure represents a new variation of the cytochrome *c* fold. The oxidized state reveals a novel sixth ligand, Asn, which moves away from the iron upon reduction or when small molecules bind. The distal side of the heme has a striking resemblance to other heme proteins that bind gaseous compounds.

The expression level of this type of cytochrome *c* during respiration is very low; therefore it is unlikely to be the physiological substrate for cytochrome *c* oxidase.

#### **4.3.2 Membrane bound cytochromes *c* of *Rhodobacter sphaeroides* and Related Bacteria**

Until recently no membrane-bound cytochrome *c* had been purified or had its gene cloned from *Rhodobacter sphaeroides*, but some had been discovered and characterized earlier in *Paracoccus denitrificans* (cytochrome *c*<sub>552</sub>), a species that is closely related to *Rhodobacter sphaeroides* (Turba *et al.*, 1995), and in *Rhodobacter capsulatus* cytochrome *c*<sub>γ</sub> (Jenney and Daldal, 1993)

##### **4.3.2.1 Cytochrome *c*<sub>552</sub>**

Among the *c*-type cytochromes found in *Paracoccus denitrificans* the membrane-bound cytochrome *c*<sub>552</sub> is most likely the mediator between cytochrome *bc*<sub>1</sub> and cytochrome *aa*<sub>3</sub>. Under certain conditions of solubilization and purification, a supercomplex containing these complexes together with cytochrome *c*<sub>552</sub> can be isolated (Berry and Trumpower, 1985; Haltia *et al.*, 1988). The high internal electron transfer rates in this complex indicates the functional importance of cytochrome *c*<sub>552</sub>.

The gene for cytochrome  $c_{552}$  (*cycM*) has been cloned and sequenced (Turba *et al.*, 1995). The N-terminal portion of cytochrome  $c_{552}$  contains a hydrophobic segment which functions as a membrane anchor, while the C-terminal part is similar to that of mitochondrial cytochrome *c*. The primary structure shows the presence of many acidic residues resulting in an unusually low isoelectric point. The crystal structure of the soluble domain of the membrane bound cytochrome  $c_{552}$  from *Paracoccus denitrificans* was determined at 1.5 Å for the oxidized and at 1.4 Å for the reduced state (Harrenga *et al.*, 2000). In general, the structure has the same features as known eukaryotic cytochromes *c*. However; cytochrome  $c_{552}$  has a strongly negatively charged surface on the back side, and a smaller positively charged area on the front side around the solvent-exposed heme group but this area contains most of the lysines that are important in the oxidase binding (Lys 8,13,72 and 86). Reduction of the oxidized crystals does not influence the conformation of the protein, in contrast to eukaryotic cytochrome *c*, although the oxidized form appears to be more flexible than the reduced one.

The isolation of the complex between  $bc_1$ , cytochrome  $c_{552}$  and  $aa_3$  oxidase (Berry and Trumpower, 1985), along with the similarity to the mammalian cytochrome *c* as well as high expression levels during aerobic growth, suggest the importance of this membrane-bound cytochrome *c* in shuttling electrons from the  $bc_1$  complex to the  $aa_3$  oxidase, perhaps in a solid-state mode where no diffusion is required (Ferguson-Miller *et al.*, 1986; Berry and Trumpower, 1985).

#### 4.3.2.2 Cytochrome $c_y$

In *Rhodobacter capsulatus*, a species that is closely related to *Rhodobacter sphaeroides* but without an  $aa_3$ -type oxidase, there are two electron carriers that transfer electrons from the  $bc_1$  complex to the cytochrome  $cbb_3$  oxidase; these are a soluble cytochrome  $c_2$  and a membrane-bound cytochrome  $c_y$  (Gray *et al.*, 1994). Until recently it was thought that *Rhodobacter sphaeroides* lacked cytochrome  $c_y$ , but a gene highly homologous to *Rhodobacter capsulatus* *cycY* (encoding cytochrome  $c_y$ ) was identified in *Rhodobacter sphaeroides* (Zeillstra-Ryalls and Kaplan, 1995). Daldal and coworkers found the polypeptide corresponding to *Rhodobacter sphaeroides* cytochrome  $c_y$  and characterized its functional properties (Myllykallio *et al.*, 1999). Their study shows that cytochrome  $c_y$  is a membrane-attached electron carrier that participates only in respiratory electron transfer, unlike in the *Rhodobacter capsulatus* counterpart, which is functional for both photosynthetic and respiratory electron transport. Furthermore, using chimeric cytochrome  $c_y$  constructs, they established that the different photosynthetic capabilities of these cytochromes are related, at least partly, to their redox active domains as well as the length of the flexible attachment region between the soluble part and the membrane domain.

In a recent study, Daldal and coworkers demonstrated that cytochrome  $c_y$  is able to carry electrons efficiently from the  $bc_1$  complex to either cytochrome  $cbb_3$  oxidase or cytochrome  $aa_3$  oxidase during respiratory growth of *Rhodobacter sphaeroides* (Daldal *et al.*, 2001). Results from these studies and the high homology between cytochrome  $c_y$  and cytochrome  $c_{552}$  of *Paracoccus denitrificans* make  $c_y$  a strong candidate for the physiological substrate of  $aa_3$  oxidase.

#### 4.4 Summary

In bacteria, including *Rhodobacter sphaeroides*, several aerobic and anaerobic electron transfer chains are used under different growth conditions. The multiple electron transfer chains create a physiological need to transfer electrons to their appropriate destinations. Thus in these bacteria, unlike mitochondria which have one conserved cytochrome *c*, multiple cytochromes *c* function in parallel as electron carriers.

In *Rhodobacter sphaeroides* a number of the *c*-type cytochromes are expressed at different levels during photosynthetic and aerobic growth. This may suggest their involvement in photosynthesis and aerobic respiration, respectively. However, mutagenesis studies of some of the cytochromes *c* under both growth conditions argue against any simplistic assignment, and the question of who is the physiological substrate of the *aa*<sub>3</sub> oxidase remains. However most of the evidence points to cytochrome *c*<sub>γ</sub> as the likely the substrate, since it participates only in the respiratory electron transfer (Myllykallio *et al.*, 1999) and it is highly homologous to the *c*<sub>552</sub> of a closely related species, *Paracoccus denitrificans*, which is involved in electron transfer to *aa*<sub>3</sub> oxidase in that bacterium.

It therefore seems that, although the *Rhodobacter* species simultaneously expresses several highly homologous electron carriers, they also have endowed them with pronounced specificity towards their redox partners to direct electron flow efficiently to the different branches of their electron transfer chains, therefore maximally supporting their physiological needs.



Knowing the right substrate is very important for understanding the binding and kinetics and for obtaining the correct complex between the enzyme and the substrate that could be used for crystallization.

## 5. Importance and Classification of Membrane Lipids

### 5.1 Importance of Membrane Lipids

The most striking feature of membrane lipids is their enormous diversity. Although the multiple roles of lipids are well known, the reason for this diversity is not clear. Certainly a major role of membrane lipids is to form the bilayer matrix with which membrane proteins interact (Gennis, 1988).

Biological protein/lipid membranes partition cells and organelles into separate aqueous compartments with unique environments. The hydrophobic bilayer phase supports a wide range of important metabolic processes, including energy transduction, solute transport, protein transport, signal transduction and motility (McAuley *et al.*, 1999).

Although many studies have been done investigating membrane lipids, still the importance of those lipids in the structure of membrane proteins was underestimated until recent crystal structures showed that lipids are resolved in the crystal structure from bacterial and mammalian enzymes even after the processes of protein isolation and purification (Yoshikawa, 1998; Luecke *et al.*, 1999). These results imply that lipids may play an integral role in membrane protein structures, stabilizing a homogenous conformation at the molecular level (Garavito and Ferguson-Miller, 2001). The X-ray structure of *Rhodobacter sphaeroides* oxidase dramatically illustrates the critical role of lipids, showing six phospholipids deeply embedded in the subunits (Figure 1.4). Since one of my goals is to establish conditions for crystallization of cytochrome *c* oxidase, I did lipid analyses of the membranes of *Rhodobacter sphaeroides* as well as lipid analyses for the purified enzyme at different purification levels and compared the lipid composition at

each stage. Many of the major lipid classes were found in *Rhodobacter sphaeroides* membranes and remained associated with cytochrome *c* oxidase at different ratios through the purification and crystallization.

The major lipid classes and their involvement in *Rhodobacter sphaeroides* membrane structures will be discussed below.

### **5.1.1 Glycerophospholipids**

The glycerophospholipids are the most commonly found membrane lipids in eukaryotes and prokaryotes. One of the glycerol hydroxyls is linked to a polar phosphate-containing group and the other two hydroxyls are linked to fatty acid chains giving it the required amphipathic character.

Most phosphoglycerides have the phosphate at the sn-3 position of glycerol. The phosphate is usually linked to one of the several hydrophilic groups such as choline, ethanolamine, inositol, serine and glycerol to form phosphatidyl choline (PC), phosphatidyl ethanolamine (PE), phosphatidylinositol (PI), phosphatidylserine (PS) and phosphatidylglycerol (PG) respectively. Phosphatidylcholine is a major component in animal cell membranes, whereas phosphatidylethanolamine is often a major component in bacterial membranes.

### **5.1.2 Phosphosphingolipids**

Phosphosphingolipids are not derived from glycerol like other phospholipids in membranes. Instead, the backbone in phosphosphingolipids is sphingosine, an amino alcohol that contains a long unsaturated hydrocarbon chain. Sphingomyelin or ceramide 1-

phosphorylcholine is a phosphosphingolipid that is widely found in animal cell plasma membranes. Other phosphosphingolipids are also found in different quantities in animal cells such as ceramide 1-phosphorylethanolamine and ceramide 1-phosphorylinositol. Phosphosphingolipids in general are rarely found in plants or bacteria.

### **5.1.3 Glycosphingolipids**

This type of lipid has a glycosidic linkage to the terminal hydroxyl of ceramide. The classification scheme is according to the carbohydrate moiety, which can range from a single sugar to very complex polymers. The glycosphingolipids are found on the outer surface of animal cell plasma membranes and form an important components of lipid “rafts” domains involved in signaling (Xu *et al.*, 2001). Monogalactosyl ceramide is the largest single component of the myelin sheath of nerves. In some cases, the glycosphingolipids are present in intracellular membranes rather than in the plasma membrane. In erythrocyte membranes the glycosphingolipids carry blood group antigens (Gennis, 1988). Glycosphingolipids are not found in bacteria.

### **5.1.4 Glycoglycerolipids**

Glycoglycerolipids are polar lipids in which the sn-3 position of glycerol forms a glycosidic link to a carbohydrate such as galactose. Glycoglycerolipids are predominant in the chloroplast membrane and are also found in substantial quantities in blue-green algae and bacteria. The main types of lipids in this class are: monogalactosyldiglyceride (MGD), digalactosyl diglyceride (DGD) and sulfoquinovosyl diacylglycerol (SL).

Monoglactosyl diacylglycerol has been termed “the most abundant polar lipid in nature” since it comprises half of the lipid in chloroplast thylakoid membrane.

### **5.1.5 Sterols**

Sterols are found in many plant, animal and microbial membranes. Cholesterol is the most commonly found sterol. This molecule is a compact, rigid hydrophobic entity with a polar hydroxyl group. Cholesterol is found in animal cell plasma membranes, lysosomes, endosomes and Golgi. It forms 30% of the mass of the membrane lipids of many animal cell plasma membranes and appears to play an important role in forming “rafts”, membrane domains involved in signaling (Xu and London, 2000; Barenholz, 2002). Other sterols such as sitosterol and stigmasterol are found in higher plants whereas hopanoids, which are steroid-like lipids, are found in bacteria and some plants.

## **5.2 Membrane lipids in *Rhodobacter sphaeroides***

The membranes of *Rhodobacter sphaeroides* are commonly known to contain two classes of polar lipids: phospholipids and nonphosphorous glycolipids including sulfolipids. In addition, ornithine-containing lipids as well as betaine lipids can be present in substantial amounts (Benning *et al.*, 1995). The growth conditions can affect the lipid composition, and the abundance of polar lipids as well as other lipids is highly variable under respiratory or photosynthetic growth, although results of lipid analysis, in our lab, from cells grown photosynthetically and under high oxygen showed almost the same lipid composition under each growth conditions.

### 5.2.1 Phospholipids

The structure of phospholipids that are found in *Rhodobacter sphaeroides* is characterized by a 1,2-diacyl-3-phospho-sn-glycerol, also known as the phosphatidyl moiety, and a variable headgroup attached to the phosphate.

Under different growth conditions the membranes of *Rhodobacter sphaeroides* contain substantial amounts of phosphatidylethanolamine. Four phosphatidylethanolamines and two other unidentified phospholipids were clearly identified in the crystal structure of cytochrome *c* oxidase from *Rhodobacter sphaeroides* (Svensson *et al.*, 2002) and five phosphatidylethanolamines were observed in the crystal structure of the bovine heart cytochrome *c* oxidase (Yoshikawa *et al.*, 1998).

Phosphatidylglycerol is found in significant amounts under photosynthetic growth conditions, and also found under respiratory growth conditions in variable amounts. The crystal structure of bovine heart cytochrome *c* oxidase identified three phosphatidylglycerol associated with the enzyme. Diphosphatidylglycerols, also known as cardiolipins, are present in high levels in mitochondria and strongly associated with cytochrome oxidase such that their removal can cause loss of activity. They are also found in *Rhodobacter sphaeroides* membranes.

Phosphatidylcholine is rarely found in membranes of bacteria; however, it is present in many species of purple nonsulfur bacteria including *Rhodobacter sphaeroides*. The presence of phosphatidylinositol is not very common in bacteria, and it is only well studied in the photosynthetic bacteria *Chloroflexus aurantiacus*.

### 5.2.2 Glycolipids

Typical glycolipids found in bacterial membranes do not contain phosphorus and are characterized by a 1,2-diacyl-sn-glycerol moiety to which a mono- or a disaccharide is attached at the sn-3 position.

Under different growth conditions, *Rhodobacter sphaeroides* membranes contain different types as well as different amounts of glycolipids. The sulfolipid sulfoquinovosyldiacylglycerol in *Rhodobacter sphaeroides* is identical to that of the sulfolipid present in chloroplasts of higher plants, with the exception of the fatty acid substituents. The two major fatty acids found in the sulfolipids in higher plants are palmitic and linolenic, whereas in *Rhodobacter sphaeroides* vaccenic acid, a monosaturated 18-carbon fatty acid commonly found in bacteria (18:1, cis $\Delta$ 11) is substituted for the linolenic fatty acid (Gage *et al.*, 1992). For a long time it was thought that this sulfolipid was important for photosynthesis, but a study by Benning and colleagues shows that it is not required for photosynthetic electron transport in *Rhodobacter sphaeroides* but enhances growth under phosphate limitation. It represents between 2% and 16% of polar lipids depending on the growth conditions (Benning *et al.*, 1993).

Several glycolipids containing galactose have been reported in *Rhodobacter sphaeroides* membranes. Monogalactosyldiacylglycerol (MGD) and  $\beta$ -digalactosyldiacylglycerol (DGD) are the most common ones, especially under phosphate-limited growth (Benning *et al.*, 1995).

### **5.2.3 Other Polar Lipids**

These are unusual lipids which cannot be classified as phospholipids or glycolipids, or which are only conditionally synthesized in some species including *Rhodobacter sphaeroides*.

#### **5.2.3.1 Ornithine Lipids**

Ornithine lipids are phosphorus-free, ornithine-containing membrane lipids. The characteristic feature of these lipids is the long chain 3-hydroxy fatty acid attached via an amide bond to the  $\alpha$ -amino group of ornithine. A second long-chain fatty acid is esterified to the 3-hydroxy group of the first fatty acid.

#### **5.2.3.2 Betaine Lipids**

Betaine lipids were previously assumed to be restricted to algae and lower plants (Siegenthaler and Murata, 1998). Recently this lipid was discovered in *Rhodobacter sphaeroides* cells that are grown under phosphate limitation (Benning *et al.*, 1995).

#### **5.2.3.3 Xenobiotic Lipids**

Xenobiotic lipids are synthesized in *Rhodobacter sphaeroides* using unnatural chemicals as head groups of the buffer substance Tris (Donohue *et al.*, 1982). The synthesis of this xenobiotic lipid phosphatidyl-Tris is a good example for the remarkable metabolic flexibility of bacteria and their ability to tolerate drastic changes in membrane lipid composition.



#### **5.2.4 Fatty Acids Composition in *Rhodobacter sphaeroides***

Saturated and monounsaturated fatty acids are the dominant components in *Rhodobacter* species. Sixteen and eighteen-carbon fatty acid chains are the majority in this species, whereas fatty acids shorter than fifteen-carbon are present in specific strains and in trace amounts below 0.1% of the total fatty acids (Imhoff, 1991). Imhoff's study showed that *Rhodobacter sphaeroides* fatty acid composition as follows: more than 70% C18:1, 11-16% C18:0, 4-8% C16:0, 1-2% C16:1 and traces of C14:0, C14:1, C17:0 and C20:1.

#### **5.3 Factors Affecting Membrane Lipid Composition**

The composition of the membrane lipids in bacteria is highly affected by two major factors: the subcellular location of the lipids and the growth conditions of the bacterial cells.

Polar lipids are synthesized by enzymes that are associated with the cytoplasmic membrane. Differences in the polar lipid composition in the cytoplasmic membranes, intracytoplasmic membranes and outer membranes might be expected in bacterial species as in eukaryotes, but some data for *Rhodobacter sphaeroides* suggested that there is no major differences in polar lipid composition of the cytoplasmic membrane and the intracytoplasmic membrane (Siegenthaler and Murata, 1998).

In *Rhodobacter sphaeroides* as well as in many other bacterial species, the membrane lipid composition is affected by different growth conditions such as oxygen concentration, light intensity, phosphate limitation, and addition of medium such as Tris

buffer and salt concentration. The effect of chemotrophic versus phototrophic growth is controversial; some studies showed no difference in lipid composition between these two growth conditions, whereas another study suggested that the relative amounts of phosphatidylethanolamine and phosphatidylglycerol increase with increasing light intensity (Siegenthaler and Murata, 1998).

Phosphate-limiting growth conditions result in the accumulation of novel lipids in *Rhodobacter sphaeroides*. Under these conditions, the relative amount of phospholipids decreases, but that of sulfoquinovosyl diacylglycerol and ornithine lipid increases. In addition monogalactosyldiacylglycerol as well as the betaine lipid accumulate (Benning *et al.*, 1995). The observed changes in lipid composition can be viewed as a requirement of the cell to maintain certain ratios of negative to positive charge, and bilayer to non-bilayer forming lipids, in order to provide a functional membrane.

In our studies, unusual growth conditions were used to maximize respiration versus photosynthesis, including high oxygen concentration, high pH and minimal carbon sources. These factors could affect the lipid composition in the membranes, therefore we analyzed our membranes and compared them with those obtained under photosynthetic conditions.

## 6. Statement of Problem

Cytochrome *c* oxidase, the terminal enzyme in the respiratory chain, is involved in electron transfer, which is coupled to proton pumping across the membrane, generating a membrane potential and synthesis of ATP. The overall goal of the research in our laboratory is to elucidate the mechanism and regulation of energy conserving electron transfer in cytochrome oxidase from *Rhodobacter sphaeroides*, which is highly homologous to the mammalian oxidase, but simpler and mutationally accessible.

To understand the molecular mechanism of electron transfer and proton pumping, crystal structures at high resolution are required. My goal was to optimize conditions for achieving high resolution 3-dimensional crystal structure for wild type and different mutant forms of *Rhodobacter sphaeroides* cytochrome *c* oxidase. The structure of oxidase mutants may help us to know how residues in the vicinity of the reactive center and in the proton pathways are involved in the functions of the enzyme.

The first approach was to produce the enzyme and isolate it with the purity, stability and in the quantities that are demanded for structural analysis. Our initial hypothesis was that the type and purity of detergent and the purity and the homogeneity of the protein were critical factors in obtaining good crystals. Using new and very pure detergents from the Anatrace company designed for membrane protein crystallization, I attempted to crystallize the *Rhodobacter sphaeroides* enzyme, both wild type and stable mutants such as H333N, a Cu<sub>B</sub> ligand mutant whose alteration inhibits the activity of the enzyme without destabilizing the structure. In order to reach this goal I tried a variety of purification and crystallization conditions.

The crystal structure of several membrane proteins were reported at very high resolution and showed that lipids are associated with the protein subunits, suggesting the importance of lipids in the protein structure. This observation lead to a new hypothesis, that in order to obtain high resolution x-ray structure, lipids may need to be retained. In order to investigate this hypothesis and to standardize our crystallization procedure, in my second project I attempted to define how the various steps of purification affected the lipid contents of *Rhodobacter sphaeroides* cytochrome *c* oxidase and its ability to form good crystals.

A further hypothesis that was considered was that, obtaining good crystals may also depend on the size of the protein domain external to the membrane. To address this idea, I attempted to develop a method to allow the crystallization of the oxidase with its soluble substrate, cytochrome *c*<sub>2</sub>, bound. One of the efforts in our lab in collaboration with Dr. Leslie Kuhn in the Biochemistry Department and Dr. Victoria Roberts at Scripps, was to apply computational and mutational methods to assist in accurately defining the binding site between cytochrome *c* and cytochrome *c* oxidase. With that information my goal was to redesign *Rhodobacter sphaeroides* cytochrome *c*<sub>2</sub> to produce a better binding substrate to maximize the chances of producing a stable complex that may be useful for crystallization. This was done by mutation to lysines of specific residues at the binding site, residues 13 and 72, which are proposed to be important for binding and are lacking in cytochrome *c*<sub>2</sub>. In addition, I attempted to produce covalent cytochrome *c*-cytochrome oxidase complexes by introduction of sulfhydryl groups at the binding site of both cytochrome *c* and cytochrome *c* oxidase to enable cross-linking between the protein.

**CHAPTER II**  
**PURIFICATION AND CRYSTALLIZATION OF *RHODOBACTER***  
***SPHAEROIDES* CYTOCHROME *C* OXIDASE**

## INTRODUCTION

The cytochrome *c* oxidases are members of a large superfamily of heme and copper containing terminal oxidases. Members of this superfamily, both eukaryotic and prokaryotic, are redox driven proton pumps that couple the reduction of molecular oxygen to translocation of protons across the membrane. The active transport of protons generates a proton and voltage gradient that is converted to more useful energy forms, via energy conserving systems such as ATP synthase, or to heat by uncoupling proteins.

During the past 15 years, many site-directed mutagenesis studies combined with spectroscopy have been performed to reveal the structure-function relationships in bacterial cytochrome *c* oxidases, which serve as models for the this key mitochondrial enzyme. In spite of all these efforts, the mechanism of energy transduction involving the coupling of proton translocation and electron transfer is not understood at a molecular level. As a prerequisite for understanding this mechanism, the crystal structure at high resolution of many different states of the oxidase is required. In this chapter we report several strategies to purify and characterize the wild type enzyme and the H333N mutant, which is a ligand of the copper atom at the binding site where oxygen is reduced to water. This mutant is completely inactive without global disruption of the structure. It is a good candidate for crystallization because its structure may help us to know how changes of residues in the vicinity of the reactive center could affect the function of the enzyme. We also show the effect of different detergents on the stability and crystallization of the enzyme. Finally, we show crystallization results using different purification protocols and crystallization conditions.

## **MATERIALS AND METHODS**

### **Growth of *Rhodobacter sphaeroides***

Cells were grown on Sistrom's plates with 50 µg/ml spectinomycin, 50µg/ml streptomycin and 1 µg/ml tetracycline pH 7.0 at 30°C for 3 days. Cells were inoculated in 6X100 ml flasks of Sistrom's media with the same antibiotics and grown for two days at 30°C. These starter cultures were used to inoculate 12 Fernbach flasks with 800 ml Sistrom's media containing 1 µg/ml tetracycline. The cultures grew at 30°C with vigorous swirling in New Brunswick shakers for two days or until the absorbance reading at 660 nm was about 1.7, which indicates that the cells are near the end of the exponential phase. Cells were harvested by centrifugation in a GS-3 rotor at 14,000x g for 20 minutes at 4°C. The pellets that contained whole cells were saved at -80°C.

### **Membrane preparation**

Cells were resuspended by gentle swirling in 50 mM KH<sub>2</sub>PO<sub>4</sub> and 1 mM EDTA with 50 µg/ml DNase I at pH 6.5, then homogenized and broken with two passages through the French press at 18,000 psi. Whole cells and debris were removed by centrifugation at 20,000 x g for 30 minutes at 4°C. The supernatant was centrifuged at 200,000x g for 1.5 hour in the ultracentrifuge. The pellet was frozen and stored at -80°C without detergent; this step is critical for crystallization. The pellets were resuspended in six volumes of 10 mM Tris, 40 mM KCl, 1% lauryl maltoside final concentration, at pH 8.0.

The mixture was homogenized and stirred at 4°C for 20 minutes. The sample was centrifuged again at 200,000x g for 1 hour at 4°C and the supernatant containing cytochrome oxidase was used immediately for chromatography.

## **Protein Purification**

### **Protocol 1:**

#### **Ni<sup>2+</sup>-NTA affinity chromatography**

This is a rapid and highly efficient affinity purification scheme using Ni-nitrilotriacetic acid agarose and a six histidine-tag fused to subunit I of the oxidase. This improved purification technique was developed for the *aa3*-type cytochrome oxidase from *Rhodobacter sphaeroides* with the aim of providing a convenient protocol to obtain a sufficient supply of the enzyme for experiments (Mitchell and Gennis, 1995).

The amount of cytochrome oxidase present in the membrane preparation is estimated spectroscopically by taking reduced minus oxidized difference spectra on the solubilized membranes. The Ni<sup>2+</sup>-NTA resin was added at a ratio of 0.5ml resin for 1mg enzyme. Imidazole (10mM final concentration) was also added to inhibit non-specific binding and stirred for 1 hour at 4°C for binding. The mixture was loaded onto a gravity-flow column and washed with 5 column volumes of 10 mM Tris-HCl pH, 40 mM KCl, 0.1% lauryl maltoside and 10 mM imidazole pH 8.0. This was followed by 5 column volumes of 20 mM imidazole, 200 mM KCl, 10 mM Tris-HCl and 0.1% lauryl maltoside pH 8.0. Then the imidazole was washed away with 5 column volumes of 10 mM Tris, 40 mM KCl and 0.1% lauryl maltoside pH 8.0. The sample was eluted with 100 mM histidine, 10 mM Tris-HCl, 40 mM KCl and 0.1% lauryl maltoside pH 8.0, then



concentrated with a Centricon concentrator (molecular weight cut off 50,000). The contaminating histidine-nickel complex was washed away with three volumes of 10 mM Tris-HCl, 40 mM KCl and 0.1 % lauryl maltoside pH 8.0.

### **FPLC-DEAE Ion Exchange Chromatography**

Approximately 15 mg of  $\text{Ni}^{2+}$ -NTA purified cytochrome oxidase was loaded onto two tandem DEAE-5PW columns (8 mm x 7.5 cm, TosoHaas) connected to an FPLC system. The columns were pre-equilibrated with 10 mM  $\text{KH}_2\text{PO}_4$ , 1 mM EDTA and 0.2% lauryl maltoside pH 7.5. The enzyme was eluted with a 45 ml of linear gradient from 0-1M KCl in the same buffer at a flow rate of 0.5 ml / min. One ml fractions were collected and the enzyme concentration was determined from an absolute reduced spectrum measured with a Perkin-Elmer spectrophotometer from 400-700 nm, the extinction coefficient is  $\Delta E_{(606-640 \text{ nm})} = 40 \text{ cm}^{-1} \text{ mM}^{-1}$ . The purified enzyme was concentrated and stored at  $-80^\circ\text{C}$ .

### **Protocol 2:**

#### **Mono Q Anion Exchange Chromatography**

Approximately 15 ml of sample containing 10-20 mg oxidase, purified with  $\text{Ni}^{2+}$ -NTA affinity column similarly to the first protocol, was loaded onto the MonoQ column (HR 10/ 10). The column was pre-equilibrated, before loading the sample, with 40 ml of 10 mM Tris, 0.05% lauryl maltoside, pH 8.0, then with 80 ml of 10 mM Tris, 0.5 M KCl, 0.05% lauryl maltoside, pH 8.0 and finally with 40 ml of 10 mM Tris, 0.05% lauryl maltoside, pH 8.0 at a rate of 4 ml/ min. The sample was loaded at a rate of 2ml/ min.

The protein was eluted with 20-25 column volumes of 0-0.5 M KCl gradient in the same buffer. The sample was washed and concentrated in 10 mM Tris and 0.24% decylmaltoside pH 8.0.

### **Protein Assay**

BCA (bicinchoninic acid) protein assay system from Pierce was used to determine the total protein contents in the sample (Smith *et al.*, 1985). Bovine serum albumin (BSA) was used as the standard. BSA and all the oxidase samples were diluted with 10mM Tris, 40mM KCl, 0.25% deoxycholate, pH 11.2 and then mixed with 2ml working buffer (a mix of reagent A (1% BCA- $\text{Na}_2$ , 2%  $\text{Na}_2\text{-CO}_3\cdot\text{H}_2\text{O}$ , 0.16%  $\text{Na}_2\text{.tartrate}$ , 0.4% NaOH, 0.95%  $\text{NaHCO}_3$ , pH11.25) and reagent B (4%  $\text{CuSO}_4\cdot 5\text{ H}_2\text{O}$  in dd $\text{H}_2\text{O}$ ) in 50:1 ratio), followed by incubation at 60°C for 30 min. The absorbance at 562 nm for the samples was measured on Perkin-Elmer  $\lambda$  40P-UV/visible spectrometer.

### **Visible spectra**

Visible spectra for the protein were detected with a Perkin-Elmer  $\lambda$  40P UV-visible spectrophotometer. The protein was diluted in 50 mM  $\text{KH}_2\text{PO}_4$  pH 7.2, 0.1% lauryl maltoside. Samples were scanned from 700 nm to 400 nm and the amount of enzyme was estimate using the extinction coefficient:  $\Delta E_{(606-640\text{ nm})} = 40\text{ cm}^{-1}\text{ mM}^{-1}$  for an absolute spectra of dithionite reduced enzyme, and  $\Delta E_{(606-640\text{ nm})} = 24\text{ cm}^{-1}\text{ mM}^{-1}$  for dithionite reduced minus ferricyanide oxidized difference spectra.

## **SDS-PAGE**

Sodium dodecyl sulfate polyacrylamide gel electrophoresis was used to detect the number of subunits of the protein and the impurities contained in the sample. Approximately 10 µg of protein in sample buffer (25 mM Tris pH 6.5, 40% glycerol, 8% SDS and 0.08% bromophenol blue) was loaded on an 8% acrylamide stacking gel at pH 6.8 and 14% acrylamide separating gel at pH 8.8. The gel was polymerized for 2 hours and run for 1 to 1.5 hours at 200V using a BioRad mini-Protean II apparatus. The gel was then stained with Coomassie blue in 7% glacial acetic acid and 50% methanol, and destained with 7.5% glacial acetic acid. Polypeptide sizes were estimated from low-molecular weight range markers from Bio-Rad.

## **Activity measurement**

Oxygen consumption was measured polarographically using an oxygen electrode at 25°C in 50 mM KH<sub>2</sub>PO<sub>4</sub> pH 6.5 containing 2.8 mM ascorbate, 1.0 mM TMPD (N-N-N'-N' Tetramethyl-p-phenylene diamine) 0.05% LM, 4 mg/ml phospholipids and 30 µM horse heart cytochrome *c*. The turnover number (molecular activity) was calculated as electrons per second per molecule of oxidase.

## **pH-Dependence Assay**

Oxidase activity at different pH values was measured polarographically under the same conditions as the previous protocol but using buffers with different pK values as follows: sodium cacodylate buffer (50 mM) was used for pH ranges of 5.0, 5.2 and 6.0;

potassium phosphate buffer (50 mM) was used for pH 6.5, 7.0 and 7.5; Tris buffer (50mM) was used for pH 7.5, 8.0, 8.5 and 9.0.

### **CO-binding Assay**

The CO-binding ability of the oxidase was measured from the CO difference spectrum of CO bound form minus the reduced form of the oxidase. To prepare CO bound oxidase, the enzyme at a concentration of about 1  $\mu$ M in a solution of 100 mM Tris, pH 8.0, 0.1% LM was reduced with dithionite, and a reduced spectrum was taken. Then 1 ml of CO was bubbled slowly (5min total time) into 1 ml of the dithionite-reduced oxidase at 25°C, and a second spectrum was taken. The CO binding is monitored at 447 nm in the difference spectrum using the extinction coefficient  $\Delta E_{(447-475 \text{ nm})}$  of 80  $\text{mM}^{-1}\text{cm}^{-1}$  (Hosler *et al*, 1992).

### **Detergent Exchange by Gel Filtration**

When exploring crystallization conditions, a variety of detergents need to be tested. The exchange of one detergent for another is therefore an important step in preparation of most membrane proteins for crystallization. A Pharmacia Hi Prep 16/60 Sephacryl S-200 column with fractionation range of 5000- 250,000 molecular weight was connected to a Pharmacia FPLC system and used to exchange detergents. Purified sample was stirred in 0.6% of the detergent of interest and loaded into the Sephacryl column, which was pre-equilibrated with 10 mM Tris-HCl, 40 mM KCl pH 7.5 and 0.2% detergent. The sample was collected with a flow rate of 1 ml/ min and concentrated

using a Centricon concentrator (50,000 M.wt. cut off) by spinning at 2000 x g. The final sample concentration was about 10 mg/ml.

### **Spin column**

Detergent concentration is very critical in crystallizing membrane proteins. Spin column chromatography was used to adjust the detergent concentration. A 3 ml G-75 Sephadex column was pre-equilibrated with 10 mM Tris-HCl, 40 mM KCl pH 7.5 and 0.2% detergent. The column was first partially dried by spinning at 2,000 rpm for 8 minutes to avoid dilution of the sample. After loading the sample (500µl of 10mg/ ml protein solution), the column was centrifuged again at 2,000 rpm for 7 minutes, and the sample was collected and saved for crystallization. During this process, the sample buffer was exchanged for the column buffer, and excess detergent was removed.

### **Thin Layer Chromatography**

The enzyme was checked for the composition of detergents that it contained after gel-filtration and spin column. The protein sample concentration was 10mg/ml. A 20µl sample was added to 75µl methanol/chloroform in a 1:1 ratio. The mixture was vortexed for 30 seconds, spun down at 13000 rpm for 2 minutes and the supernatant was dried and re-dissolved in 40µl chloroform. Then the sample was applied slowly as a small spot to a pre-activated Silica gel plate that had been heated for 3 hours at 120°C (Benning and Somerville, 1992). The solvent system was 130 ml of acetone/ toluene/ water (91:30:8). Then the plate was dried, and stained with  $\alpha$ - naphthol for sugars to determine the position of detergents.

### **Stability of cytochrome *c* oxidase in different detergents**

The enzyme, which was purified in 0.1% lauryl maltoside, was incubated in excess of each of the four detergents to be tested (0.6%), which are lauryl maltoside, decyl maltoside, CYMAL-6 and Empigen. The incubation time was 72 hours at room temperature, or 120 hours at 4°C. Fifty mM Tris-HCl at pH 7.5 was used as buffer. The structural and functional integrity of the enzyme was investigated by spectroscopy and oxygen consumption activity respectively.

### **Melting Temperature Assay**

Cytochrome *c* oxidase denaturation experiments were conducted as another way of measuring the stability of the enzyme in different detergents. The enzyme was purified in dodecyl maltoside and decyl maltoside separately. Approximately 1.7  $\mu$ M of the sample in 50 mM potassium phosphate buffer (400 $\mu$ l total volume) was used. Denaturation was monitored from 30°C to 80°C, with the rate of 1°C/ min, by measuring the absorbance at 420 nm in 0.5 ml quartz cuvettes (path length = 1.0 cm), using Beckman DU650 spectrophotometer equipped with a Peltier heating system. Spectra for samples were recorded and the transition phase was determined.

### **Crystallization**

The hanging drop vapor diffusion method was used in which 2  $\mu$ l of 10-20 mg/ ml protein was mixed with 2  $\mu$ l of reservoir solutions on a well-siliconized cover slips and inverted over the wells that contain reservoir solutions (from Hampton company) such as PEG (polyethylene glycol) and ammonium sulfate which function as precipitants. The

wells are covered and sealed using vacuum grease, and incubated at constant temperature (room temperature and 4°C). Water vapor leaves the less concentrated drop and enters the reservoir. The drop components concentrate as the volume decreases. This continues until the drop and the reservoir vapor pressure are equilibrated. During the equilibration period as the protein very slowly becomes insoluble and leaves the solution, crystals will form.

The other protocol that we adopted from the Swedish group who succeeded in crystallizing *Rhodobacter sphaeroides* oxidase at 2.3 Å was also a hanging drop method. The drop consisted of 2µl protein solution (15 mg/ml cytochrome *c* oxidase purified by protocol 2), 1µl reservoir solution that include 21-23% PEG400, 100 µl of 1 M sodium citrate and 50 µl of 2M sodium chloride to a 1ml total volume, pH 5.6 and 5.7. One microliter of (0.1 M MgCl<sub>2</sub>, 15% heptanetriol and 10 x CMC (critical micel concentration) lauryl maltoside 1:1:1 mixture) were also added. The wells were covered and sealed using vacuum grease, and incubated at 14°C for 12 hours and gradually the temperature was decreased to 4°C in another 12 hours and kept at constant temperature at 4°C for about two weeks.

Images in this thesis are presented in color.

## RESULTS

### **Growth of *Rhodobacter sphaeroides***

The plasmid pYJ-pRK123H was used and transformed into *Rhodobacter sphaeroides* JS100 which had subunit I deleted from its genome to create the overexpressing strain YZ100 (Zhen *et al.*, 1998). In that strain, three genes for the structural subunits of cytochrome *c* oxidase and two assembly genes are linked together in the multicopy plasmid pRK 415-1 plasmid. This strain when grown aerobically gives 4-5 fold higher production of the enzyme than the parent Ga strain. The expression of cytochrome *aa*<sub>3</sub> was compared by the ratio of absorbance at 606 nm to that of 560 nm (cytochrome *a*/ cytochrome *b* or *a/b* ratio). The wild type non-overexpressed strain gave an expression of *a/b* ratio of 0.2 while *a/b* ratio for YZ100 the overexpressed strain was 0.8 (Figure 2.1). Using this strain increased the yield dramatically and ten liters of media after two days gave approximately 50g wet cells, which contained about 60 mg of oxidase.

The expression level of H333N is much lower than YZ100 wild type, because it is not in an overexpression strain and the yield is about 10-15 mg oxidase/ 10L culture.

### **Purification with Ni<sup>2+</sup>-NTA**

Approximately 90% of wild type and mutant cytochrome oxidase from the membranes was recovered from Ni<sup>2+</sup>-NTA purification. Addition of 10 mM of imidazole to the solubilized membrane eliminated the non-specific binding. An additional step of using a



**Figure 2.1 Comparison between the expression level of the wild type strain (CY91) and wild type overexpressed strain (YZ100). The expression was measured as cytochrome *a*/cytochrome *b* or *a/b* ratio and calculated as  $A_{606}/A_{560}$ .**

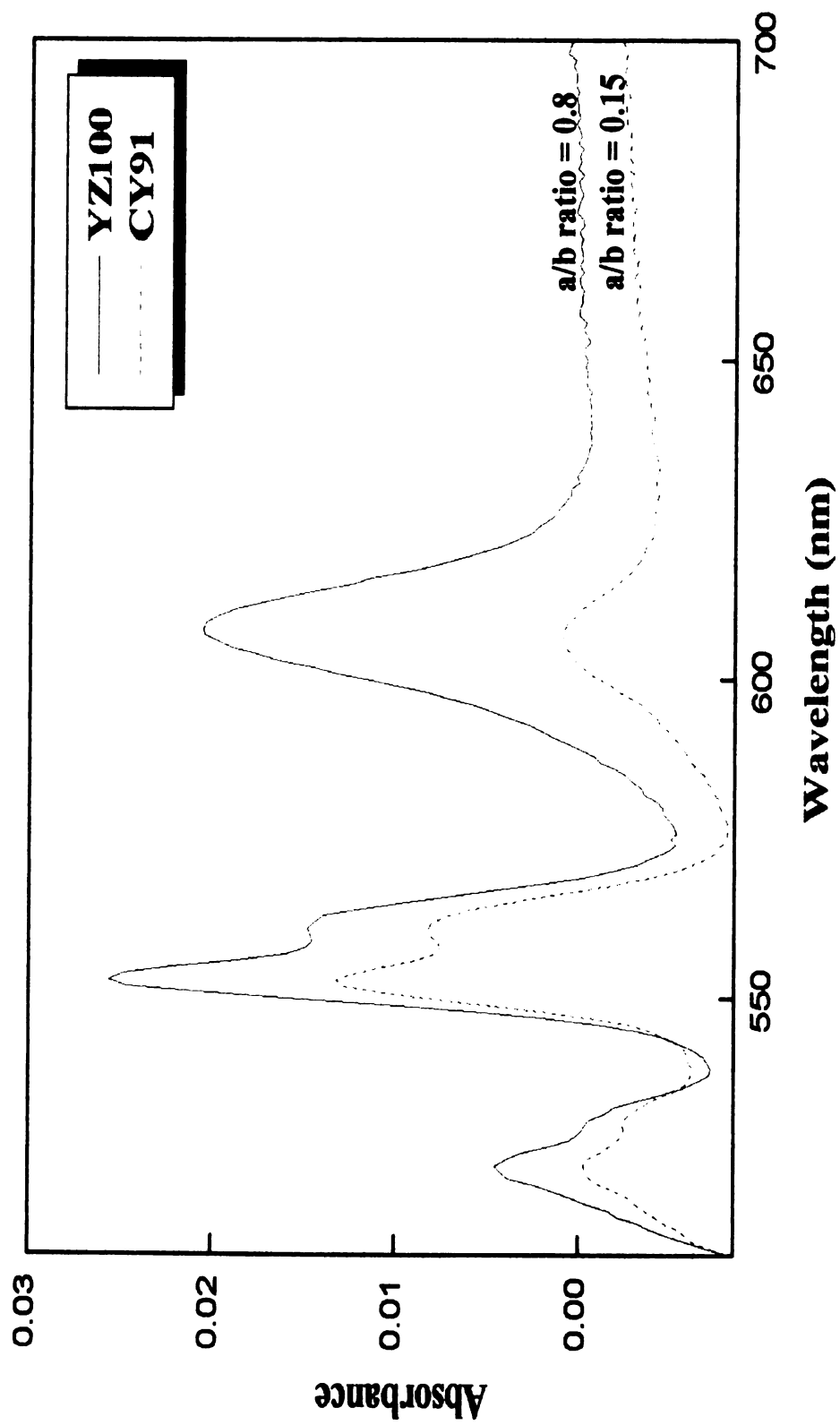


Figure 2.1

relatively high salt (200 mM KCl) wash, after the first low salt wash (40 mM KCl) and before the elution step, minimized the impurities (Figure 2.2). On an SDS gel the enzyme that was washed with high salt (200 mM KCl) shows a more pure fraction than the one that was washed with low salt buffer (40 mM KCl) only. The wash did not contain a significant amount of the enzyme and did not result in loss of any of the subunits. The gel also shows an extra band representing a 63 kDa polypeptide which is not removed with this purification system, and probably represents a dimer of subunit I and II that may be prevented from forming at high ionic strength.

Due to the high selectivity of the histidine-tag, contaminants were efficiently removed; neither photosynthetic pigments, nor other membrane proteins had any apparent effects on the binding or purity of the histidine-tag oxidase. This purification took about 6-7 hours and yielded about 4-5 mg oxidase/ 1L culture.

To get a more reproducible enzyme preparation for crystallography, the protein concentration was determined by the protein assay as mentioned in the Materials and Methods, and the protein/detergent ratio was calculated. The best crystals were achieved at 15mg/ml protein and 1.5 % lauryl maltoside when used in dissolving the membrane pellet for application to the  $\text{Ni}^{2+}$ -NTA column (Qin, personal communication).

### **DEAE anion exchange chromatography**

When using a DEAE column for further purification, 70-75% of the oxidase was recovered. The sample eluted at 250 mM KCl. The ratio of  $A_{280}$  to  $A_{420}$  (total protein per oxidase ratio) for enzyme purified through both metal-affinity and DEAE columns is 1.8, compared to 2.2 for the enzyme purified with  $\text{Ni}^{2+}$ -NTA alone, suggesting that combining

**Figure 2.2 Combination of  $\text{Ni}^{2+}$ -NTA and FPLC columns as well as using relatively high salt wash (200 mM KCl) to improve the enzyme purity.**

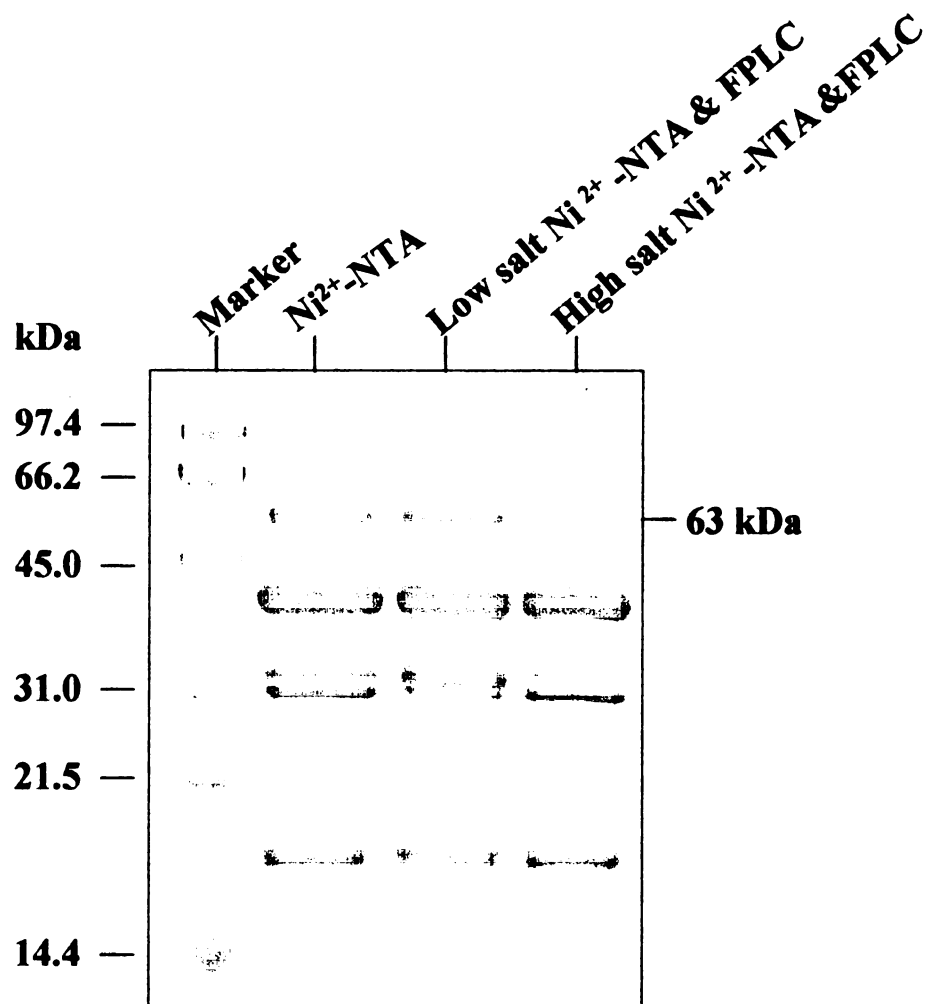


**Figure 2.2**

the two methods result in a better purification system and pure enzyme that may be suitable for crystallization, but the fact that these columns cause a significant lipid depletion that may be important for crystallization process.

### **Visible spectra**

Visible spectra can detect impurities and the overall structural integrity of the protein. The spectra for the purified wild type and H333N mutant showed a highly pure enzyme with no *b* or *c* cytochromes. The reduced wild type oxidase had peaks at 444 nm and 606 nm, which are the *soret* and  $\alpha$  absorption regions for heme *a* and heme *a*<sub>3</sub>; and the spectra for H333N mutant have the same absorption maxima in the  $\alpha$  and the *soret* regions indicating that the heme sites of this mutant were not altered (Figure 2.3).

After bubbling 1 ml of CO into dithionite-reduced cytochrome oxidase, 100% of the wild type was converted to the CO-bound form, compared to 60% for H333N, which suggested that by changing a histidine to asparagine at this position, a conformational change at the binuclear center has occurred, though not detectable by the visible spectrum.

### **SDS-PAGE**

Polyacrylamide gel electrophoresis of the purified wild type oxidase (Figures 2.2 & 2.4) showed 3 distinct bands representing the three subunits of the enzyme with apparent molecular masses of 42-44, 32-34 and 19 kDa. The gene for subunit II codes for a 35 kDa protein after an N-terminal leader sequence is removed. The C-terminal of subunit II is also subject to processing, but processing is incomplete, resulting in two

**Figure 2.3 Checking the native structure of the wild type and the mutant H333N by monitoring the absolute reduced spectra at the solet (444nm) and  $\alpha$  (606nm) absorption regions for heme  $a$  and heme  $a_3$ .**

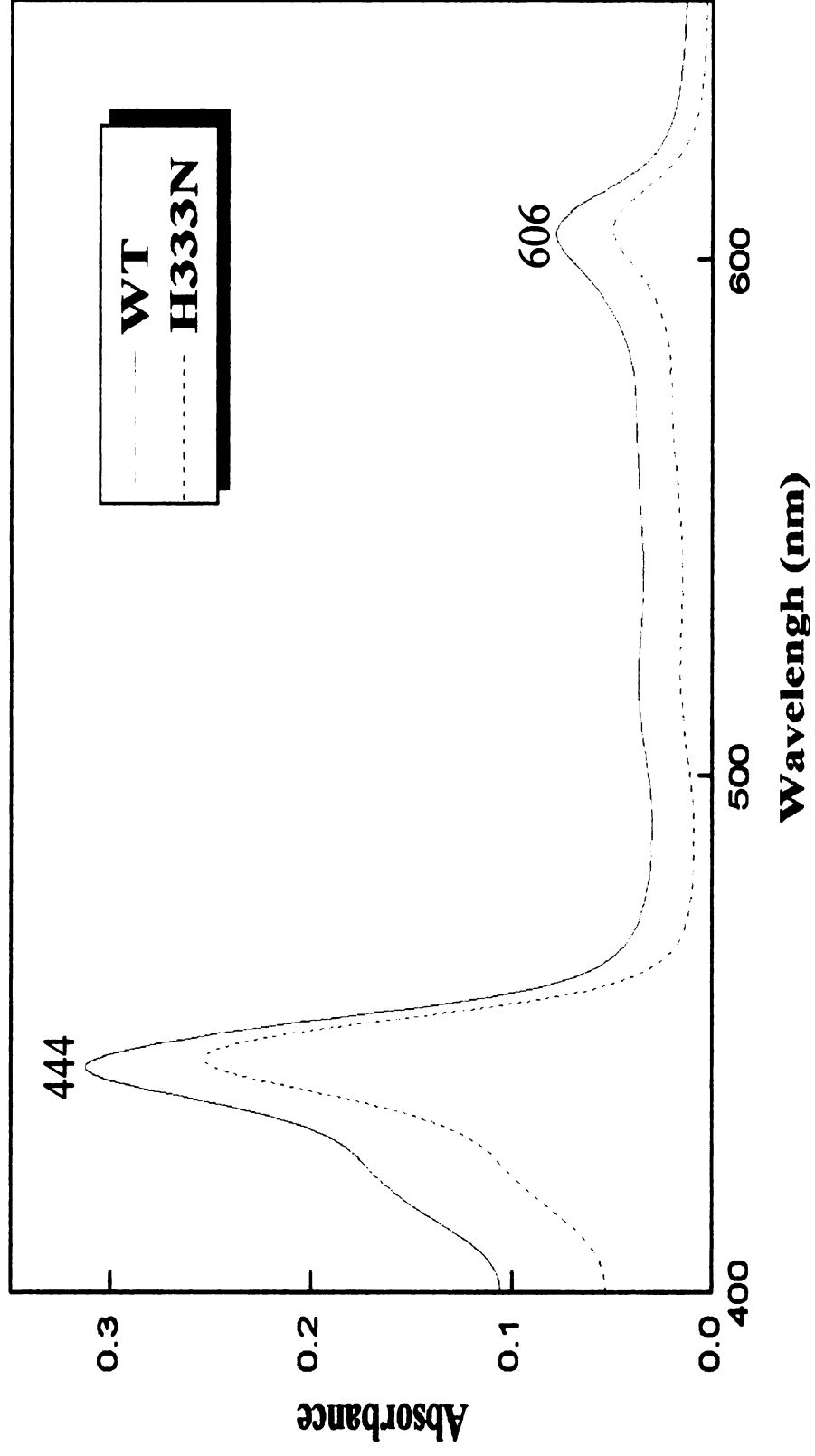


**Figure 2.3**





**Figure 2.4 Improving the homogeneity of the enzyme.** Lane 1 of the SDS gel is for  $\text{Ni}^{2+}$ -NTA column purified wild type oxidase showing both processed and unprocessed forms of subunit II, with apparent molecular weights of 34 and 36 respectively. Lane 2 shows  $\text{Ni}^{2+}$ -NTA column purified wild type oxidase with only the processed form (short) of subunit II, created genetically by altering the gene for subunit II. Identification of subunit polymers based on specific fluorescence labeling of all subunit (Schmidt, personal communication).

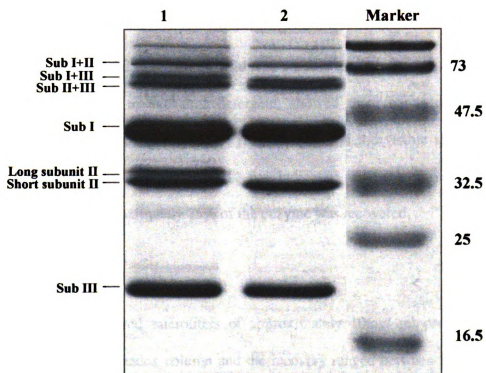


**Figure 2.4**

bands for subunit II of 34-36 & 32 kDa. Carrie Hiser in our lab engineered a gene for subunit II that is artificially processed by a 2 kDa segment (Figure 2.4). This version of the enzyme is more homogenous and a better candidate for crystallization. Variable amounts of contaminants or polymerized forms in the 63-70 kDa range, are also seen in the SDS gel (Figures 2.2 & 2.4).

### **Gel Filtration**

SDS-PAGE of a purified wild type oxidase that ran through a Sephacryl S-200 gel filtration column to exchange detergent, showed three bands representing the three subunits of cytochrome *c* oxidase (Figure 2.5), and the visible spectra shows the two normal peaks at 606 nm and 444 nm indicating that the enzyme was not changed structurally. Approximately 75% of the enzyme was recovered.

### **Spin column chromatography**

Five hundred microliters of approximately 10mg/ ml protein (wild type) was loaded to the Sephadex column and the recovery ranged between 80-95%. The enzyme activity was decreased, but the spectrum and the enzyme subunit composition remained unchanged (Figure 2.5).

After gel-filtration and the spin column, the sample was applied to a TLC plate to determine what types of detergents were in the sample. By running a control of both lauryl maltoside(LM) and decyl maltoside (DM), it was very clear that a major part of LM was exchanged with DM after the spin column (Figure 2.6), but by no means complete exchange was obtained.

**Figure 2.5 SDS-polyacrylamide gel electrophoresis (14% separating and 8% stacking) of oxidase purified with different columns. First and second lanes show wild type oxidase, purified with Ni<sup>2+</sup>-NTA and FPLC, in two different concentrations (10 and 20 µg). Third lane shows the oxidase after gel filtration that was used to exchange detergents, and the last lane shows the oxidase after a spin column was used to adjust the detergent contents in the protein sample.**

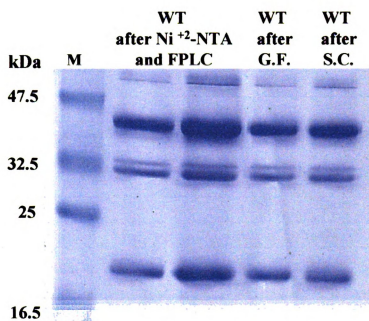


**Figure 2.5**

**Figure 2.6 Measurement of detergent content by thin layer chromatography (TLC).**

Decyl maltoside and lauryl maltoside were run along with protein samples before and after gel filtration and spin column, to examine the efficiency of the detergent exchange process. In this experiment the sample was purified in lauryl maltoside, and the detergent exchanged with decyl maltoside by gel filtration and spin column procedure. Before detergent exchange, the sample was concentrated 10 fold and the concentrated lauryl maltoside appears as large spot on the TLC plate overlapping somewhat with the position of decyl maltoside. Detergent concentration was adjusted by spin column and on the gel there are two bands for lauryl maltoside and decyl maltoside showing that complete exchange was not obtained.

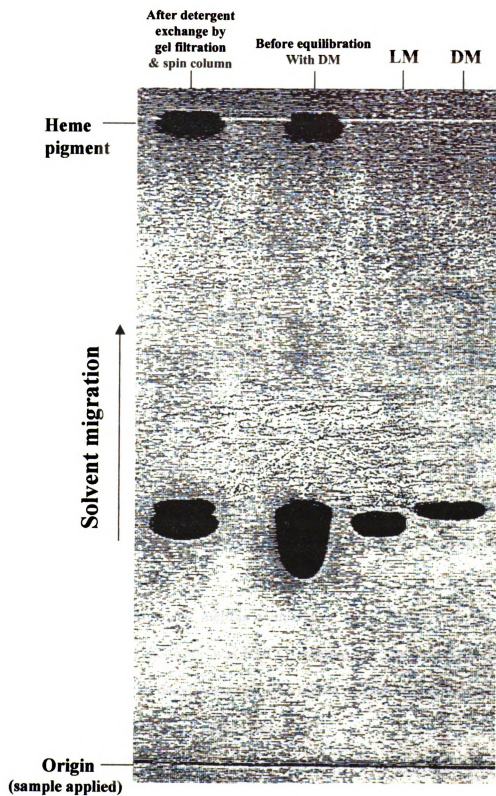


**Figure 2.6**



### **Activity assay**

The turnover number of the purified enzyme was approximately  $1800\text{ s}^{-1}$  at pH 6.5 in  $\text{KH}_2\text{PO}_4$  buffer with lipids. The enzyme lost some activity after gel filtration where the turnover number decreased to  $1600\text{ s}^{-1}$ , whereas after spin column the turnover number was  $1400\text{ s}^{-1}$ , probably due to loss of lipids during the stages of purification.

To determine a maximum turnover a pH- dependent experiment was made, and we found that the highest activity can be determined at pH 6.5 (Figure 2.7).

### **Stability of the enzyme in different detergents**

The stability of the wild type oxidase was determined functionally by measuring the oxygen consumption using the polarograph, and structurally by spectral analysis. The enzyme behaved differently in different detergents at different temperatures. When incubated at room temperature for three days the enzyme lost ~50% of its activity in lauryl maltoside, 90% in CYMAL-6 and 85% in decyl maltoside. When incubated at  $4^\circ\text{C}$ , the enzyme lost 25% activity in lauryl maltoside or CYMAL, and 20% in decyl maltoside (Figure 2.8)

Results from the melting temperature assay shows that  $T_m$  for the enzyme purified in lauryl maltoside was  $65.8^\circ\text{C}$ , whereas the  $T_m$  for the one purified under the same conditions in decyl maltoside was  $60.8^\circ\text{C}$ , which means that enzyme purified in lauryl maltoside was more stable (Figure 2.9).

**Figure 2.7 Effect of pH on cytochrome *c* oxidase activity.**

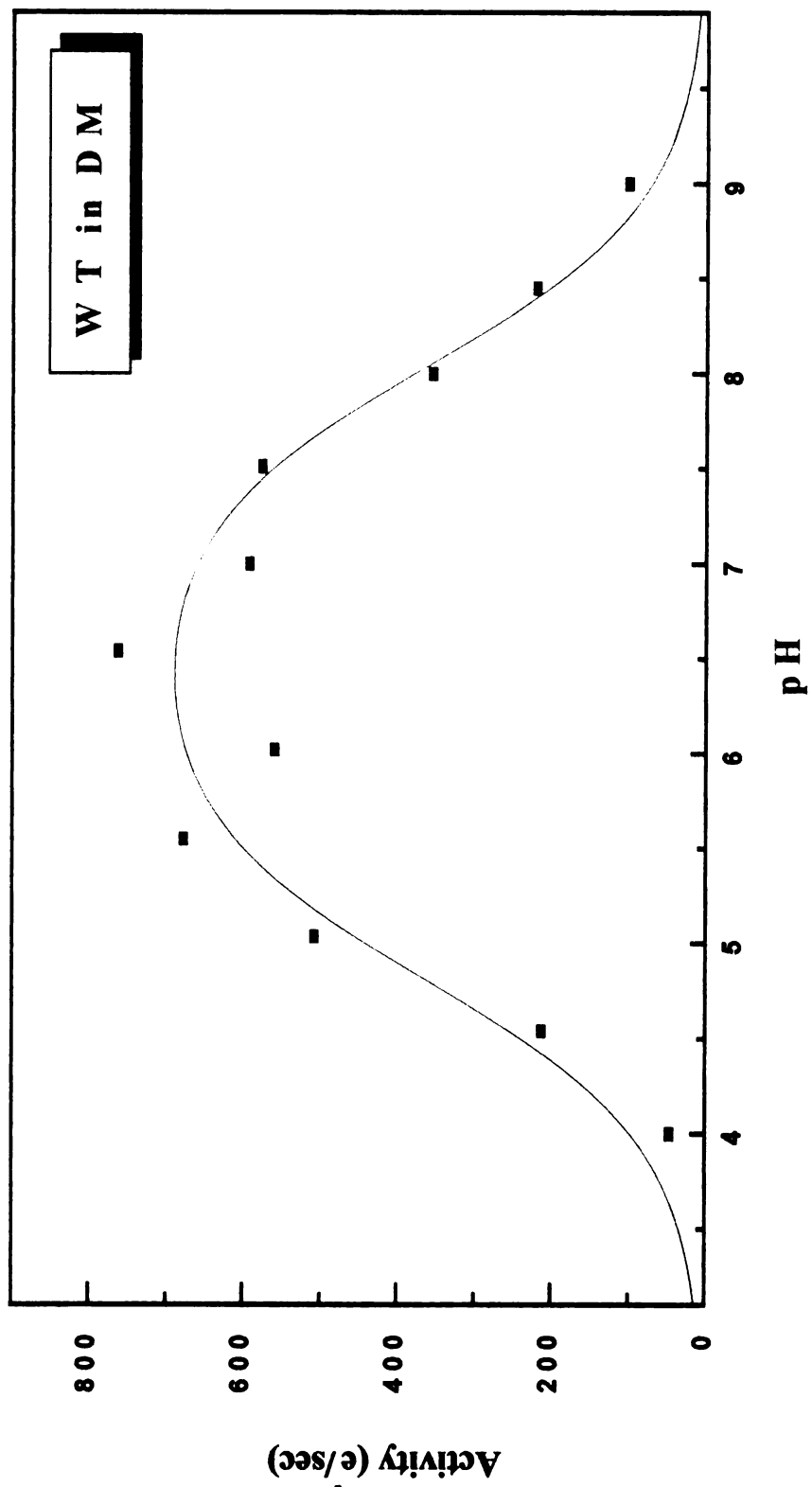


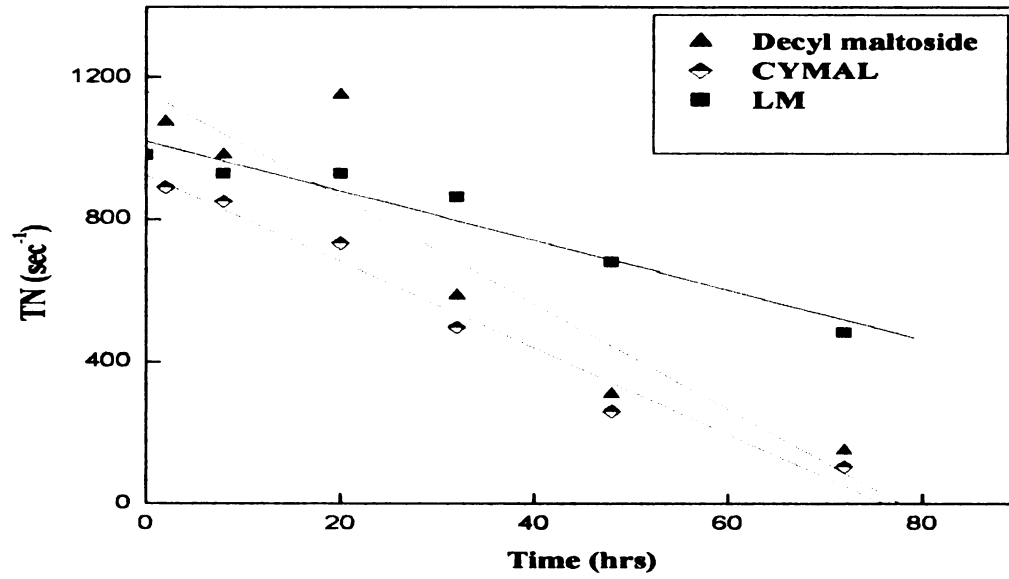
Figure 2.7



**Figure 2.8. Stability of the enzyme in different detergents.** Figure A shows the effect of detergents on the stability of the enzyme at room temperature where the enzyme lost 50- 90% of its activity depending on the detergent type. Figure B shows the loss of activity of the oxidase when incubated in different detergents at 4°C resulting in an activity loss of 20-25 %.

TN: Turnover number.

### A: Assay at Room Temperature



### B: Assay at 4°C

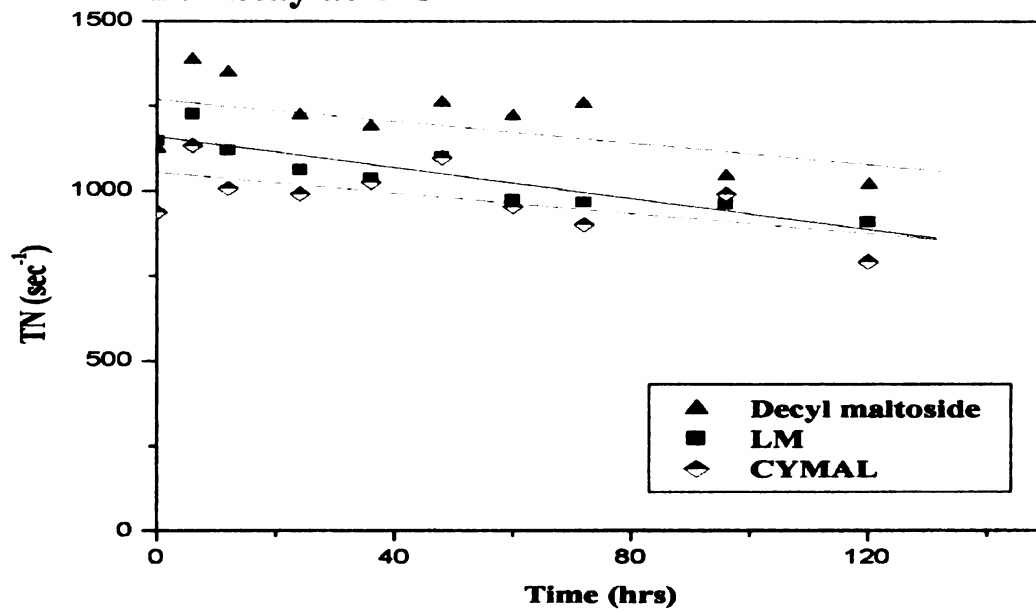


Figure 2.8

**Figure 2.9 Enzyme stability measured by melting temperature assay.** Enzyme purified with either lauryl maltoside or decyl maltoside was used for the denaturation experiment to measure the stability of the enzyme under each condition. Denaturation was monitored from 30°C to 80°C by measuring the absorbance at 420nm.

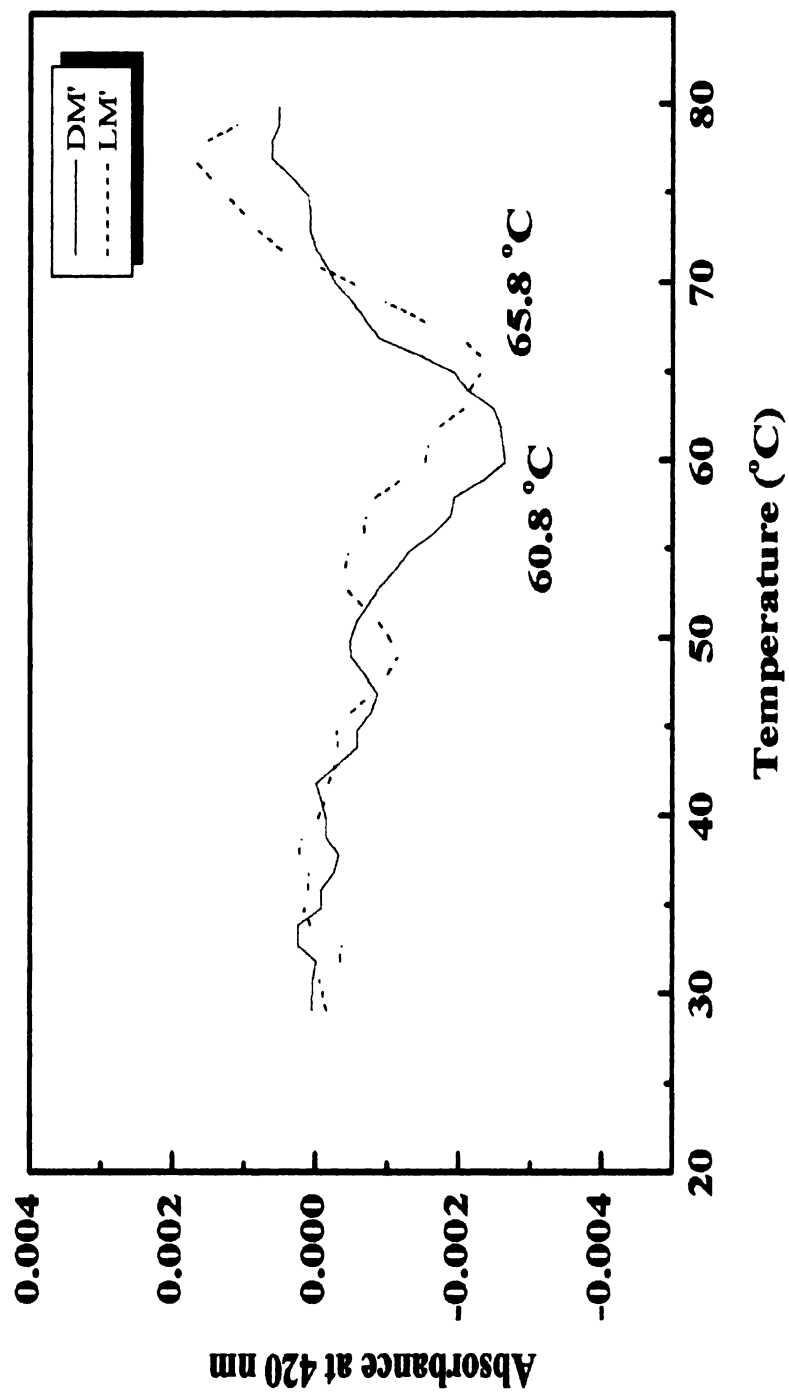


Figure 2.9



## Crystallization

After screening more than 1000 variations, including several precipitants and precipitant concentrations, different additives, different pHs and two temperatures, microcrystals were observed after two weeks under 10 of these conditions. The common precipitant in all 10 wells that had crystals was polyethylene glycol (PEG) and the pH range for the reservoir solutions was 6.5-7.5. Crystals of wild type oxidase grew at both room temperature and 4°C, and in both lauryl maltoside and decyl maltoside. In order to improve the quality and the size of the crystals, modifications of the previous extreme conditions, used for the initial screening, was required. Using mild conditions such as lower PEG concentration, created a protein instability problem. Use of protein inhibitors, formate and azide, was tried to overcome this problem. The protein was more stable when using the inhibitors, but the crystal formation did not improve.

In parallel with our efforts, a group in Sweden (Svensson Ek, M. and Iwata, S.) were successful in achieving crystals of *Rhodobacter sphaeroides* oxidase that diffract at 2.3Å resolution. Their procedure differed importantly in the purification method, using Mono-Q instead of DEAE-5PW and not as vigorous detergent exchange, by using an Amicon concentrator instead of the gel filtration and spin columns in our protocol. They crystallized the protein in 0.24% decyl maltoside detergent and the protein concentration was 15-20 %.

By using this protocol we were able to see crystals after 2-3 days and they can grow bigger for about another 10 days (Figure 2.10). So far the best diffraction has been achieved to 3.2 Å. Efforts continue toward achieving higher resolution.

**Figure 2.10. Crystal of *Rhodobacter sphaeroides* wild type cytochrome *c* oxidase.**  
Crystals were grown under conditions mentioned in the Materials and Methods section and the overall dimensions are 0.3 x 0.3 x 0.15 mm.

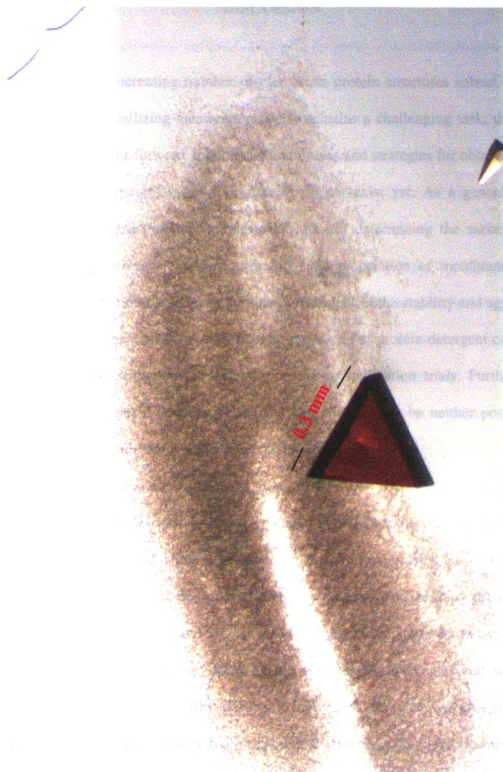
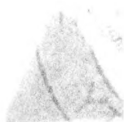


**Figure 2.10**



## DISCUSSION

Despite the increasing number of membrane protein structures solved by X-ray crystallography, crystallizing membrane proteins remains a challenging task; this is due to the fact that straight-forward, reliable methodologies and strategies for obtaining X-ray quality crystals of integral membrane proteins do not exist yet. As a general rule in crystallizing membrane proteins, the critical factors in determining the success of the crystallization experiments are the purification and preparation of membrane protein samples. Another important factor is the role of detergent in the stability and aggregation of membrane proteins, as well as the colloidal properties of protein-detergent complexes that need to be controlled before and during the crystallization trials. Further it has recently become apparent that complete removal of lipids may be neither possible nor desirable (Garavito and Ferguson-Miller, 2001).

In order to follow these general rules and in our first attempts to crystallize *Rhodobacter sphaeroides* cytochrome *c* oxidase, we purified the enzyme with affinity chromatography combined with DEAE ion-exchange chromatography. Ni<sup>2+</sup>-NTA affinity chromatography is known to be the most effective method for separating cytochrome *c* oxidase from other proteins; and DEAE ion-exchange chromatography is capable to a large extent in separating the two forms of the enzyme with long and short subunit II. This problem of having two forms of subunit II is due to the presence of a proteolytic cleavage site located at the C-terminal of subunit II (Hosler *et al.*, 1992; Rumbley *et al.*, 1997). This site is subjected to partial processing during growth, resulting in two forms of

the enzyme. Combining these two methods of purification improved the purity and homogeneity of the enzyme remarkably.

Then gel filtration was used to exchange detergents. The protein sample was very diluted after gel filtration and the concentration process concentrates the detergent as well as the enzyme, and since the detergent concentration is very critical in crystallizing membrane proteins, a spin column was then used to adjust the detergent concentration. These procedures also cause lipid depletion, where naturally associated lipids were substituted with detergents.

Further, the enzyme was analyzed by thin layer chromatography, which revealed that the detergent exchange was not complete, even with the gel filtration and spin column. Since most membrane protein purification/ crystallization methods do not determine extent of exchange, thin layer assay was used as a valuable tool for monitoring the detergent content and lipid composition in order to standardize procedures.

Although incubation of the enzyme in any of the different detergents caused some decrease in activity with time, still after three days at room temperature and five days at 4°C the enzyme remains active. Lauryl maltoside kept the enzyme more active at room temperature whereas decyl maltoside kept it more active at 4°C. Incubation in CYMAL-6 has the lower activity, but the enzyme is still active and it could be considered for crystallization.

The initial screening involved searching for the parameters and optimum conditions for crystals growth. As for many other membrane proteins, PEG proved to be the best precipitant for *Rhodobacter sphaeroides* cytochrome oxidase. The enzyme in both lauryl maltoside and decyl maltoside formed crystals although in lauryl maltoside

more successes were observed. Unexpectedly the microcrystals grew at both temperatures, leading to a perhaps wrong conclusion that temperature had little effect, but later studies revealed that it is a critical factor in getting large and stable crystals useful for X-ray analysis. The fact that the enzyme had highest activity at pH 6.5 and that crystals grew at pH range of 6.5-7.5, seemed to be a reasonable result, though this is by no means a common observation.

After purification the enzyme showed a satisfactory purity, homogeneity and activity to be crystallized. It also showed a reasonable stability while growing crystals. These were encouraging results for proceeding with crystallizing this membrane protein, but after continuous efforts we were not able to improve the size and the quality of our crystals.

As part of a collaboration between our lab and a Swedish group in Uppsala, we modified our purification protocol and crystallization conditions to match their protocols since they had succeeded to solve the crystal structure of *Rhodobacter sphaeroides* cytochrome *c* oxidase at 2.3 Å. In their protocol, the enzyme was purified with Ni-affinity chromatography as above but using an imidazole gradient to elute rather than 100mM histidine. The next purification step used a Mono Q column instead of DEAE/5PW-HPLC ion-exchange column. These two columns have the same DEAE ion-exchange chemistry but a different resin is used as a support. No gel filtration or spin column was used for detergent exchange, just a concentrator-filtration method. This lesser level of manipulation and different DEAE resins may be critical for maintaining the necessary native lipids.

By using more and different column systems (affinity chromatography, DEAE ion-exchange chromatography, gel-filtration and spin column, compared to use affinity chromatography and Mono-Q column) we were achieving higher purity, homogeneity and detergent exchange, but undoubtedly we were losing more of the native membrane lipids. The maintenance of some lipid-protein interactions may be critical for crystallization (Garavito and Ferguson-Miller, 2001). As many as 19 lipids were resolved in the 2.0 Å resolution structure of bovine cytochrome oxidase (Yoshikawa, personal communication), and six were resolved in the *Rhodobacter sphaeroides* structure (Svensson-Ek *et al.*, 2002). Eighteen lipids were also found associated with bacteriodopsin at 1.55 Å resolution (Luecke *et al.*, 1999). Nussberger and colleagues document the requirement of 4 molecules of digalactosyl diacyl glycerol lipids per molecule of plant light harvesting complex to achieve 2-dimensional crystallization. Another example of the importance of lipids in crystallizing membrane proteins is the requirement of re-addition of lipids in crystallizing the sarcoplasmic  $\text{Ca}^{++}$  pump (Toyoshima *et al.*, 2000). Therefore, even when reasonably active forms of the enzyme are isolated, solubilized and purified by using non-ionic detergents such as lauryl maltoside to substitute for the lipid bilayer, still the structural integrity and homogeneity of the membrane proteins may be influenced by retained lipids.

Using the Swedish purification protocol and a hanging drop method for crystallization under modified conditions, as mentioned in the Materials and Methods section, we were able routinely to get crystals as large as 0.3 X 0.3 X 0.15 mm in our lab. This encourages us to continue with our efforts at refining the method to crystallize mutant forms and in the future of forming and crystallizing a complex between



cytochrome *c*- cytochrome *c* oxidase to reveal more information about the binding sites and the process of electron transfer between the two proteins.

### **CHAPTER III**

#### **USE OF THIN LAYER CHROMATOGRAPHY AND MASS SPECTROMETRY TO ANALYZE MEMBRANE LIPIDS FROM *RHODOBACTER SPHAEROIDES* MEMBRANES**

## INTRODUCTION

Membrane lipids play a variety of key roles in biomembrane function. Although very little is known about the molecular basis of these lipid-protein interactions, it is well understood that a major role of membrane lipids is to form the bilayer structure that provides the immediate environment for the integral membrane proteins, allowing them to perform important physiological processes such as photosynthetic and respiratory energy transduction (Gennis, 1988; McAuley, 1999).

The membranes of *Rhodobacter sphaeroides* are commonly known to contain two classes of polar lipids: phospholipids and non-phosphorous glycolipids (Benning *et al.*, 1995). Growth conditions can affect the lipid composition: the abundance of polar lipids, as well as other lipids, changes under respiratory or photosynthetic growth.

Under all growth conditions the membranes of *Rhodobacter sphaeroides* contain substantial amounts of phosphatidylethanolamine. Four phosphatidylethanolamines and two other unidentified phospholipids were clearly seen in the crystal structure of cytochrome *c* oxidase from *Rhodobacter sphaeroides* (Svensson *et al.*, 2002). For comparison, five phosphatidylethanolamines were observed in the crystal structure of the bovine heart cytochrome *c* oxidase (Yoshikawa *et al.*, 1998) as well as three phosphatidyl glycerols. In *Rhodobacter sphaeroides*, phosphatidylglycerol is found in significant amounts under photosynthetic growth, and also found under respiratory growth in variable amounts. Diphosphatidylglycerol, also known as cardiolipin, is also found in *Rhodobacter sphaeroides* membranes. There is strong evidence of the functional importance of some anionic membrane lipids, in particular cardiolipin, which is found to

be associated with the oxidase even after the protein isolation and purification (Robinson *et al.*, 1980).

In this section we analyzed for the presence of the major lipids, such as the phosphorus-containing and non-phosphorus-containing lipids: phosphatidylglycerol, phosphatidylethanolamine, phosphatidylserine, phosphatidylcholine and cardiolipin sulfolipids and ornithine lipid that associated with *Rhodobacter sphaeroides* cytochrome *c* oxidase, during different purification steps and in the crystals. Thin layer chromatography and mass spectrometry were used to identify and quantify the lipid content. The goal was to establish the nature of the lipid retained during purification and to determine the importance of lipid in obtaining crystals with good diffraction characteristics.

## **MATERIALS AND METHODS**

### **Growth of *Rhodobacter sphaeroides***

Cells were grown on Sistrom's plates with 50µg/ml spectinomycin, 50µg/ml streptomycin and 1 µg/ml tetracycline pH 7.0 at 30°C for 3 days. Cells were inoculated in 6X100 ml of Sistrom's media with the same antibiotics and grown for two days at 30°C. These starter cultures were used to inoculate 12 Fernbach flasks with 800 ml Sistrom's media containing the same antibiotics. The cultures grew at 30°C with vigorous swirling to achieve maximum aeration in New Brunswick shakers for two days or until the absorbance reading at 660 nm was about 1.7, which indicates that the cells are near the end of the exponential phase.

Cells were harvested by centrifugation in a GS-3 rotor at 14,000x g for 20 minutes at 4°C. The pellets containing whole cells were saved at –80° C.

### **Basic Lipid Extraction**

The protein sample concentration was 10mg/ml. 20µl sample (membranes or purified enzyme) was added to 75µl methanol/chloroform in a 1:1 ratio. The mixture was vortexed for 1 minute, spun down at 13000 rpm for 2 minutes and the supernatant containing lipids was saved for further analysis.

### **Acetone Extraction of Lipids**

Approximately 100µl sample containing 10mg/ml was lyophilized and 10 times volume of anhydrous acetone was added. Sample was vortexed for 1 minute and kept in

ice for 1 hour. The mix was spun at 2500 rpm for 3-5 minutes and the supernatant was removed, dried and re-dissolved in 40 µl chloroform/methanol 1:1 ratio. Then the pellet was extracted with 75µl chloroform/methanol 1:1 ratio, vortexed for 1 minute and spun at 13000 rpm for 2 minutes. The supernatant was dried and re-dissolved in 40 µl chloroform/ methanol 1:1 ratio.

### **Ammonia Extraction**

An approximately 100µl sample containing 10mg/ml was lyophilized and a 10 times volume of acetone was added. The sample was vortexed for 1 minute and kept in ice for 1 hour. The mix was spun at 2500 rpm for 3-5 minutes and the supernatant was removed, dried and re-dissolved in 40 µl chloroform/methanol 1:1 ratio. The pellet was then extracted with chloroform/methanol 2:1 twice, ethanol/diethylether 1:1 once and finally with chloroform/methanol/ammonia (100: 50: 2) twice to extract the cardiolipin. The supernatant from all extraction steps were kept together and evaporated with nitrogen gas, then dissolved in 40 µl chloroform/methanol 1:1 ratio and saved for further analysis.

### **Thin Layer Chromatography (TLC)**

Samples that were either extracted with chloroform/methanol, acetone or ammonia were applied to a pre-activated Silica gel plate treated with sulfuric acid and heated at 120°C for 3 hours (Benning and Somerville, 1992). The solvent system that used was 128 ml of acetone/ toluene/ water (91:30:7). The plate was run for about 50 minutes, dried and stained with iodine for all lipids and with  $\alpha$ - naphthol for sugars to determine

the existing detergents, as well as molybdenum blue for phosphate groups to confirm phospholipids bands.

Some of the bands were cut and the Silica was precipitated by adding 200 $\mu$ l chloroform, vortexed for 1 minute and spun at 2500 rpm for 3-5 minutes. The supernatant was removed, dried with argon gas and re-dissolved in 10-20 $\mu$ l chloroform to be analyzed by mass spectrometry.

### **Fast Atom Bombardment Tandem Mass Spectrometry (FAB)**

FAB mass spectra were obtained using a JEOL HX-110 double-focusing mass spectrometer (JEOL USA, Peabody, MA) operating in  $\pm$  ion mode. Ions were produced by bombardment with a beam of Xe atoms (6 keV). The accelerating voltage was 10kV and the resolution was set at 1000. For FAB-CAD-MS/MS, helium was used as the collision gas in a cell located in the first field-free region. The helium pressure was adjusted to reduce the abundance of the parent ion by 50%. A JEOL data system generated linked scans at a constant ratio of magnetic to electrical fields (B/E). The instrument scanned from 50-1500 m/z.

Approximately 0.1 $\mu$ g of lipids extract was mixed with 1 $\mu$ l of matrix, either triethanolamine or glycerol, and injected into the system.

### **Matrix-Assisted Laser Desorption Ionization Mass Spectrometry (MALDI)**

The matrix 2,5-dihydroxybenzoic acid was purchased from Aldrich (Milwaukee, WI). A matrix solution with a concentration of 25 mg/ml was prepared using a 1:1 acetonitrile/water solution. Lipids were dissolved in chloroform and samples were

prepared by spotting 1µl of matrix solution on a gold sample plate, air-dried and then 1µl of the analyte was added.

For whole protein analysis (protein and associated lipids), 1µl sample was cocrystallized with the matrix and then injected into the system.

Reflectron and post- source decay (PSD) MALDI mass spectra were recorded on a PerSeptive Biosystems (Farmingham, MA) Voyager STR delayed extraction time-of-flight linear (TOF) mass spectrometer equipped with nitrogen laser (337 nm, 3 ns pulse).

Analysis of mass spectrometry data was facilitated by using calculated molecular weights for lipids with different acyl groups as shown in Table 3.1.

### **Phosphate Analysis**

Typical samples used were 10µl of 60mg/ ml protein. Water was added to 2ml final volume. Samples and a blank (2ml water) were heated in a preheated oven at 150-160°C for at least 3 hours. Then 50µl of phosphorous-free hydrogen peroxide were added to each sample and incubated for another 1.5 hour to complete the combustion and to decompose all the peroxide. Then 0.2ml of 5% ammonium molybdate and 0.2ml of Fiske-SubbaRow reagent (15g anhydrous sodium bisulfite, 0.25g 1-amino-2-naphthol-4-sulfonic acid, 0.5g anhydrous sodium sulfite in 100 ml water) were added, mixed thoroughly and heated for 10 minutes in a boiling water bath. The tubes were cooled down and the absorbance at 830nm was recorded by using a Perkin Elmer UV/VIS Lambda 40 spectrometer.

For the standard curve, tubes containing 0.02, 0.04, 0.06, 0.08, 0.1 and 0.12µmole phosphate were prepared and 0.5ml 10 N H<sub>2</sub>SO<sub>4</sub> was added and vortexed. Then the



**Table 3.1 Molecular Weights of Major Lipids in *Rhodobacter sphaeroides***

Lipid	Head	Head + Acyl groups 18:0 18:0	Head + Acyl groups 18:1 18:1	Head + Acyl groups 18:0 16:0	Head + Acyl groups 18:1 16:0	Head + Acyl groups 18:1 16:1	Head + Acyl groups 16:0 16:0	Head + Acyl groups 16:1 16:1
Phosphatidyl glycerol (PG)	154	777	773	749	747	745	721	717
Phosphatidyl ethanolamin (PE)	124	747	743	719	717	715	691	687
Phosphatidyl serine (PS)	167	790	786	762	760	758	734	730
Phosphatidyl choline (PC)	166	789	785	761	759	757	733	729
Sulfoquinovosyl diacylglycerol (SL)	226	849	845	821	819	817	793	789
Ornithine Lipid	131	680	676	652	650	648	624	620
Diphosphatidyl glycerol (Cardiolipin)	216	1462	1458	1434	1432	1430	1350	1346

molybdate and the Fiske-SubbRow reagent were added, mixed, heated and the absorbance was recorded as mentioned above.

## RESULTS

### Lipid Extraction

Membranes and purified enzymes from wild type cells grown under the conditions indicated in the Materials and Methods section, initially were extracted with chloroform-methanol (2:1 by volume), a solvent universally used for lipid extraction. This system was efficient in extracting most of the polar lipids (phospholipids and glycolipids) as well as the neutral lipids including detergents. Since our purified enzyme contains significant amounts of detergents that extract along with other lipids and interfere with further lipid analysis, this method was not very useful for our purposes.

Acetone pre-extraction was used as an alternative method. This is the simplest and often the most efficient procedure for separating polar lipids from neutral lipids and detergents. The method depends on the general insolubility of polar lipids in cold, dry acetone, and the fact that other neutral lipids and detergents are soluble in cold, dry acetone (Awasthi *et al.*, 1971). It was found that this method of separation was only successful if the sample was lyophilized before acetone extraction to maintain a minimum water content in the sample that could affect lipid extraction and separation by TLC. By using this method, followed by the basic chloroform- methanol system, we were able to separate polar lipids from neutral lipids (pigments and detergents) to a great extent.

One of the important polar lipids in *Rhodobacter sphaeroides* membranes is the tightly bound diphosphatidyl glycerol (cardiolipin). The chloroform/methanol method partially extracted this lipid. Therefore we used another system to extract cardiolipin:

acetone extraction to remove detergents, followed by chloroform/ethanol (2:1), then ethanol/diethyl ether (1:1) and finally chloroform/ methanol/ ammonia (100: 50: 2) to ensure the extraction of cardiolipin. When analyzing this extract we were able to detect cardiolipin by mass spectrometry (Figure 3.1), even though it tended to run off the top of the plate in the thin layer system used.

Combining acetone pre-extraction with ammonium extraction is a good procedure to get a high yield of lipid contents without interference from detergents and pigments that might affect the lipid analysis.

### **Thin Layer Chromatography**

To examine the lipids that associate with *Rhodobacter sphaeroides* oxidase, wild type membranes and purified enzyme were extracted and separated by thin layer chromatography. This separation revealed a consistent pattern of polar lipids in all samples and showed phospholipids as a major class of lipids under our growth conditions. Phosphatidylethanolamine was found to be the most abundant lipid in the extract; this is in agreement with a previous study (Benning *et al*, 1995). Phosphatidylcholine and phosphatidylglycerol were also found in significant amounts. Phosphatidylserine appears as a small spot running close to and sometimes co-migrating with phosphatidylethanolamine. All these lipids were confirmed with lipid standards (Figure 3.2).

**Figure 3.1 MALDI spectra (Matrix-Assisted laser Desorption Ionization Mass Spectrometry) showing the presence of cardiolipins with a molecular weight of 1458 kDa, corresponding to cardiolipin with 4(18:1) alkyl chains. Sample was extracted first with acetone to remove detergents and the pellet was further extracted with chloroform/ethanol 2:1 twice; ethanol/diethyl ether 1:1 once and chloroform/methanol/ammonium 100:50:2 once, to extract the tightly bound cardiolipins.**

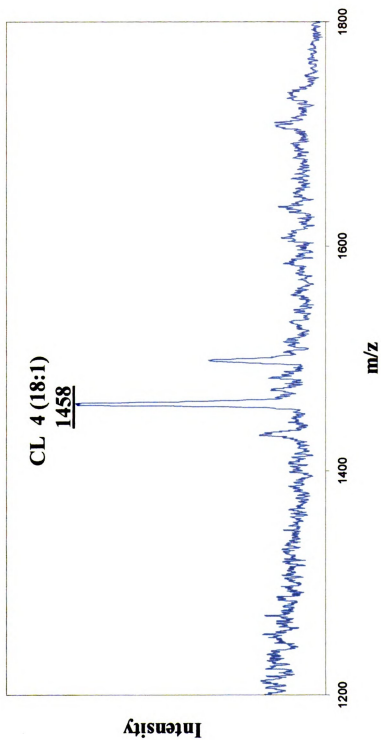
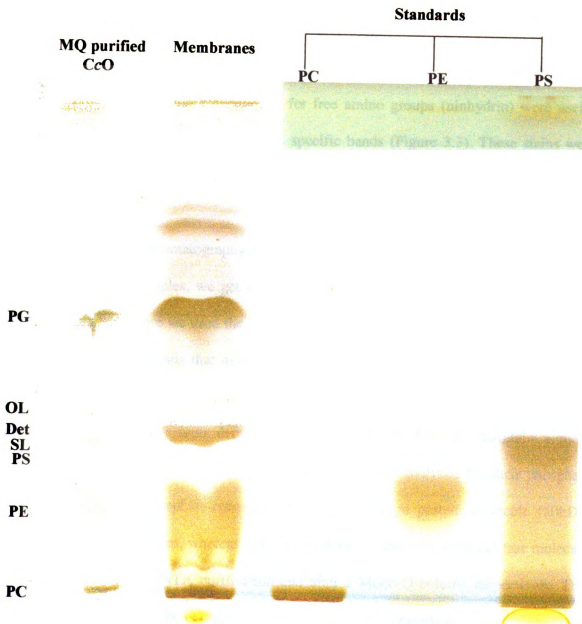


Figure 3.1

**Figure 3.2. Thin layer chromatography (TLC) of membrane and purified enzyme extracts.** Samples and lipid standards were applied to TLC plate, run for 50 minutes and stained with iodine. Both samples contained phosphatidylglycerol (PG), phosphatidylethanolamine (PE), phosphatidylcholine (PC), sulfolipids (SL) and ornithine lipid. The Mono-Q purified sample showed an extra band (yellow), between ornithine lipid and sulfolipid, that represents detergents since membranes samples do not contain any detergents.



**Figure 3.2**



Sulfolipids and ornithine lipids were also identified in our samples. These are phosphorus-free lipids are found in wild type *Rhodobacter sphaeroides* cells under normal growth conditions (Benning, 1997) (Figure 3.2).

Diagnostic spray reagents specific for phosphate groups (molybdenum blue), for sugar residues ( $\alpha$ -naphthol reagent) and for free amino groups (ninhydrin) were useful tools to provide more information about specific bands (Figure 3.3). These stains were particularly useful for distinguishing the sulfolipids band from ornithine lipid and phosphatidylserine.

Thin layer chromatography is a semi-quantitative method; when we apply the same amounts of samples, we get almost the same size of bands for each type of lipid (Figure 3.4). Therefore we used the thin layer chromatography technique to determine the relative amounts of lipids that associated with the oxidase in the membranes and after each purification step. The same types of lipids were found in membranes and after all purification stages, but with decreasing amounts (Figure 3.5). To maintain a more quantitative measure of lipids, these samples were further analyzed for their phosphate contents. Over 70 phosphate-containing lipids per average protein molecule (50kDa) were found in membranes, whereas only 16-23 and 8-11 phospholipids/ oxidase molecule were found after  $\text{Ni}^{2+}$ -NTA purification and after a Mono-Q column respectively. This value does not include the non-phospholipids that are clearly present in the TLC analysis. These results suggest that 10-15 lipids may be associated with a single oxidase at the time of crystallization.

An interesting result was found when membranes from cells grown photosynthetically and cells grown under high oxygen were extracted and analyzed with

**Figure 3.3 Diagnostic spray reagents for specific groups.** Membrane extracts, chloroform/methanol extract (lane 1 of each set) and the prior acetone extract (lane 2), were applied to a TLC plate and stained with molybdenum blue for phosphate groups: phosphatidyleglycerol (PG), phosphatidylethanolamine (PE) and phosphatidylcholine (PC).  $\alpha$ -naphthol (outer panel) was used to detect the sugar-containing lipids (sulfolipids SL). Ninhydrin (right panel) stain is specific for free amino groups. This stain over-reacted and all bands showed up including the expected ornithine lipid and phosphatidylserine. Cardiolipin (CL), heme and photosynthetic pigments co-migrate at the top of the plate.

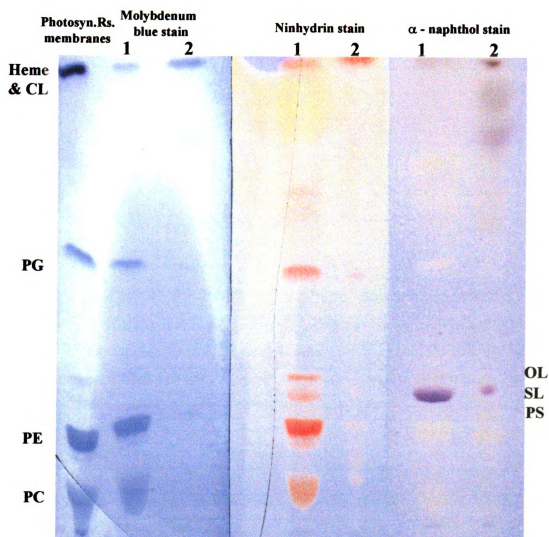


**Figure 3.3**

**Figure 3.4 Semi-quantitative analysis for membrane lipids by Thin Layer Chromatography.** Membrane samples, containing 1 mg cytochrome *c* oxidase, were extracted with acetone and then with chloroform/methanol 1:1 and applied to TLC plate. The same amount of sample was applied to each lane and the band positions, densities and sizes are almost the same in each extract, showing the consistency of the method in relative quantification of lipid composition.

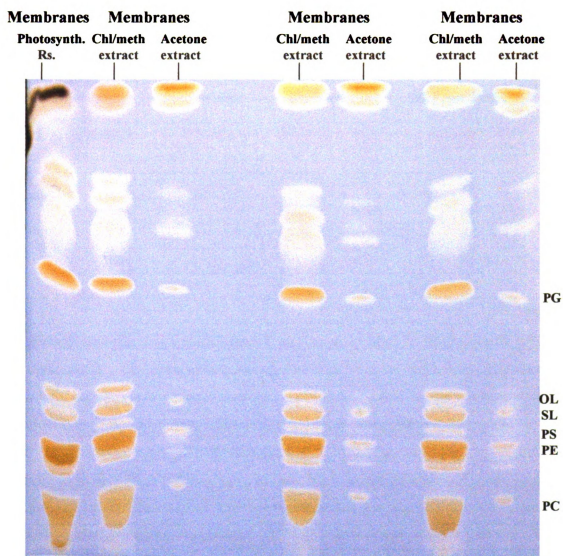


**Figure 3.4**

**Figure 3.5 Comparison of lipid composition in membranes and after each stage of purification.** *Rhodobacter* cells were either grown photosynthetically (first lane) or under high oxygen (second lane). Cytochrome *c* oxidase from aerobic cells purified with  $\text{Ni}^{2+}$ -NTA affinity chromatography (third lane) followed by Mono Q column (last lane) were extracted and applied to a TLC plate. All samples have the same types of lipids with variable amounts. Known amounts of the extract of cytochrome *c* oxidase were applied to each lane: amount of cytochrome *c* oxidase in the membranes sample was 0.1 mg, in  $\text{Ni}^{2+}$ -NTA purified enzyme was 0.5 mg and in the Mono-Q column purified enzyme was 1 mg.

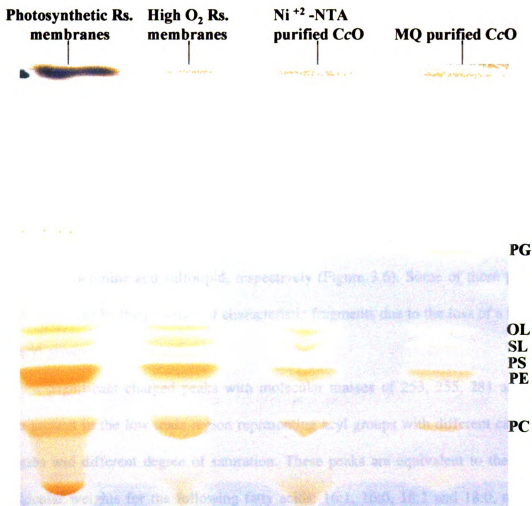


**Figure 3.5**

TLC. There was no significant difference in lipid composition in each extract except for the presence of variable amounts of phosphatidyl serine in cells grown under high oxygen (Figure 3.5, first lane).

### **Mass Spectrometry**

The presence of phosphatidylethanolamine, phosphatidylglycerol, phosphatidylcholine and sulfolipid was further verified by FAB and MALDI mass spectrometry. The FAB mass spectrum in either the positive or negative ion mode showed high-mass ions indicative of the molecular weights corresponding to the above lipids. In the FAB-mass spectrometry profile, significant peaks were identified at 743, 773, 789 and 819 m/z. These signals represent phosphatidylethanolamine, phosphatidylglycerol, phosphatidylcholine and sulfolipid, respectively (Figure 3.6). Some of these peaks were also confirmed by the presence of characteristic fragments due to the loss of a head group or acyl group.

Significant charged peaks with molecular masses of 253, 255, 281 and 283 are also present in the low mass region representing acyl groups with different carbon chain lengths and different degree of saturation. These peaks are equivalent to the calculated molecular weights for the following fatty acids: 16:1, 16:0, 18:1 and 18:0, respectively (Figure 3.7). This result is consistent with a previous study on fatty acid composition in *Rhodobacter* species where they found that the dominant fatty acids are long chains with 16 and 18 carbon atoms (Imhoff, 1991).

MALDI mass spectrometry was used as another powerful technique to analyze lipids without requiring previous sample extraction. This method provides useful data on



**Figure 3.6 Membrane lipid analysis by Fast Atom Bombardment Tandem Mass Spectrometry (FAB).** *Rhodobacter sphaeroides* membranes were extracted with acetone followed by chloroform/methanol 1:1 ratio and analyzed by FAB mass spectrometry to reveal the presence of phosphatidylthanolamine (PE), phosphatidylglycerol (PG), phosphatidylcholine (PC) and sulfolipids (SL). The numbers (underlined) indicate the mass and the calculated alkyl chains.

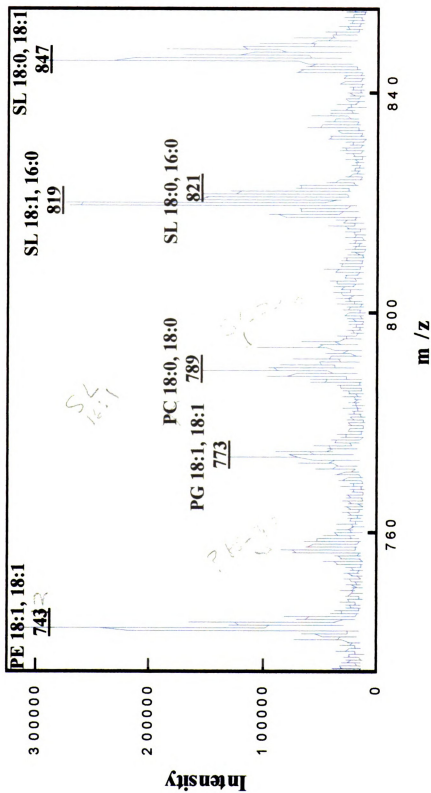


Figure 3.6

**Figure 3.7 Fatty acid composition by Fast Atom Bombardment Tandem Mass Spectrometry (FAB).** The underlined numbers indicate the mass of the peak, followed by the type of the alkyl chain.

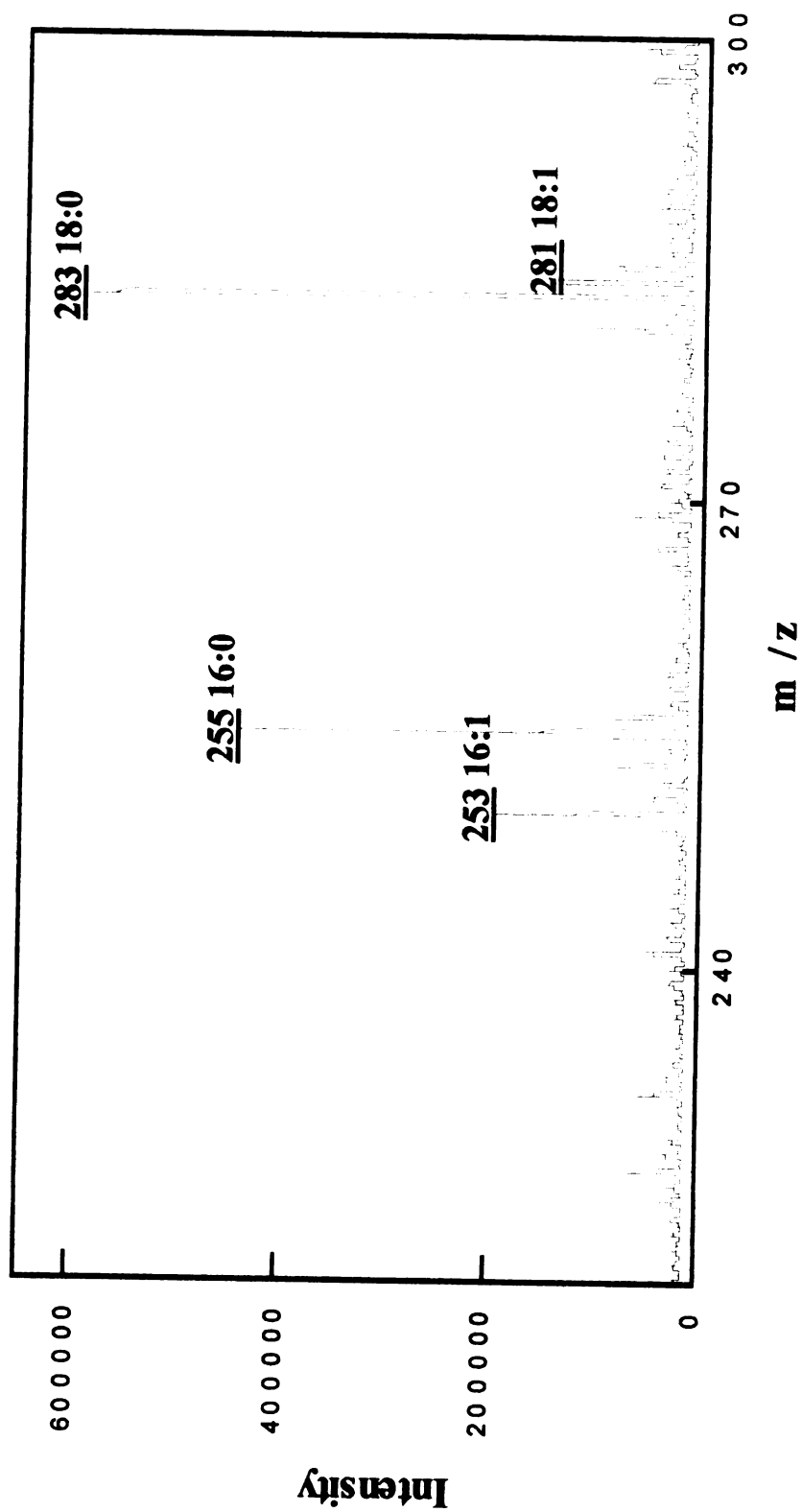


Figure 3.7

lipid composition, consistent with previous results from TLC and FAB techniques. With MALDI we were able to see the association between lipids and the protein subunits such as the association between cardiolipin and subunit IV of the oxidase (Figure 3.8). In addition, MALDI has the power of showing the intact protein with lipids associated (Figure 3.9), although this does not give quantitative information about relative amounts of the different lipids. A combination of TLC chromatography and MALDI spectrometry was also performed. Extracted samples were separated on a TLC plate, and each band from the plate was further analyzed with MALDI. These peaks were identified at 777, 745 and 787 m/z representing PG, PE and PC, respectively (Figure 3.10).

A more detailed mass spectrum (ms/ms) of a specific region provides more information about fragmentation of certain molecules, for example, the 184 m/z peak is a characteristic peak for the head group of phosphatidyl choline (Figure 3.10).

Interesting results were found when one crystal was re-dissolved and analyzed with MALDI (Figure 3.11). It was clear that the crystal contains phosphatidylcholine and it also contains phosphatidylethanolamine as reported in the crystal structure of *Rhodobacter sphaeroides* cytochrome *c* oxidase (Svensson-Ek *et al.*, 2002) (Figure 1.4).

**Figure 3.8 The association between cardiolipin and subunit IV of *Rhodobacter sphaeroides* cytochrome *c* oxidase.** The analysis was made by Matrix-Assisted Laser Desorption Ionization Mass Spectrometry (MALDI). Cardiolipin (CL) bound to the long form of subunit IV, and phosphatidylcholine (PC) bound to the short form of subunit IV. A potassium adduct was also detected (subunit IV + potassium ion).

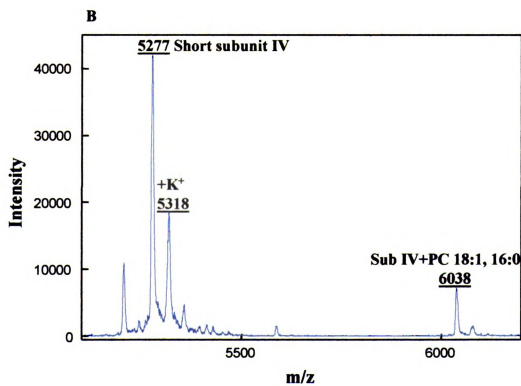
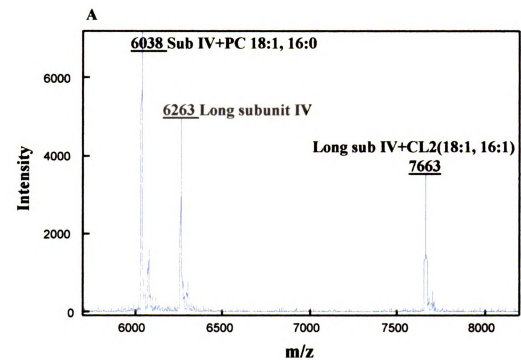


**Figure 3.8**

**Figure 3.9 Analysis of Ni<sup>2+</sup>-NTA purified cytochrome *c* oxidase by MALDI mass spectrometry.** Whole purified enzyme was analyzed with MALDI and phosphatidylethanolamine (PE), phosphatidylglycerol(PG) and sulfolipids (SL) were detected, with the indicated alkyl chain.



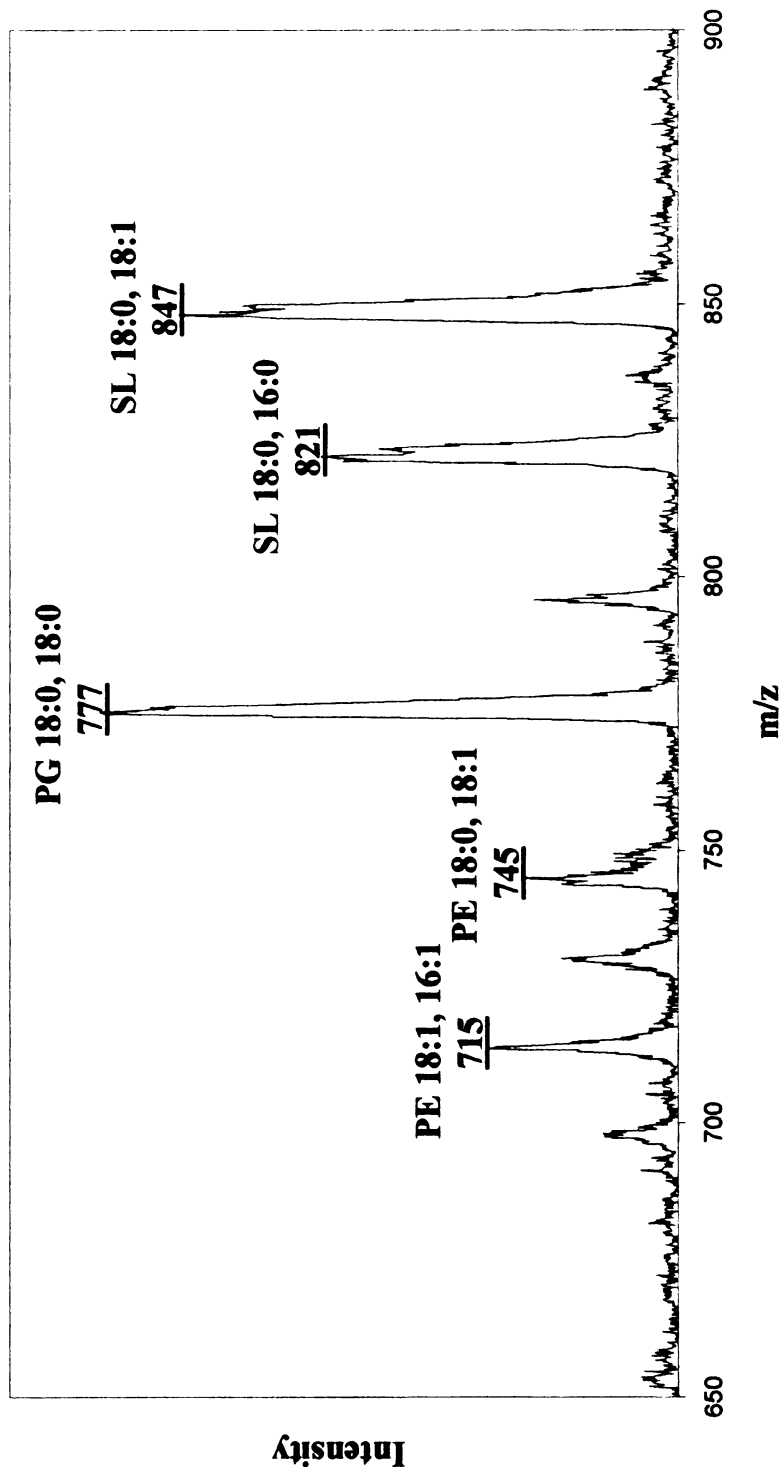
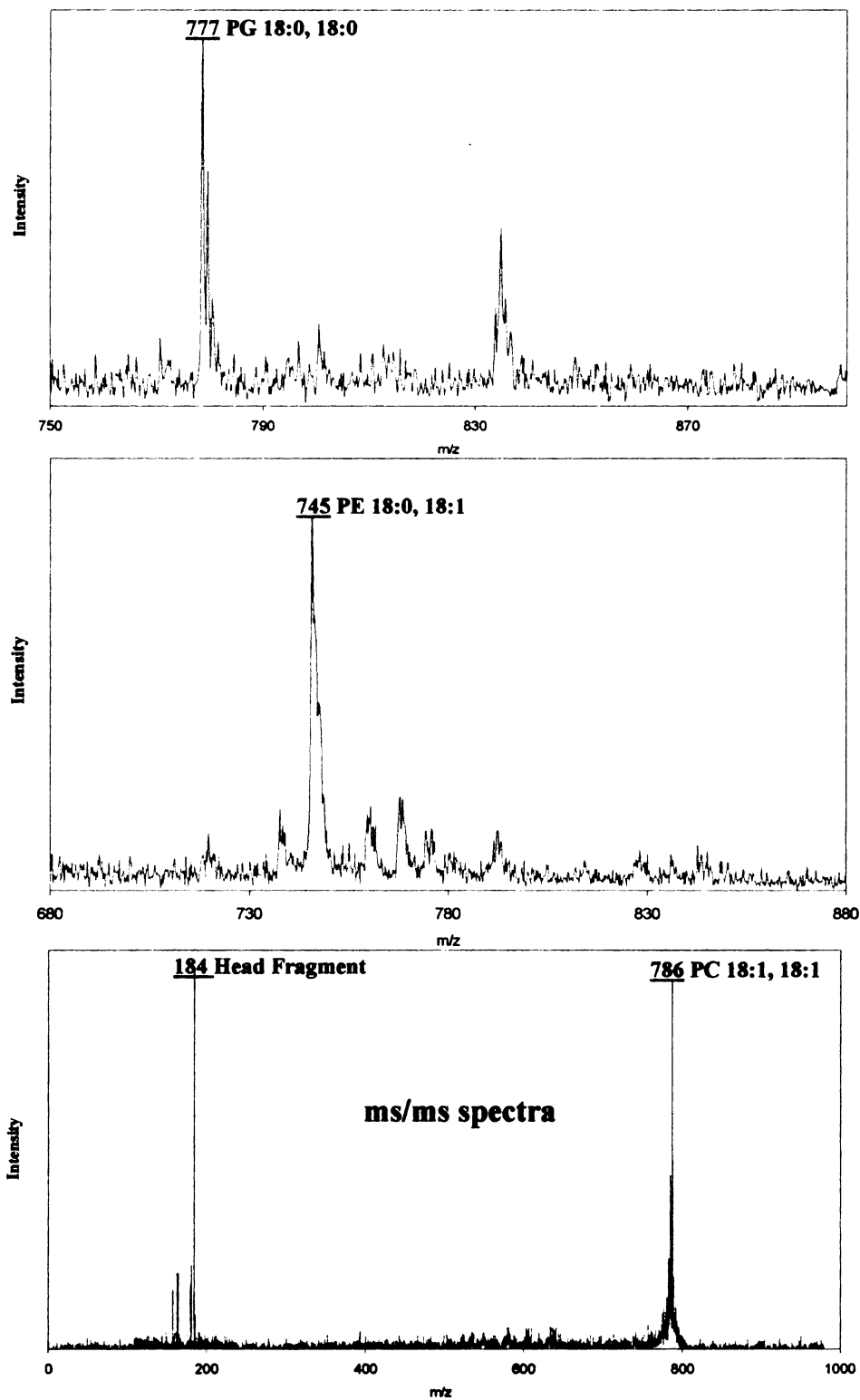


Figure 3.9

**Figure 3.10 Combining Thin Layer Chromatography and MALDI mass spectrometry for lipid analysis.** Membranes of *Rhodobacter sphaeroides* were lyophilized, extracted with acetone followed by chloroform/methanol extraction and applied to TLC plate. Specific bands were scratched from the plate and the silica was precipitated by centrifugation. The lipids were dissolved in chloroform and analyzed with MALDI. Top panel contains phosphatidylglycerol (PG) and band B contains phosphatidylethanolamine (PE). A more detailed spectrum (ms/ms) for band C showed a peak for phosphatidylcholine and a characteristic peak for its head group at 184 m/z.



**Figure 3.10**

**Figure 3.11 Lipid composition of a re-dissolved crystal analyzed with MALDI.** This data shows the presence of two major lipid components in *Rhodobacter sphaeroides*: phosphatidylcholine (PC) and phosphatidylethanolamine (PE), in a re-dissolved crystal, the crystal spectrum also contains sulfolipids (not shown in this figure). The crystal was dissolved in 10 µl of 10 mM Tris, 0.1% LM and directly analyzed with MALDI. In the crystallization procedure we use polyethylene glycol (PEG), as a protein precipitant, it shows strong peak signals in the spectrum.

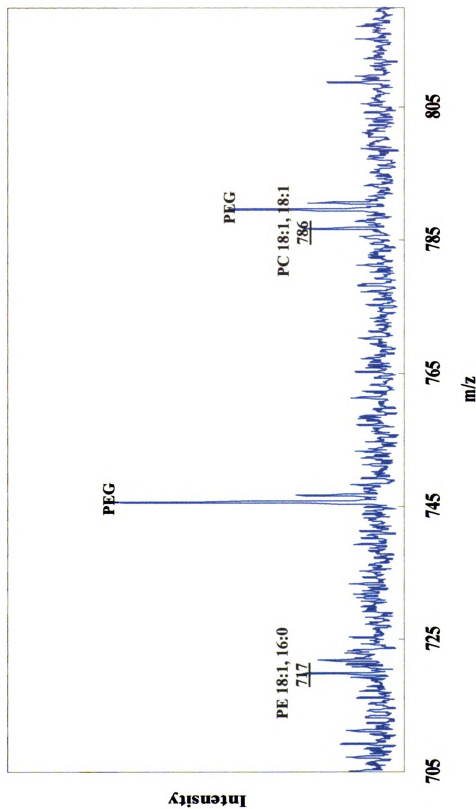


Figure 3.11

## DISCUSSION

Fast atom bombardment and matrix-assisted laser desorption ionization mass spectrometry are powerful methods for directly characterizing underivatized lipids, even in mixtures. These methods show mass ions indicative of the molecular weights of each of the molecular species present in the sample as well as fragments derived from elimination of the head groups or acyl groups. However, it is difficult to obtain quantitative information and to characterize the structure of some molecular species in a mixture with these methods, because the amount of each species desorbed from the probe is not proportional to the amount in the sample. In addition, the molecular ions of isomeric species overlap and fragments may be attributable to more than one molecular species. Therefore in this study we used mass spectrometry along with thin layer chromatography and phosphate analysis to analyze the lipid composition of *Rhodobacter sphaeroides* membranes and each stage of the oxidase purification.

Spectra from MALDI and FAB mass spectrometry show consistent peaks at certain regions that are equivalent to the calculated molecular weights for phosphatidylethanolamine, phosphatidylglycerol, phosphatidylcholine, cardiolipin and sulfolipid. The same samples were separated by a TLC method that provided an efficient separation, but since it is hard to control differences in humidity that allow lipids to migrate differently, we used standard lipids to confirm the types of lipids present in each sample at each condition.

Lipid analysis by thin layer chromatography and FAB mass spectrometry and in some cases by MALDI requires lipid extraction. The extraction efficiency is a major factor in lipid determination. When we used chloroform/methanol alone versus combined with ammonium extraction, tightly bound cardiolipin was resolved from the latter extraction method, but not detected in the former extract.

Another important factor is the water content in the sample, which is a variable that affects the lipid extraction and migration in thin layer chromatography; therefore all through our study we used lyophilized samples to control the water content. This was particularly important in permitting the extraction of detergents with dry acetone: if water was present in the sample, the acetone was not dry, and most of the lipids were extracted along with the detergent.

The purification method can be critical in permitting lipid retention. In order to maintain lipids that may be critical for crystallization, purification needs to be conducted very carefully with special attention to the nature and concentration of the detergent and the type of resin used. Ion exchange columns are not all alike, even when they have the same active groups. Both Mono Q and DEAE 5PW resins have the same ion-exchange chemistry, but are attached to different supporting matrices. Evidence suggests that the 5PW resin strips off more lipids than Mono Q (Hosler *et al.*, 1992).

In order to purify cytochrome *c* oxidase, as other membrane proteins, it must be solubilized with detergent to substitute for the native lipid bilayer where the membrane protein is naturally found. If too much or too strong detergent is used, more lipids may be removed. Hence it is sometimes necessary to sacrifice yield of oxidase by using a

relatively mild detergent and in lower concentration in order to retain the lipids (Qin, personal communication).

From this study we can conclude several major points:

- 1- Significant amounts of lipids remain bound to the oxidase after purification, at the level of about 10-15 molecules of lipids/molecule of oxidase from phosphate analysis and thin layer chromatography. Phosphate analysis shows 8-11 molecules phospholipids per purified oxidase, and TLC shows, besides the phospholipids, non-phosphorous containing lipids: sulfolipids and ornithine lipids.
- 2- Membranes from *Rhodobacter sphaeroides* cells that are grown under low and high oxygen contain the same type of lipids, though with slightly different ratios, with the exception of phosphatidylserine, found in the high oxygen conditions.
- 3- MALDI data provides interesting results on the association of certain lipids with specific subunits; for example, the association between the long form of subunit IV with cardiolipin, and the short form of subunit IV with phosphatidylcholine. In the unit cell of the crystal structure, subunit IV and subunit II form the major contacts between monomers of the oxidase. These lipids may thus be critical in maintaining the right form to allow crystal formation. In bovine heart oxidase structure at 2.0Å resolution, lipids were found associated with specific subunits. For example, five cardiolipins were found at interfaces between different subunits, III-VIa, III-VIIa, I-II-Vc, I-VIIc and I-II-IV. They also found one phosphatidylcholine, three phosphatidylethanolamine and five phosphatidylglycerol each at subunit interfaces. (Yoshikawa, personal communication). This further emphasizes that lipids are integrated in the protein molecules, apparently maintaining a stable homogenous



structure, and not just randomly distributed on the surface. A similar integration of lipid into the *Rhodobacter sphaeroides* oxidase structure is found in the crystal structure (Figure 1.4).

- 4- Purification of *Rhodobacter sphaeroides* oxidase affects the amounts of lipids associated with these proteins but not the types of lipids remaining even after several purification steps. This might seem somewhat surprising, but in fact it is consistent with the finding in the high resolution structure bovine oxidase that all the major lipids were found to co-crystallize with the protein each at different, highly specific sites.

In bacteriorhodopsin, a light-driven ion pump, 18 lipid molecules/protein monomer were identified in the crystal structure at 1.5 Å resolution (Luecke *et al.*, 1999). Crystals of this membrane protein were grown in lipidic cubic phase, a novel approach for crystallizing membrane proteins. The system consists of lipids (monooleoylglycerol and palmitoyl-lysophosphatidylcholine for two different phases), water (buffer) and protein in certain proportions to form a structured three-dimensional lipidic array that keeps the protein in a more membrane-like environment all through the crystallization process (Landau and Rosenbusch, 1996). In spite of this, the lipid that is found in the crystal, is that which had copurified from the native membrane, not that which had been added. In some other cases, as in crystallization of  $\text{Ca}^{+}$ -ATPase, a membrane protein that transfers ions across the membrane against a concentration gradient, lipid (phosphatidylcholine) was added to achieve a crystal structure at 2.6Å resolution, providing further evidence for the importance of lipids in achieving high resolution structures of integral membrane proteins.

The results of these studies, and results from crystallizing other membrane proteins, suggest a new paradigm for membrane protein structure: Lipids of many different kinds associate specifically, not randomly, with the protein structure and are important for maintaining a molecularly homogeneous configuration suitable for crystallization at high resolution (Garavito and Ferguson-Miller, 2001).

**CHAPTER IV**

**ENGINEERING OF *RHODOBACTER SPHAEROIDES* CYTOCHROME  $C_2$**   
**TO TEST THE MODEL OF THE Cc/CcO COMPLEX BY**  
**MAKING A COVALENT COMPLEX**

## INTRODUCTION

Cytochrome *c* is a soluble, highly charged, small (12 kDa), heme-containing protein that is an essential component of the terminal segment of the mitochondrial respiratory chain.

Mitochondria of higher eukaryotes contain a single, soluble and a highly conserved cytochrome *c* that functions as an electron carrier between the membrane-associated cytochrome *bc<sub>1</sub>* complex and cytochrome *c* oxidase, in the linear electron transfer chain of aerobic respiration. On the other hand, in some bacteria such as *Rhodobacter sphaeroides*, which are used widely for functional and structural studies on biological energy transduction, several aerobic and anaerobic electron transfer chains are used under different growth conditions. In these bacteria the presence of multiple electron transfer chains creates a physiological need to funnel electrons specifically to appropriate destinations. Thus in these species, unlike mitochondria, multiple cytochromes *c* function in parallel as electron carriers with seemingly overlapping function.

Photosynthetic and respiratory electron transfer chains of *Rhodobacter sphaeroides* provide a useful model system for studies on cellular energy transduction. In this species photosynthetic growth depends on the cyclic electron transfer between the photochemical reaction center and the cytochrome *bc<sub>1</sub>* complex. In this process cytochrome *c<sub>2</sub>* or its functional analogue isocytochrome *c* are needed as an electron carrier between the two proteins. During aerobic respiratory growth *Rhodobacter sphaeroides* appears to use a membrane bound cytochrome *c<sub>y</sub>* as an electron carrier between the *bc<sub>1</sub>* complex and cytochrome *c* oxidase (Myllykallio *et al.*, 1999). A recent

study provides some evidence of the involvement of cytochrome  $c_2$  as well as cytochrome  $c_y$  in the electron transfer process during the respiratory growth (Daldal *et al.*, 2001).

In this study we used cytochrome  $c_2$  as a substrate, since it is a soluble protein and the gene sequence for it is available, and we had access to an overproducing strain so that we could obtain adequate amounts for our studies. On comparison between cytochromes  $c$  from different species, we found that some of the lysine residues that are important for specific binding between cytochrome  $c$  and cytochrome  $c$  oxidase were missing in *Rhodobacter sphaeroides* cytochrome  $c_2$  (Figure 4.1). Therefore we modified cytochrome  $c_2$  by putting back Lys 13 and Lys 72 for a better binding (Figure 4.2). Then we introduced a histidine-tag at the C-terminus of the protein to facilitate the purification of the enzyme (Figure 4.2) We also introduced a cysteine residue (Cys 39 and Cys 60) at the back of the molecule to attach a ruthenium group to study the rapid electron transfer process between cytochrome  $c$  and cytochrome  $c$  oxidase and thus test our success in creating a good interaction with cytochrome oxidase (Figure 4.2).

A goal of this study was to use a further modified cytochrome  $c_2$  to obtain a stable complex between cytochrome  $c$  and cytochrome  $c$  oxidase to serve as an effective tool for crystallizing the oxidase and to test the accuracy of the predicted native interaction of cytochrome  $c$  with the oxidase. This study involved insertion of cysteines in cytochrome  $c_2$  and in the oxidase, guided by a computational prediction of the docking interaction between cytochrome  $c$  and cytochrome  $c$  oxidase done by Roberts and coworkers (Roberts and Pique, 1999). Using this model, the best position in the two proteins for creating inter-molecular disulfide bond were between Ala 83 of cytochrome  $c$  and Ala213

**Figure 4.1 Comparison of lysine residues on the front face of cytochromes *c* from horse, *Rhodobacter sphaeroides* and *Paracoccus denitrificans*.** The conserved lysine residues that have been shown to be critical for cytochrome *c* structure and binding are labeled in horse numbering: Lys 8 (gold), 13 (light blue), 27 (brown), 72 (yellow), 73 (black), 79 (dark blue), 86 (green), 87 (red). The heme edge is bright green. The corresponding lysines are similarly color in *Rhodobacter sphaeroides* *c*<sub>2</sub> and *Paracoccus denitrificans* *c*<sub>550</sub>. The missing Lys13 is indicated as white circle in *Rhodobacter sphaeroides* *c*<sub>2</sub>, while the missing Lys72 is indicated by the lack of the yellow residue close to the black Lys73. Other lysines that are not conserved or critical are indicated in magenta. This figure was made by Dr. Y. Zhen (unpublished).

## Comparison of Cytochromes *c*

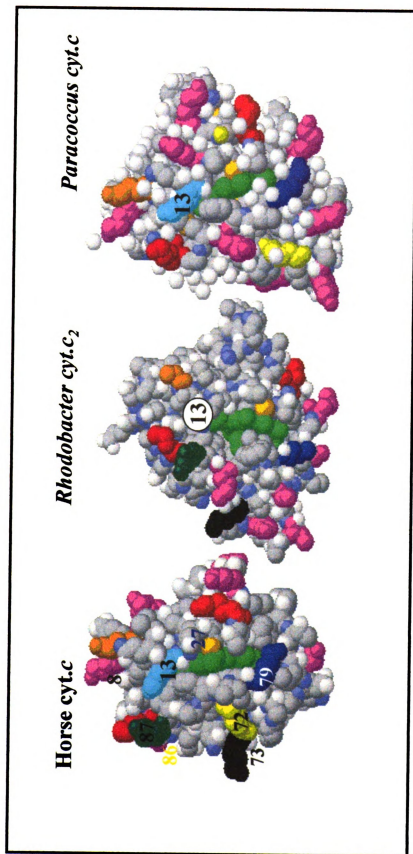


Figure 4.1





**Figure 4.2 Crystal structure of horse cytochrome *c*.** The lysines that are involved in binding with oxidase are shown in yellow and magenta. The yellow ones (Lys 8, Lys 86, Lys 87 and Lys 73) are found in *Rhodobacter sphaeroides* cytochrome *c*<sub>2</sub>, whereas Lys13 and Lys72 are not. Residues 13 and 72 were changed to lysines as mentioned in Materials and Methods. Cys 39 and Cys 60 (green) indicated the position of cysteine mutations at these positions (in two different mutants) to measure the intrinsic electron transfer by attaching ruthenium groups at these positions. This figure also shows the C-terminal where the five histidines were inserted to facilitate the purification process by Ni affinity chromatography.

## Cytochrome *c*

Front view



Side view

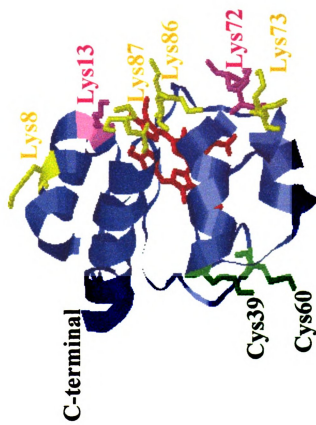


Figure 4.2

of the oxidase on one hand, and Gln 12 of cytochrome *c* and Tyr 159 of the oxidase on the other (Figure 4.3). We changed each of these pairs of residues to cysteines in order to form a covalent cytochrome *c*/cytochrome *c* oxidase complex, assuming that the predicted complex is correct and therefore the engineered cysteine pairs will be brought into close proximity.

**Figure 4.3 Cysteine mutants at the interface between cytochrome *c* and subunit II of the oxidase.** The coordinates for the position of cytochrome *c* (red) and subunit II of the oxidase (green) are from (Roberts and Pique, 1999). Two residues on cytochrome *c*, glutamine 12 (blue) and alanine 83 (blue), and two residues on the oxidase, tyrosine 159 (black) and alanine 213 (black), were changed to cysteines to test for sulfhydryl linkage between the two proteins. For cytochrome *c* the horse numbering is used and for oxidase residues *Rhodobacter sphaeroides* numbering is used.

**Cytochrome *c***

**CcO subunit II**

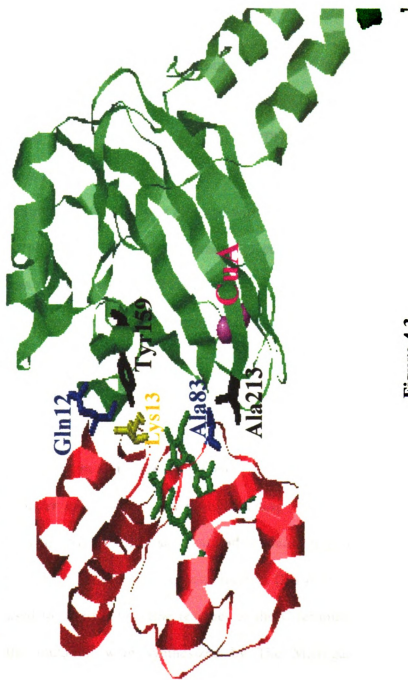


**Figure 4.3**



## MATERIALS AND METHODS

### Site-Directed Mutagenesis on Cytochrome $c_2$

The *Rhodobacter sphaeroides* cytochrome  $c_2$  mutants were made by a PCR overlapping method (Ho *et al.*, 1989). For each mutant four oligo primers were synthesized and used (Figure 4.4). The plasmid pC2PH19 containing *cycA*, a gene encoding cytochrome  $c_2$ , was used as a template (Donohue *et al.*, 1988). The 1583 bp PCR product containing the mutation was digested with PstI/HindIII restriction enzymes, subcloned into the plasmid pUC19 and sequenced to confirm the mutation. Then the pUC19 plasmid was digested with EcoRI/HindIII and a 1605 bp fragment carrying the mutated gene was subcloned to pRK415 plasmid and transformed into JM109 and S17-1 *E.coli* strain. Finally S17-1 was conjugated with *Rhodobacter sphaeroides* CYCA1, a cytochrome  $c_2$  deleted strain.

### Insertion of Histidine-Tag in Cytochrome $c_2$ Gene

The *Rhodobacter sphaeroides* *cycA* gene, encoding for cytochrome  $c_2$ , which is contained on a 1538 bp PstI/HindIII restriction endonuclease fragment, was subcloned into pUC19 plasmid. A PCR-based mutagenesis method (Ho *et al.*, 1989) utilizing Pfu polymerase was used to insert 5 histidine residues at the C-terminus. The primers that were used for the mutation were synthesized by The Michigan State University Molecular Structural Facility and are shown in (Figure 4.5). The fragment containing the mutation was subcloned into the plasmid pUC19 after it was digested with PstI/Hind III

**Figure 4.4** Oligonucleotide sequences of wild type and mutants of *Rhodobacter sphaeroides* cytochrome  $c_2$ .



WT 5'- TTC AAC CAG TGC CAG ACC TGC CA - 3'

Q13K 5'- TTC AAC AAG TGC CAG ACC TGC CA - 3'

WT 5' – GAT CCG ACC AAG TTC CTG AAG G – 3'

T72K 5' – GAT CCG AAG AAG TTC CTG AAG G – 3'

WT 5' – G GCC TTC AAC CAG TGC CAG AC – 3'

N12C 5' – G GCC TTC TGC CAG TGC CAG AC – 3'

WT 5' – G ATG ACC TTC AAG CTG AAG AA – 3'

K83C 5' – G ATG ACC TTC TGC CTG AAG AA – 3'

WT 5' – TC GTG GGC CGC ACC GCG GGC – 3'

T39C 5' – TC GTG GGC CGC TGC GCG GGC – 3'

Figure 4.4

**Figure 4.5 Wild type and histidine-tag insertion oligonucleotide sequences of *Rhodobacter sphaeroides* cytochrome  $c_2$**

WT 5'- AG CAG GTC GCC GTC CGG CCC TGA – 3'

His-tag 5'-AG CAG GTC GCC GTC CGG CCC CAC CAC CAC CAT CAT TGA–3'

Figure 4.5

restriction enzymes, and sequenced. After successful insertion of a histidine tag, the fragment containing the *cycA* gene was subcloned to pRK415 plasmid and transformed to JM109 and S17-1 *E.coli* strains and finally conjugated with *Rhodobacter sphaeroides* CYCA1, a cytochrome  $c_2$  deleted strain.

### **Prediction of Positions for Cysteine Interactions**

Based on the original computational model for the cytochrome *c*/cytochrome *c* oxidase complex by Roberts and coworkers (Roberts and Pique, 1999), Hespenheide searched for all the possible pairs of disulfide forming residues in this complex using the computer program Insight II. His search resulted in four possibilities: Cc 12 with CcO 159, Cc 83 with CcO 213, Cc 83 with CcO 214 and Cc 77 with CcO 183. These pairs were identified by searching for any pair of C- $\alpha$  atoms between the *Rhodobacter sphaeroides* oxidase and the docked cytochrome *c* that were at a distance of 4-7.5 Å (Hespenheide, personal communication).

### **Cell growth and Membrane Preparation**

*Rhodobacter sphaeroides* cytochrome  $c_2$  was isolated from a cytochrome  $c_2$  overexpression strain CYCA1 (pC2P404.1) (Brandner *et al.*, 1989). The cells were grown photosynthetically to maximize cytochrome  $c_2$  expression, and harvested at late exponential phase; this increases cytochrome  $c_2$  yield by 2-4 fold. The harvested cells were resuspended in a solution of 100 mM  $\text{KH}_2\text{PO}_4$ , pH 7.0, in the presence of small amounts of DNase and RNase, and were broken by two passages through a French pressure cell at 20,000 psi. Whole cells and debris were removed by centrifugation at

20,000 g for 20 min. The supernatant was centrifuged again at 45,000 g for 1 hour. The red photosynthetic pigments and membranes were precipitated in this step. The supernatant containing cytochrome *c* was saved in a  $-80^{\circ}\text{C}$  freezer.

### **Hydroxylapatite Column**

The supernatant from the ultracentrifugation was loaded onto a hydroxylapatite column pre-equilibrated with 10 column volume of 10mM  $\text{KH}_2\text{PO}_4$  pH 7.0. After loading the sample the column was washed with 100 mM  $\text{KH}_2\text{PO}_4$ , pH7.0, and cytochrome *c*<sub>2</sub> was eluted with 150 mM  $\text{KH}_2\text{PO}_4$ , pH 7.0. The fractions containing cytochrome *c*<sub>2</sub> were washed and concentrated in 5 mM Tris, pH 7.0 to be further purified with DEAE-cellulose column

### **DEAE-Cellulose Column**

The fractions containing cytochrome *c*<sub>2</sub> were loaded onto a DEAE-cellulose column pre-equilibrated with 5 mM Tris, pH 7.0. The column was washed with 5 mM Tris, 25 mM NaCl, pH 7.0. Cytochrome *c*<sub>2</sub> was eluted with 5 mM Tris, 100 mM NaCl, pH 7.0. The sample was then concentrated and kept in  $-80^{\circ}\text{C}$ .

### **$\text{Ni}^{+2}$ -NTA Affinity Chromatography Column**

A supernatant from membrane preparation was mixed with Ni resin (1 ml resin/ 2 mg protein) and stirred for one hour at  $4^{\circ}\text{C}$ . The mixture was loaded onto a gravity column and washed with 5 mM imidazole, 10 mM Tris, 40 mM KCl, pH 8.0.

Cytochrome *c* was eluted with 100 mM imidazole, 10 mM Tris, 40 mM KCl, pH 8.0. The eluant was washed and concentrated in 10 mM Tris, 40 mM KCl, and stored at a  $-80^{\circ}\text{C}$ . In the case of cysteine mutants, all buffers contained 5 mM dithiothreitol reducing agent (DTT) to prevent dimerization.

### Visible Spectra

Visible spectra for cytochrome *c*<sub>2</sub> were detected with a Perkin-Elmer Lambda 40P UV-visible spectrophotometer. The protein was diluted in 50 mM KH<sub>2</sub>PO<sub>4</sub> pH 7.0 and scanned from 700 nm to 400 nm and the amount of enzyme was estimated using the extinction coefficient:  $\Delta E_{(550-600\text{ nm})} = 28\text{ cm}^{-1}\text{ mM}^{-1}$  for dithionite reduced spectra and  $\Delta E_{(550-540\text{ nm})} = 16.5\text{ cm}^{-1}\text{ mM}^{-1}$  for dithionite reduced minus ferricyanide oxidized difference spectra.

To compare the purity of cytochrome *c* with different purification methods, absorbance of total protein at 280 nm was recorded and  $A_{280}/A_{410}$  was calculated.

### Activity measurement

Oxygen consumption was measured polarographically using an oxygen electrode at  $25^{\circ}\text{C}$  in 50 mM KH<sub>2</sub>PO<sub>4</sub>, pH 6.5 containing 2.8 mM ascorbate, 1.0 mM TMPD, 0.05% LM, 4 mg/ml phospholipids and 20  $\mu\text{M}$  horse heart cytochrome *c* in 1.8 ml total volume. The turnover number (molecular activity) was calculated as electrons/second/molecule of oxidase. For analysis of steady- state kinetics, 0.05 n moles of *aa*<sub>3</sub> and a range of concentrations of cytochrome *c*<sub>2</sub> (1- 22  $\mu\text{M}$ ) were used.

### **Spin Column**

A spin column was used to wash the dithiothreitol, a reducing agent, from the proteins. A 1 ml syringe was used and 0.5 ml of G-10 Sephadex resin was loaded into the column. The column was then washed with 10 mM Tris, 10 mM KCl, 0.15% lauryl maltoside, pH 7.0, and spun for 5 minutes at 3000 rpm to partially dry the column. 40  $\mu$ M cytochrome *c* and 40  $\mu$ M cytochrome *c* oxidase in a total volume of 100  $\mu$ l were loaded into the column. The column was spun for another 5 minutes at 2500 rpm to elute cytochrome *c* and cytochrome *c* oxidase leaving behind the dithiothreitol. The eluant was incubated for one hour at 4°C before loading onto a second gel-filtration column to test for the formation of the cross-linkage between the two proteins.

### **Gel-filtration Column**

The eluant from the spin column (100  $\mu$ L) containing approximately 30  $\mu$ M of each proteins was loaded onto a 20 cm x 0.5 cm column containing 2.5 ml Sephadex G-75 resin in it. The column was pre-equilibrated with 5 column volume of 10 mM Tris, 100 mM  $\text{KH}_2\text{PO}_4$ , 0.15% lauryl maltoside, pH 7.0. The sample was eluted with 10 mM Tris, 100 mM  $\text{KH}_2\text{PO}_4$ , 0.15% lauryl maltoside, pH 7.0 into 100  $\mu$ l fractions and spectra were taken for each fraction. High ionic strength was used to insure that any complex observed was covalently bound, not just electrostatically.

### **SDS-PAGE**

Sodium dodecyl sulfate polyacrylamide gel electrophoresis was used to detect the subunits of the oxidase and cytochrome *c* contained in the sample. Approximately 10  $\mu$ g

of sample, dissolved in 0.08% SDS in 0.5M Tris buffer, were used with an 8% stacking gel at pH 6.8 and 14% separating gel at pH 8.8 with conditions as described (Hiser *et al.*, 2001). The gel was polymerized for 2 hours and run for 1 to 1.5 hours at 200V. The gel was stained with TMB (3,3',5,5'-Tetramethylbenzidine) (Daldal *et al.*, 2001) for peroxidase activity associated with bound heme, to detect the positions of cytochrome *c*, then de-stained with sodium sulfide and stained again with Coomassie blue in acetic acid and methanol for the oxidase subunits.

### **MALDI Mass Spectrometry**

MALDI mass spectra experiments were performed by using a Voyager-DE STR MALDI-TOF mass spectrometer (PerSeptive Biosystems, Framingham, MA) equipped with delayed ion extraction. The samples were irradiated with a N<sub>2</sub> laser at 337 nm, producing 3 ns wide pulses. The spectra were acquired in positive-ion linear mode at 25 kV initial acceleration voltage.

Samples were prepared with the dried-droplet method, mixing 1 µl of sample, diluted in 60% formic acid, with 1 µl of sinapinic acid solution [10 mg/ml in acetonitrile-0.1% trifluoroacetic acid 1:1 (v/v)] and applied directly to the probe.



## RESULTS

### Design of The Mutants

To improve the binding ability between cytochrome  $c_2$  and the oxidase to make it better resemble the substrate used in docking analyses (horse cytochrome  $c$ ) and the likely physiological substrate  $c_y$ , we introduced lysine residues at two different positions: Gln 13 and Thr 72 in cytochrome  $c_2$ . These lysines residues have been shown to play an important role in binding between cytochrome  $c$  and cytochrome  $c$  oxidase (Ferguson-Miller *et al.*, 1978; Zhen *et al.*, 1999). The effect of the mutations was determined by measuring the activity and kinetics of each mutant with the oxidase. Introduction of Lys 72 by itself did not change the binding affinities estimated by the apparent  $K_m$  of the steady-state kinetics, whereas the introduction of a lysine at position 13, improved the binding significantly (Figure 4.6). As a further test of the interaction, cysteine residues were introduced at positions 39 and 60 (in different molecules) at the backside of cytochrome  $c$  mutant Q13K. These mutations were made to enable the measurement of rapid electron transfer between cytochrome  $c$  and the oxidase within the complex, by allowing the attachment of a ruthenium group as a photo-activated electron donor to cytochrome  $c$ . Our collaborators at University of Arkansas are attempting to label the T39C/Q13K and D60C/Q13K mutants with ruthenium as an electron donor, although a high tendency to self dimerize has so far made the experiments difficult.

To test the computational model of the docking site of cytochrome  $c$  on the oxidase we created two cysteine mutants K83C and N12C on cytochrome  $c$  to form a cross-linkage with cytochrome  $c$  oxidase cysteine mutants (A213C and Y159C,

**Figure 4.6 Steady-state kinetics of *Rhodobacter sphaeroides*  $c_2$  wild type and mutants with *Rhodobacter sphaeroides* cytochrome *c* oxidase.** Horse cytochrome *c* was used as a control that has higher affinity for binding with *Rhodobacter sphaeroides* oxidase than its own wild type R.s. cytochrome  $c_2$ . In this figure the steeper the curve the lower the apparent  $K_m$ , which appears to reflect higher binding affinities. All mutants that contain Lys13 showed higher affinity than the wild type. The curve in this Eadie-Hofstee plot can be analyzed as two different interactions of cytochrome *c* with the oxidase, one high affinity, one low affinity (Ferguson-Miller *et al.*, 1978; Zhen *et al.*, 1999). The introduction of lysine at position 13 appears to increase both affinities.

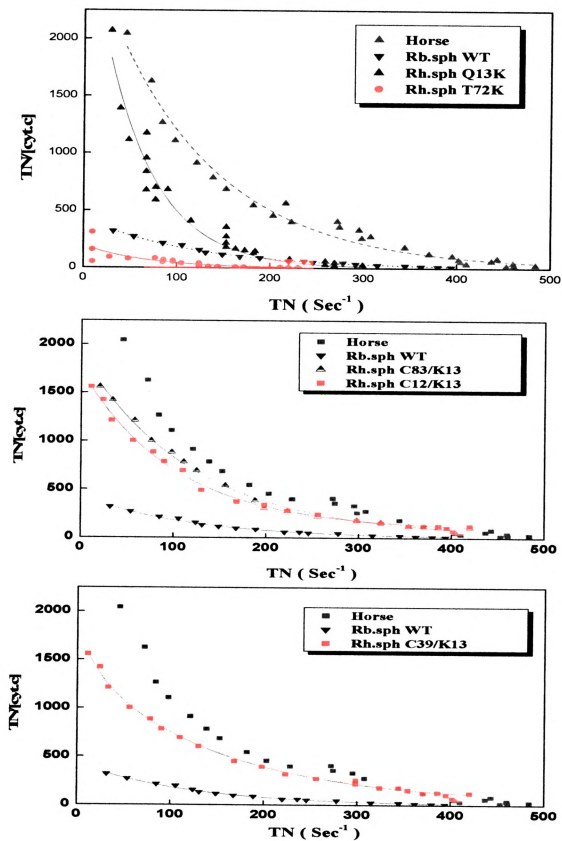


Figure 4.6

respectively). Also double mutants were made with Lys 13 as follows: Q13K/K83C and Q13K/N12C. (Table 4.1) shows all mutants that were made for these studies.

All the mutations were done successfully and sequencing of the region of the mutation showed no secondary mutation was introduced in any case. All the mutants were expressed in *Rhodobacter sphaeroides* with expression levels similar to wild type, except some of the cysteine mutants, especially (T39C), where the expression level was significantly lower (50% of the wild type).

### **Purification**

The common method that has been used for cytochrome *c* purification was hydroxylapatite followed by DEAE-cellulose ion-exchange chromatography (Meyer and Cusanovich, 1995). Hydroxylapatite chromatography is an efficient technique for separating different cytochromes *c* from other proteins and each other, but the end product is not very pure and needs further purification. DEAE-cellulose ion-exchange chromatography increased the purity significantly, but the yield decreased dramatically. Although a combination of these two methods gave a pure sample, the yield was very low especially for the cysteine mutants.

Ni<sup>2+</sup>-NTA affinity chromatography has been known to be a very rapid and efficient procedure for purifying histidine-tagged proteins. Therefore we fused five-histidine residues to the C-terminus of cytochrome *c* and used the Ni-column system for purification. The histidine-tagged protein was examined structurally and functionally and it behaves like the non-histidine-tagged wild type.

**Table 4.1 Characteristics of Cytochrome  $c_2$  Mutants From *Rhodobacter Sphaeroides***

Horse Cc Residue	R.S. Cc Residue at Same Position	Mutation	Optical Spectra (nm)	Purity $A_{280}/A_{416}$	Yield (%)
K13/his	Q14	Q $\rightarrow$ K	550	0.25	70
K72/his	T84	T $\rightarrow$ K	550	0.25	75
Q12	N13	N $\rightarrow$ C	550	2.5	18
A83	K103	K $\rightarrow$ C	550	3.0	24
K39	T47	T $\rightarrow$ C	550	NA	<5
K60	D72	D $\rightarrow$ C	550	3.0	20
K13/K39/his	Q14/T47	Q/T $\rightarrow$ K/C	550	0.15	50
K13/ K60/his	Q14/D72	Q/D $\rightarrow$ K/C	550	0.14	70
K13/ Q12/his	Q14/N13	Q/N $\rightarrow$ K/C	550	0.13	70
K13/ A83/his	Q14/K103	Q/K $\rightarrow$ K/C	550	0.13	75

R.S. *Rhodobacter sphaeroides*

Cc cytochrome *c*

his histidine-tag

This method is faster (takes about 4 hours compared to two full days for hydroxylapatite and ion-exchange chromatography), and has higher purity and higher recovery than the other two methods. Comparison between these methods is shown in (Table 4.2). Spectral analysis shows that Ni-affinity chromatography is a procedure that can result in a protein with very high purity (Figure 4.7).

### **Visible spectra and activity**

In the reduced form, wild-type cytochrome  $c_2$  from *Rhodobacter sphaeroides* has characteristic absorbance peaks at 416 nm and 550 nm, known as the Soret and  $\alpha$ -bands, respectively. All the mutants have the wild-type spectral characteristics (Figure 4.8) indicating that there is no global change in the protein structure.

The maximum turnover numbers of the cytochrome  $c$  with cytochrome  $c$  oxidase have been measured using wild-type cytochrome  $c_2$  from *Rhodobacter sphaeroides* and cytochrome  $c_2$  mutants (Q13K, T72K, N12C, K83C, Q13K/T39C, Q13K/K60C, Q13K/K83C and Q13K/N12C) from the same species at high concentration (20 $\mu$ M) of cytochrome  $c_2$ . All the mutants have the wild-type turnover at high concentrations (Figure 4.6)

### **Steady-State Kinetic Assay**

The steady-state kinetics of wild-type and mutant cytochromes  $c_2$  with *Rhodobacter sphaeroides* cytochrome  $c$  oxidase have been measured polarographically. At high level of cytochrome  $c$  (20 $\mu$ M) all mutants show high activity with the oxidase, whereas at low cytochrome  $c$  concentration, only mutants that contain Lys13 (Q13K, Q13K/K83C and Q13K/N12C) gave a high turnover with the oxidase compare to horse

**Table 4.2 Comparison Between Different Purification Techniques**

<b>Method</b>	<b>Purity <math>A_{280}/A_{410}</math></b>	<b>Yield %</b>
Hydroxylapatite	3	24%
DEAE-Cellulose Ion-Exchange Chromatography	0.25	12%
Ni <sup>2+</sup> -NTA Affinity Chromatography	0.13	75%





**Figure 4.7 Spectral analysis to test the efficiency of Ni<sup>2+</sup>-NTA method in comparison with other purification methods.** Samples were purified with Hydroxylapatite column, DEAE-Cellulose ion-exchange chromatography and Ni<sup>2+</sup>-NTA affinity chromatography. The latter method gave the highest purity, measured as  $A_{280}/A_{416}$ .

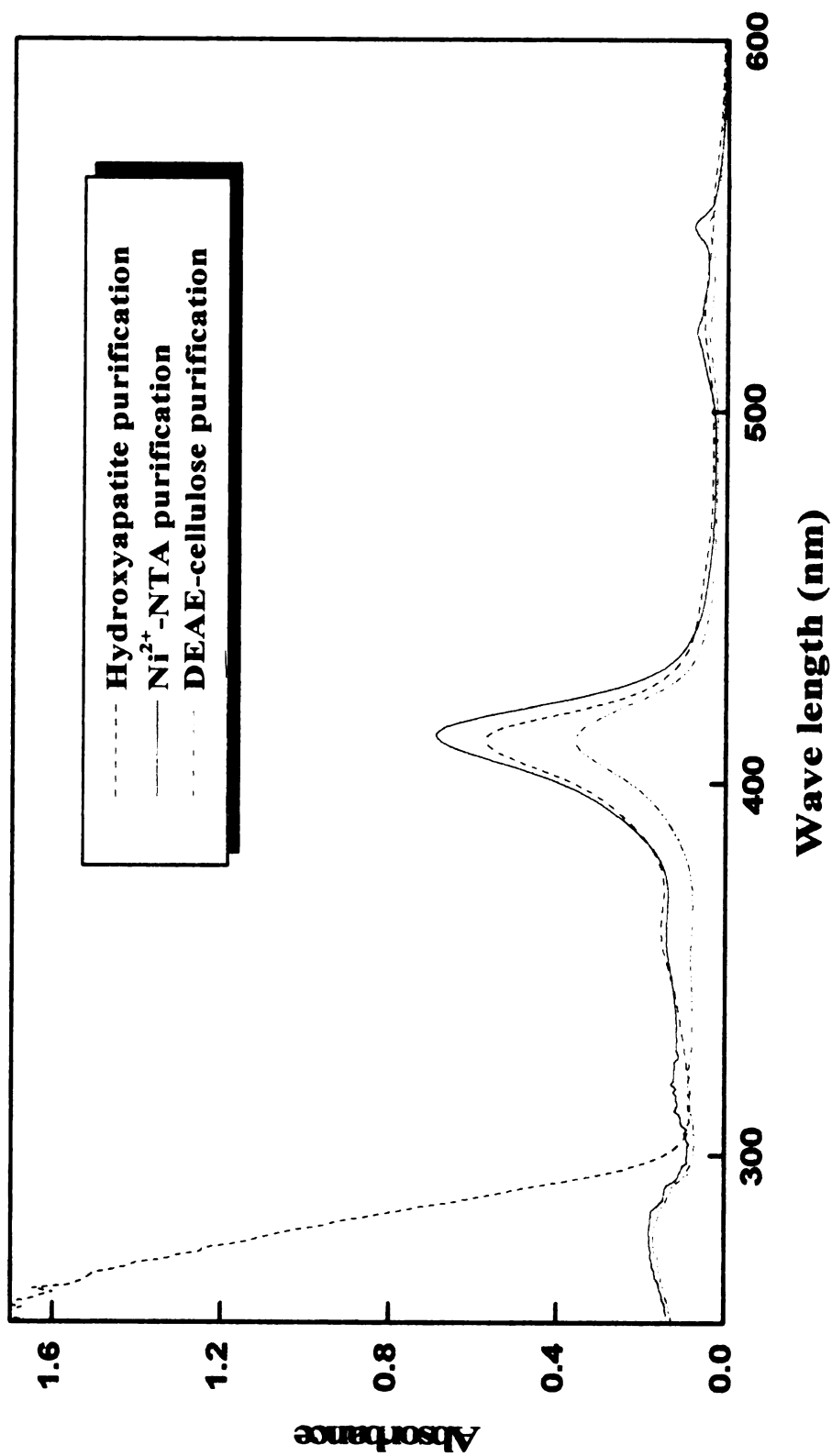
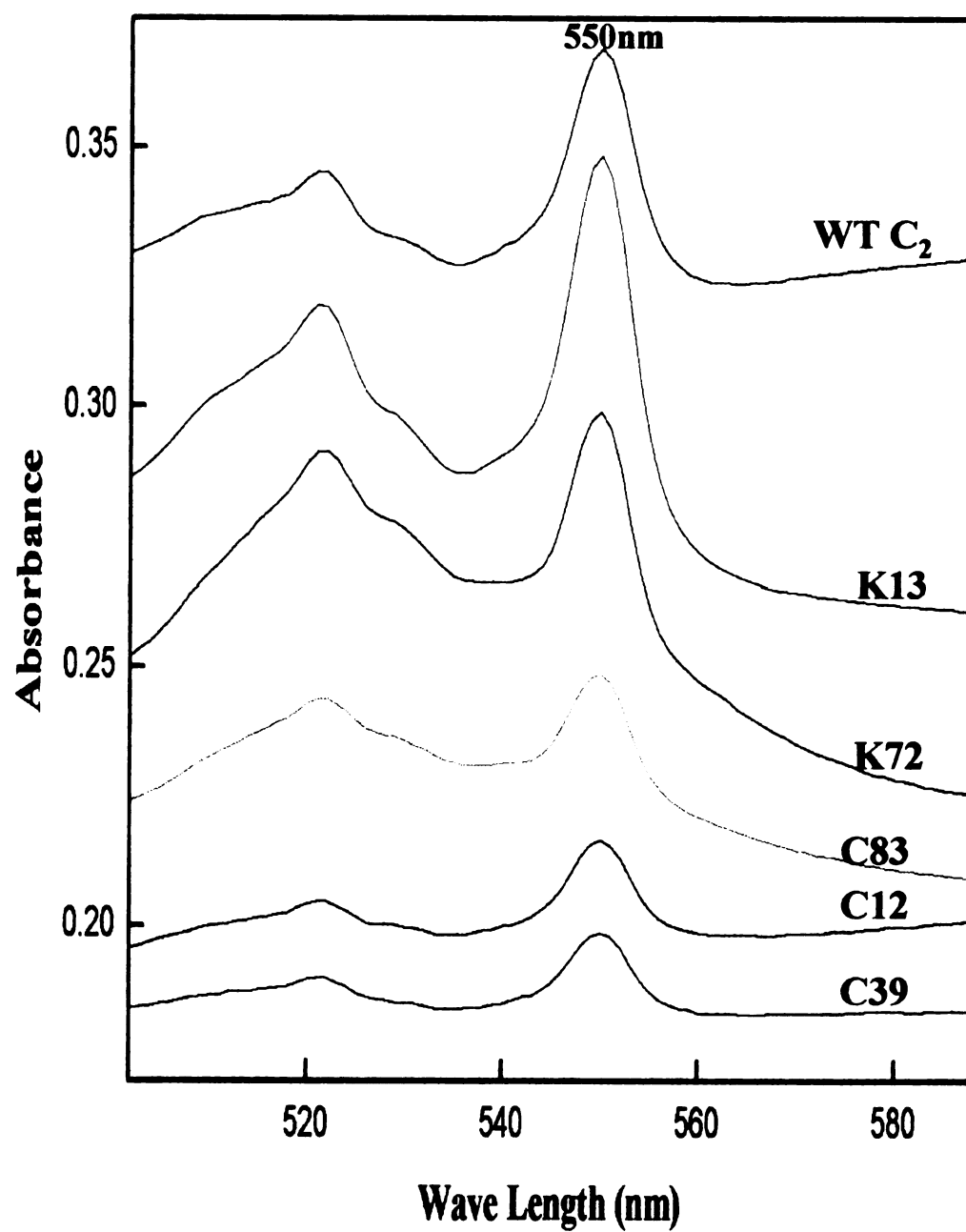


Figure 4.7

**Figure 4.8 Visible spectra for wild type and mutants of cytochrome  $c_2$  from *Rhodobacter sphaeroides*.** Dithionite-reduced absolute spectra of the purified enzyme were recorded with Perkin-Elmer Lambda 40P UV-visible spectrophotometer, showing characteristic peak at 550 nm for cytochrome  $c_2$ .



**Figure 4.8**

cytochrome *c*, indicating increased affinity for binding of these mutants with the enzyme. This is evidence for the importance of Lys13 in the binding between the two proteins (Figure 4.6).

### **Complex Formation**

Using cysteine mutants for this experiment, we were faced with dimerization of cytochrome *c*. In order to keep this protein in its monomer form we used a reducing agent (DTT) through all the purification steps. This prevented dimerization to some extent but it also prevented the cysteines on cytochrome *c* from forming cross-links with cysteine residues on the oxidase. Therefore we used a spin column to wash out the reducing agent only after the two proteins were mixed.

After one-hour incubation, without reducing agent, a solution containing cytochrome *c*<sub>2</sub> and cytochrome *c* oxidase cysteine mutant-pairs was loaded onto a gel filtration column to separate unbound cytochrome *c* from oxidase and oxidase with cytochrome *c* covalently attached (the latter two species are expected to elute together). The spectra and elution profiles provided evidence that separation between oxidase and free cytochrome *c* was sufficient to detect whether there was bound cytochrome *c* (Figure 4.9, Figure 4.10 & Figure 4.11). By plotting the data for Cc12/CcO159 (Figure 4.10) and for Cc83/CcO213 (Figure 4.11) and comparing it with the data for the wild type oxidase and wild type horse cytochrome *c* in high salt to prevent complex formation (Figure 4.12), it clearly indicated formation of a cytochrome *c*/cytochrome *c* oxidase complex.

**Figure 4.9 Elution profile for different fractions from gel-filtration column for cytochrome *c* cysteine mutant (N12C) with cytochrome *c* oxidase subunit II cysteine mutant (T159C). Ni<sup>2+</sup>-NTA purified cytochrome *c* and cytochrome *c* oxidase (40 μM each) were incubated for one hour and loaded onto sephadex G-75 gel-filtration column. Fractions containing cytochrome *c* oxidase (plus any complex) eluted first, followed by fractions containing free cytochrome *c*.**

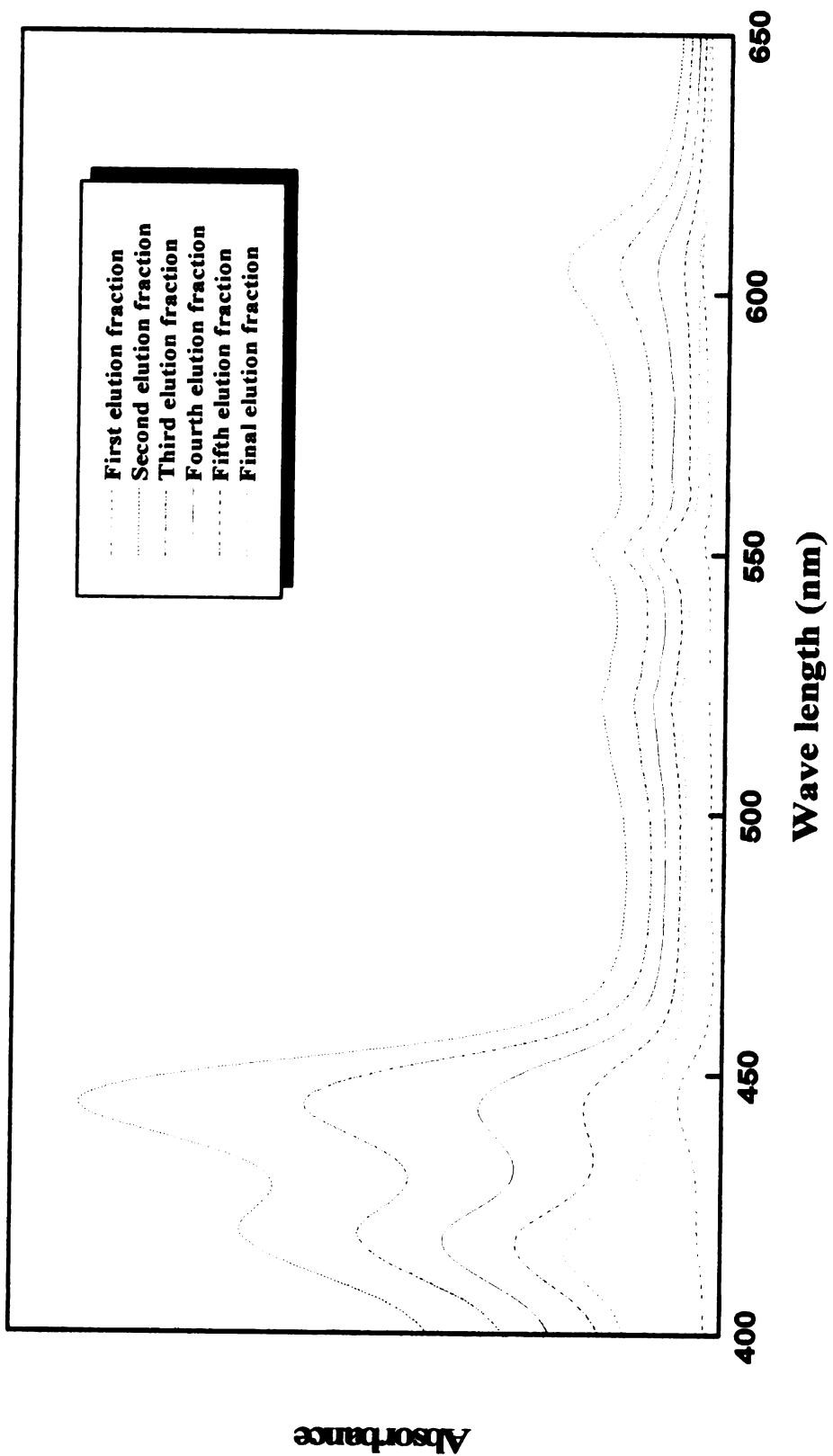


Figure 4.9

**Figure 4.10 Gel-filtration for cytochrome *c* cysteine mutant (N12C) with cytochrome *c* oxidase subunit II cysteine mutant (T159C).** Elution volume was plotted versus absorbance at 416 nm for cytochrome *c* and 444 nm for the oxidase. Each point on the oxidase plot represents the actual absorbance at 444 nm of the specific elution fraction (100  $\mu$ l). For the cytochrome *c* plot data were corrected and the absorbance of the oxidase at 416 nm was subtracted using this formula:

Cytochrome *c* absorbance at 416 = absorbance at 416 – (absorbance at 444 nm X 0.32)

where 0.32 = absorbance at 416nm /Absorbance at 444 nm for oxidase alone.



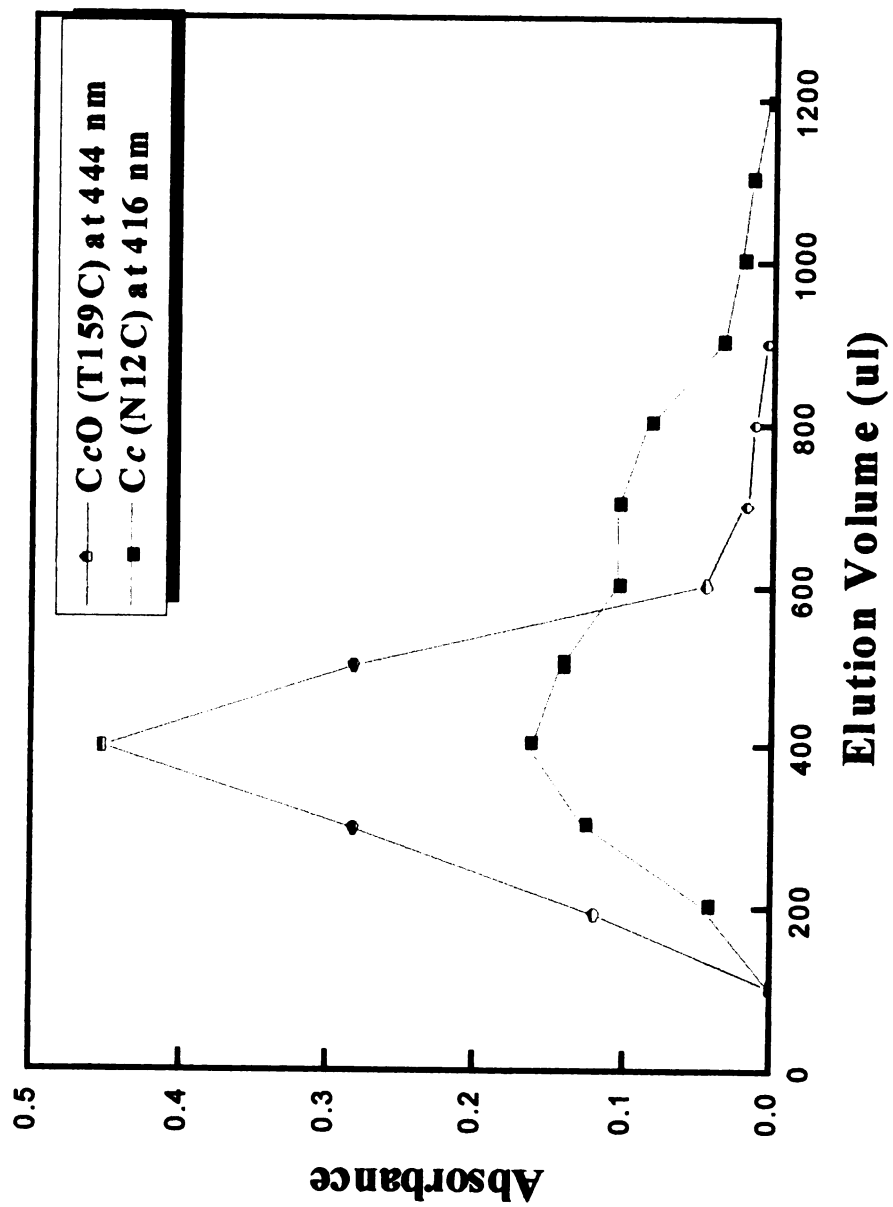


Figure 4.10

**Figure 4.11 Gel-filtration for cytochrome *c* cysteine mutant (K83C) with cytochrome *c* oxidase subunit II cysteine mutant (A213C).** Elution volume was plotted versus absorbance at 416 nm for cytochrome *c* and 444 nm for the oxidase, as in the previous figure. The cytochrome *c* mutant (K83C) was chromatographed separately, under the same conditions as the complex, to determine the position of free cytochrome *c*<sub>2</sub> on the column.

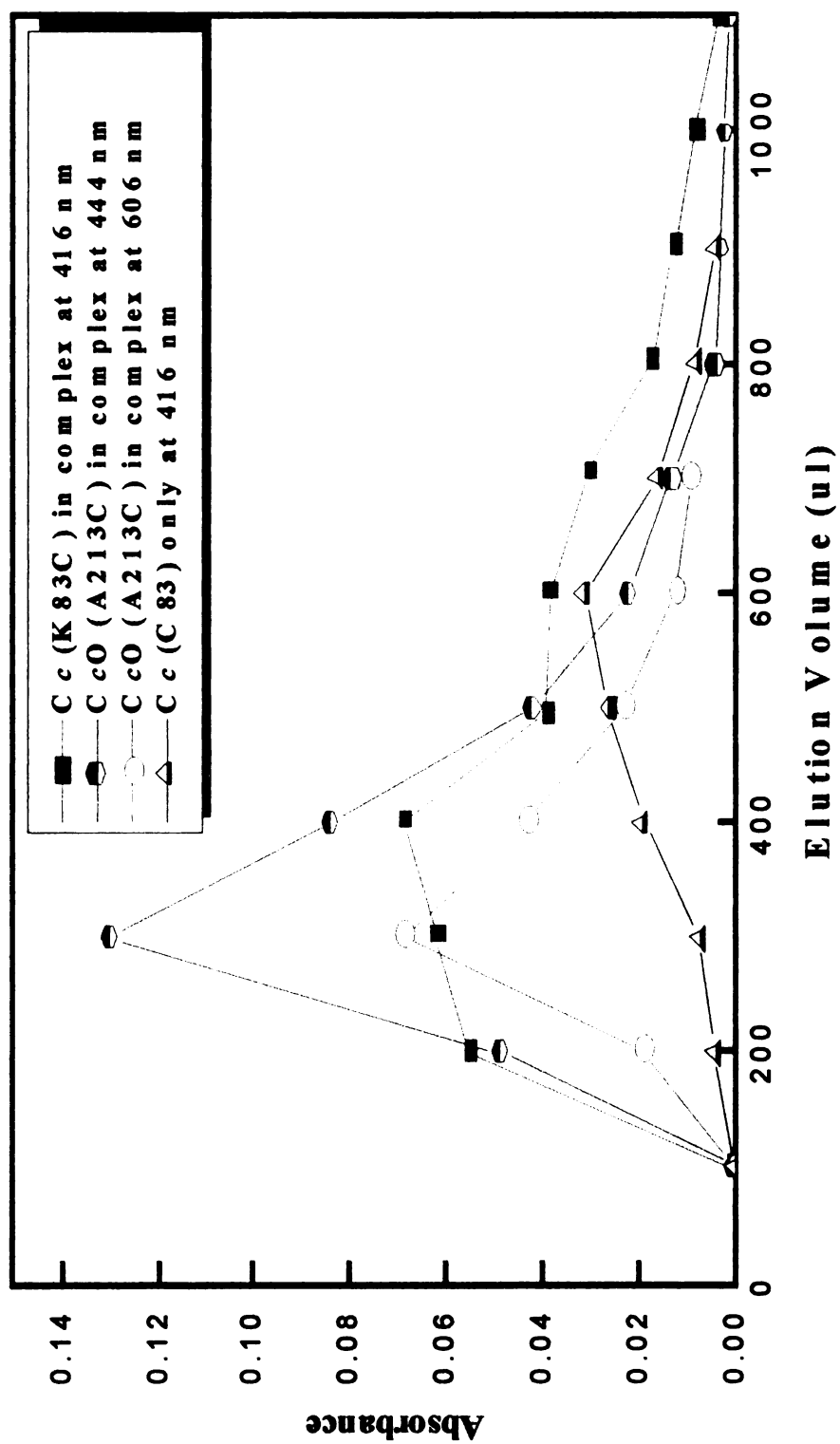


Figure 4.11

**Figure 4.12 Gel-filtration for horse cytochrome *c* with wild type *Rhodobacter sphaeroides* cytochrome *c* oxidase.** Elution volume was plotted versus absorbance at 416 nm for cytochrome *c* and 444 nm for the oxidase. The high ionic strength conditions (100 mM KPO<sub>4</sub>) would have prevented any non-covalent complex from being maintained during gel filtration.

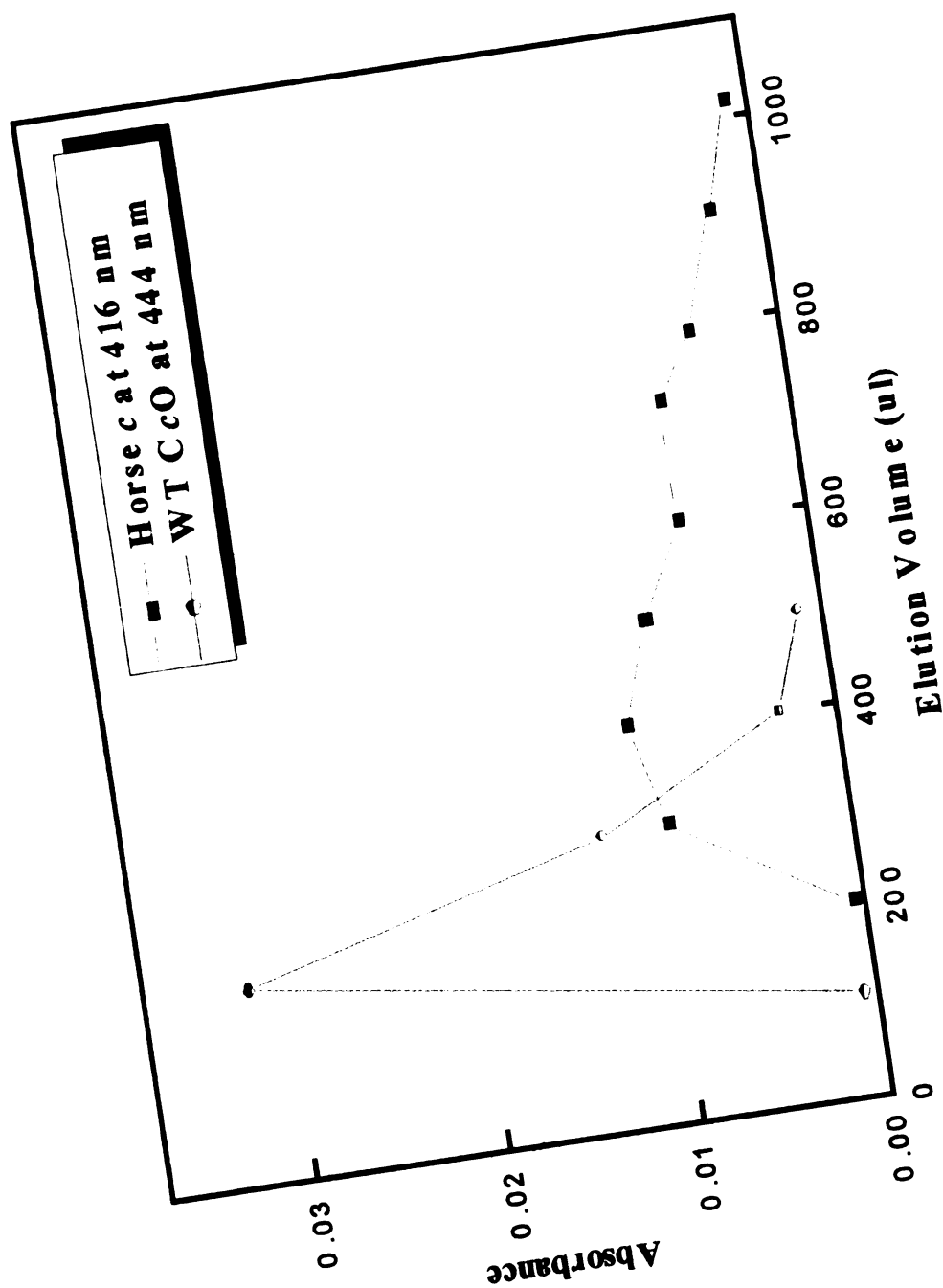


Figure 4.12



The fractions from gel filtration that contained the complex (plus uncomplexed oxidase) were run on an SDS-Page gel and stained with TMB for peroxidase activity to determine the position of cytochrome *c* by virtue of its covalently bound heme, which should be retained even in an SDS-PAGE gel. This was followed by Coomassie staining to determine the positions of the oxidase subunits. Results from this experiment and calculations based on the expected cross-linkage products between cytochrome *c* and subunit II of the oxidase using a molecular weight curve (Figure 4.13), indicated cytochrome *c*, if cross-linked with subunit II, should be at a position equal to 44 kDa on the gel. Unfortunately, this position is where a broad band of subunit I is also located, and the heme of subunit I appears also to be somewhat retained. Therefore the identification of the cytochrome *c* complex with subunit II was not possible by this approach (data not shown).

To obtain further evidence of complex formation, MALDI mass spectrometry analysis was performed on the band eluted from the gel. Analysis with MALDI shows a species that corresponds to cytochrome *c* bound covalently to subunit II of the oxidase. Cytochrome *c*<sub>2</sub> molecular weight is 14.7 kDa and the molecular weight of the naturally processed subunit II is 29.4 kDa and the expected molecular weight of the complex is 44.2 kDa. The species that were obtained by MALDI are shown in (Figure 4.14).

**Figure 4.13** The Log of molecular weights of the marker proteins were plotted versus the position on the SDS gel (actual distance from the top of gel), to calculate the position of the subunits of cytochrome oxidase and the expected position of the complex between cytochrome *c* and subunit II of the oxidase. Subunits of cytochrome oxidase do not run according to their actual molecular weights (63 for subunit I, 29.4 and 30.6 for short and long subunit II and 30 for subunit III) because of their hydrophobic character. The apparent molecular weights on SDS gel are: 44.5 kDa for subunit I, 32 kDa and 33.5 kDa for short and long subunit II, respectively and 19 kDa for subunit III. Cytochrome *c*<sub>2</sub> runs close to its actual molecular weight (14 kDa), and on the gel it is 13. The complex should therefore runs at 44-47 kDa, in the same region as subunit I. Polymer forms of subunits I, II and III are present at the top of the gel.



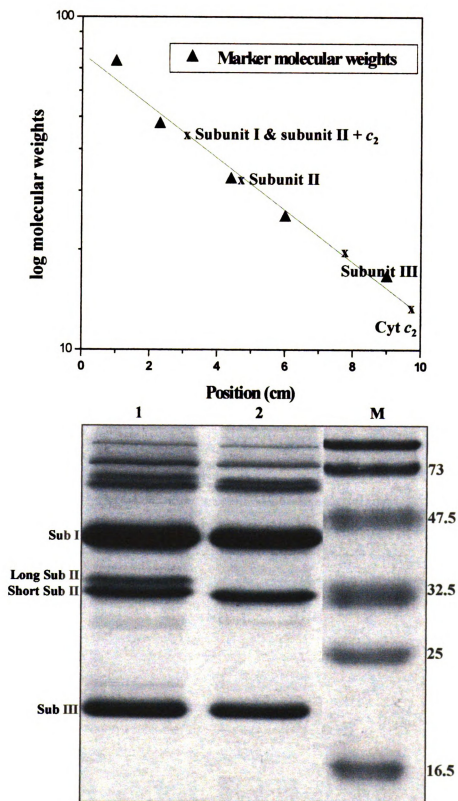


**Figure 4.13**



**Figure 4.14 MALDI analysis to confirm the formation of the complex.** 100  $\mu\text{L}$  of sample [40  $\mu\text{M}$  cytochrome  $c_2$  mutant (N12C) and 40  $\mu\text{M}$  oxidase mutant (Y159C)] were incubated for one hour without reducing agent and loaded onto a gel filtration column to separate the unbound cytochrome  $c$  from oxidase and oxidase bound covalently to cytochrome  $c$ . A fraction from the gel filtration column that appears to contain the covalently formed complex, was analyzed with MALDI mass spectrometry. Data shows peaks at 14,787, 29,467 and 44,254  $m/z$  that correspond to the actual molecular weights of cytochrome  $c_2$ , subunit II of the oxidase and the subunit II + cytochrome  $c_2$  (complex), respectively.

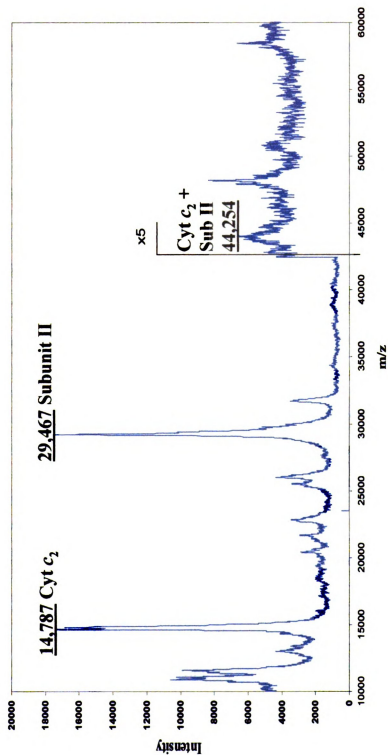


Figure 4.14

## Discussion

Prediction of protein-protein interaction sites is currently of great interest because understanding the nature of protein-ligand association is crucial both to drug design and to the ability to predict potential binding sites in physiological reactions. Computer docking has gained recognition over the past years, with interest currently shifting from the analysis of protein interactions with small ligand towards the understanding of protein-protein interactions, often involved in complex signaling pathways.

Crystallization of electron transfer complexes is extremely difficult, as the kinetics of the interaction is fast and the association is transitory and has to be stabilized during crystallization. This makes electron transfer systems are attractive for theoretical studies, and a large number of available docking programs, including DOCK and DOT, have been used for these studies.

A cytochrome *c*/cytochrome *c* oxidase complex computational model was developed by Roberts and coworker (Roberts and Pique, 1999). Knowing the docking site of cytochrome *c* on the oxidase is very important in understanding the details of the electron transport mechanism. In this study we attempted to test the docking model by designing covalent linkages between cytochrome *c* and the oxidase based on the theoretical model. Successful crosslinkage would not only confirm the model, but might provide a stable complex suitable for crystallization.

Having access to the overproducing strain and the availability of the gene sequence, in addition to the fact that it is soluble, makes cytochrome *c*<sub>2</sub> a suitable candidate for this study; However, lack of Lys 13 and Lys 72 which are important for the binding with the oxidase (Ferguson-Miller *et al.*, 1978), makes it a less good candidate.

Using site-directed mutagenesis we made two mutants: one with Lys 13 and the other with Lys 72. Introduction of Lys 13 improved the binding between the two proteins significantly whereas addition of Lys 72 didn't have much effect. Lys 72 is surrounded by a number of positively charged residues, which may make addition of another positive charge less critical, whereas Lys 13 is not. Introducing a positive charge at position 13 made a dramatic difference in the binding ability of this cytochrome *c* (cyt *c*<sub>2</sub>), confirming the previous results regarding the importance of this residue in the binding between cytochrome *c* and the oxidase (Ferguson-Miller *et al.*, 1978; Smith *et al.*, 1977; Brautigan *et al.*, 1977; Roberts and Pique, 1999). Due to the importance of this mutant (Q13/K), all mutants made for this study were made as double mutants with Q13K.

Measuring the intrinsic electron transfer in the Q13K mutant by attaching a ruthenium group, as an electron donor to cytochrome *c*, requires the presence of cysteine at positions 39 or 60 (Geren *et al.*, 1995). We made and characterize the double mutants Q13K/K39C and Q13K/K60C, which behave like wild type but have a little less activity, probably due to dimer formation, and lower expression level in the case of Q13K/K39C (50% of the W.T). Unfortunately Millett's group found that self-dimerization made labeling of these mutants with ruthenium a very difficult experiment. Efforts continue with the use of reducing agents, such as DTT and anaerobic conditions, to prevent dimerization.

Based on the computational model of the docking site of cytochrome *c* and cytochrome *c* oxidase (Roberts and Pique, 1999; Hespenheide, personal communication), cysteine mutants of cytochrome *c* (Q13K/N12C and Q13K/K83C) were successfully made, purified and characterized. Using the traditional purification methods

(hydroxylapatite and DEAE ion-exchange chromatography) was not the best choice to have a good yield of cysteine mutants. Therefore we fused a histidine-tag to the C-terminal of cytochrome *c* and used Ni<sup>2+</sup>-NTA affinity chromatography, which is increased the yield as well as the purity remarkably.

Cysteine mutants in subunit II of the oxidase (Y159C and A213C) were also made in our lab, designed to form a covalent cytochrome *c*/ cytochrome *c* oxidase.

Complex formation was confirmed, at least partially, by gel-filtration. Elution profiles provided evidence that separation between the oxidase and free cytochrome *c* was sufficient to indicate whether there is formation of a covalent cytochrome *c*/cytochrome *c* oxidase complex. SDS-PAGE was used as another confirmatory test. Unfortunately the calculated molecular weight for the complex (cytochrome *c* and subunit II of the oxidase) runs at the same position on SDS gel as subunit I, which makes the presence of the complex difficult to detect. In order to solve this problem we used TMB stain (Daldal *et al.*, 2000) that is specific for heme staining, but heme *a* in subunit I is also retained in the SDS gel, even though it is not covalently linked, making subunit I alone stain with TMB. Therefore the SDS gel and heme staining method does not provide conclusive evidence for complex formation.

MALDI mass spectrometry was used to analyze the trypsin-digested band from the SDS gel that was expected to contain both subunit I and the complex. Specific peaks were identified that indicated the presence of cytochrome *c* and subunit II along with subunit I at that position. This result gave another piece of evidence of the complex formation, although the peaks from the band confirming the mixed species did not match the theoretical predicted trypsin fragments. However, they did match the fragments

actually found in trypsin-digested subunit I, subunit II and cytochrome *c*, separately. MALDI was also used to analyze the elution fraction from gel-filtration that appears to contain the complex. Analysis detected low levels of cytochrome *c*<sub>2</sub> bound to subunit II of the oxidase (44.2 kDa). This low yield could be due to self-dimerization of cytochrome *c* or to dissociation or oxidation of the complex subsequent to gel filtration. Another possibility is that the “perfect fit” necessary to make these disulfides may not be obtained with this engineered cytochrome *c*<sub>2</sub>.

It is now possible to produce horse cytochrome *c* in *E. coli* (Patel *et al.*, 2001) and it may be possible to test the model more definitively by making the cysteine mutants in this system.



## SUMMARY AND CONCLUSION

### **1- Purification and crystallization of *Rhodobacter sphaeroides* cytochrome *c* oxidase.**

In attempts to crystallize *Rhodobacter sphaeroides* cytochrome *c* oxidase, we purified the enzyme with affinity chromatograph combined with DEAE ion-exchange chromatography. Then gel filtration was used to exchange detergents from lauryl maltoside that is used for isolation and purification, to decyl maltoside that is used for crystallization. This process dilutes the protein sample; in the concentration process the protein along with detergent concentrated to 10 fold. Since detergent concentration is very critical for crystallization, spin column was used to adjust detergent concentration.

By using many column systems, we were achieving high purity, homogeneity and detergent exchange, but undoubtedly we were losing more of the native membrane lipids. The maintenance of some lipid-protein interactions may be critical for crystallization (Garavito and Ferguson-Miller, 2001; Yoshikawa *et al*, 1998; Luecke *et al*, 1999; Toyoshima *et al*, 2000). Therefore, even when reasonably active forms of the enzyme were isolated, solubilized and purified by using non-ionic detergents to substitute for the lipid bilayer, still the structural integrity and homogeneity of the membrane proteins may be influenced by lack of native lipids. By using this purification system and a hanging drop method for crystallization, only microcrystals were formed.

As part of a collaboration between our lab and a Swedish group in Uppsala, we modified our purification protocol and crystallization conditions to match their protocols since they had succeeded to solve the crystal structure of *Rhodobacter sphaeroides* cytochrome *c* oxidase at 2.3 Å. In their protocol, the enzyme was purified

with Ni-affinity chromatography as above but using an imidazole gradient to elute rather than 100mM histidine. The next purification step used a Mono Q column instead of a DEAE/SPW-HPLC ion-exchange column. These two columns have the same DEAE ion-exchange chemistry but a different resin is used as a support. No gel filtration or spin column was used for detergent exchange, just a concentrator-filtration method. This lesser level of manipulation and different DEAE resins may be critical for maintaining the necessary native lipids.

Using the Swedish purification protocol and a hanging drop method for crystallization under modified conditions, we were able routinely to get crystals as large as 0.3 X 0.3 X 0.15 mm in our lab with diffraction of up to 3.0Å. This encourages us to continue with our efforts at refining the method to crystallize mutant forms and in the future of forming and crystallizing a complex between cytochrome *c*- cytochrome *c* oxidase to reveal more information about the binding sites and the process of electron transfer between the two proteins.

## **2- Use of thin layer chromatography, mass spectrometry and phosphate analysis to analyze lipid contents of *Rhodobacter sphaeroides* cytochrome *c* oxidase.**

Lipid contents in membranes and after each purification step through to the crystal forms of *Rhodobacter sphaeroides* cytochrome *c* oxidase were analyzed with different methods. Thin layer chromatography provided considerable information about lipid contents, but the results are dependent on the extraction process. In this study we extracted the protein samples with dry acetone that extracts detergents and pigments, which distorts the analysis. Then chloroform/methanol system was used to extract polar

lipids. To extract the tightly bound cardiolipin that is thought to be important for the enzyme function, ammonium extraction was used. These extraction systems were efficient and reproducible. However, in some cases the TLC method did not provide conclusive identification. Therefore mass spectrometry was pursued in parallel.

Fast atom bombardment (FAB) and matrix-assisted laser desorption ionization (MALDI) mass spectrometry are powerful methods for directly characterizing underivatized lipids, even in mixtures. These methods show mass ions indicative of the molecular weights of each of the molecular species present in the sample as well as fragments derived from elimination of the head groups or acyl groups

FAB provided detailed knowledge of the fatty acid components and characteristic fragments of each type of lipid, whereas MALDI enable us to analyze the intact protein without relaying on solvent extraction. MALDI is unique in showing the association of some lipids with specific protein subunits, such as the association between cardiolipin and phosphatidylcholine with two different forms of subunit IV. Also with MALDI we were able to analyze lipid contents of a single crystal. This analysis may enable us to correlate lipid contents with high resolution data as a unique way to improve the crystallization conditions.

From this study we can conclude that significant amounts of lipids remain bound to the oxidase after purification, at the level of about 10-15 molecules of lipids/molecule of oxidase from phosphate analysis and thin layer chromatography. Phosphate analysis shows 8-11 molecules phospholipids per purified oxidase, and TLC shows, besides the phospholipids, non-phosphorous-containing lipids, sulfolipids and ornithine lipids. MALDI shows cardiolipn and PC associated with subunit IV. In bovine heart oxidase at

2.8Å resolution, 9 phospholipids were identified. At 2.0Å resolution, many more lipids were resolved and seem to be associated with specific subunits. For example, five cardiolipin were found at interfaces between different subunits, III-VIa, III-VIIa, I-II-Vc, I-VIIc and I-II-IV. They also found one phosphatidylcholine, three phosphatidylethanolamine and five phosphatidylglycerol, each at subunit interfaces. (Yoshikawa, personal communication). This further emphasizes that lipids are integrated in the protein molecules, apparently maintaining a stable homogenous structure, and not just randomly distributed on the surface. A similar integration of six lipid into the *Rhodobacter sphaeroides* oxidase structure is found in the 2.3Å crystal structure; more are likely to be resolved as better structures are achieved.

Purification of *Rhodobacter sphaeroides* oxidase affects the amounts of lipids associated with these proteins, but not the types of lipids remaining even after several purification steps. This might seem somewhat surprising, but in fact it is consistent with the finding in the high resolution structure of bovine oxidase that all the major lipids were found to co-crystallize with the protein each at different, highly specific sites.

In bacteriorhodopsin, a light-driven ion pump, 18 lipid molecules/protein monomer were identified in the crystal structure at 1.5 Å resolution (Luecke *et al.*, 1999). In some other cases, as in crystallization of Ca<sup>+</sup>-ATPase, a membrane protein that transfers ions across the membrane against a concentration gradient, lipid (phosphatidylcholine) was added to achieve a crystal structure at 2.6Å resolution, providing further evidence for the importance of lipids in achieving high resolution structures of integral membrane proteins.

The results of these studies, and results from crystallizing other membrane proteins, suggest a new paradigm for membrane protein structure: Lipids of many different kinds associate specifically, not randomly, with the protein structure and are important for maintaining a molecularly homogeneous configuration suitable for crystallization at high resolution.

### **3- Engineering of *Rhodobacter sphaeroides* cytochrome $c_2$ to test the model of the Cc/CcO complex by making a covalent complex.**

As another way to optimize conditions for crystallization and to test the computational model of the cytochrome  $c$  /cytochrome  $c$  oxidase complex, we attempted to increase the hydrophilic surface area of the oxidase by making a covalent complex between a soluble cytochrome  $c_2$  and cytochrome  $c$  oxidase.

Dr. Roberts and coworkers at Scripps institute predicted a docking site of horse cytochrome  $c$  on bovine cytochrome  $c$  oxidase. In this study we used cytochrome  $c_2$  as a substrate for many reasons: it is a soluble protein; its sequence is available; we have access to the overexpressed strain and it was thought to be the physiological substrate. However, activity and binding studies show that it has lower binding affinity with the *Rhodobacter sphaeroides* oxidase than the horse  $c$  that is used in the model. This is consistent the fact that *Rhodobacter sphaeroides* cytochrome  $c_2$  is lacking lysine 13 and lysine 72 which are known to be important for binding from mutation and chemical modification studies.

Introduction of Lys13 improved the binding between cytochrome  $c_2$  and the oxidase significantly, consistent with the predicted importance of that lysine in the

cytochrome *c*/ cytochrome *c* oxidase complex; it also made cytochrome *c*<sub>2</sub> more like the horse *c* on which the prediction was based.

In order to improve the purification system for cytochrome *c*<sub>2</sub> wild type and mutants, we inserted a histidine-tag on cytochrome *c*<sub>2</sub> gene and used Ni-affinity chromatography as a purification method. Using this system improved the yield by 3-4 fold and improved the purity remarkably.

This study involved insertion of cysteines in cytochrome *c*<sub>2</sub> and in the oxidase, guided by a computational prediction of the docking interaction between cytochrome *c* and cytochrome *c* oxidase. Using this model, the best positions in the two proteins for creating inter-molecular disulfide bonds were between Ala 83 of cytochrome *c* and Ala213 of the oxidase on one hand, and Gln 12 of cytochrome *c* and Tyr 159 of the oxidase on the other. We changed each of these pairs of residues to cysteines in order to form a covalent cytochrome *c*/cytochrome *c* oxidase complex, assuming that the predicted complex is correct and therefore the engineered cysteine pairs will be brought into close proximity.

Cysteine mutants were made, purified and characterized and used for making a covalent complex by incubation of cytochrome *c*<sub>2</sub> mutants with their predicted partner mutants of the oxidase and then separate the bound form from the unbounded cytochrome *c*<sub>2</sub> by gel filtration. Gel filtration analysis and mass spectrometry provide evidence of formation of covalent cytochrome *c*/ cytochrome *c* oxidase. The results of these studies support the computational model, and suggest that making a covalent complex for crystallization is feasible.

## **BIBLIOGRAPHY**

Abramson, J.; Svensson-Ek, M.; Byrne, B. & Iwata, S. (2001) Structure of cytochrome *c* oxidase: a comparison of the bacterial and mitochondrial enzymes. *Biochim. Biophys. Acta.* 1544: 1-9.

Awasthi, Y.; Chuang, T.; Keenan, T. & Crane, F. (1971) Tightly bound cardiolipin in cytochrome oxidase. *Biochim. Biophys. Acta* 226:42- 52.

Bartsch, R.; Ambler, R.; Meyer, T. & Cusanovich, M. (1989) Effect of aerobic growth conditions on the soluble cytochrome content of the purple phototrophic bacterium *Rhodobacter sphaeroides*: induction of cytochrome *c*554. *Arch. Biochem. Biophys.* 271: 433-440.

Barenholz, Y. (2002) Cholesterol and other membrane active sterol: from membrane evolution to “rafts”. *Prog. Lipid Res.* 41: 1-5.

Benning, C. (1997) Lipids in photosynthesis: Structure, function and genetics (chapter 5). Kluwer Academic Publishers. Printed in The Netherlands.

Benning, C. Huang, Z. H. & Gage, D. (1995) accumulation of a novel glycolipid and a betaine lipid in cells of *Rhodobacter sphaeroides* grown under phosphate limitation. *Arch. Biochem. Biophys.* 317: 103-111.

Benning, C.; Beatty, J.; Prince, R. & Somerville, C. (1993) The sulfolipid sulfoquinovosyldiacylglycerol is not required for photosynthetic electron transport in *Rhodobacter sphaeroides* but enhances growth under phosphate limitation. *Proc. Natl. Acad. Sci. USA* 90: 1561-1565.

Benning, C. & Somerville, C. (1992) Isolation and genetic complementation of sulfolipid-deficient mutant of *Rhodobacter sphaeroides*. *J. Bacteriol.* 174: 2352-2360.

Beratan, D.; Betts, J. & Onuchic, J. (1991) Protein electron transfer rates set by the bridging secondary and tertiary structure. *Reports*: 1285-1288.

Beratan, D.; Onuchic, J.; Winkler, J. & Gray, H. (1992) Electron-tunneling pathways in proteins. *Science* 258: 1740-1741.

Berry, E. & Trumpower, B. (1985) Isolation of ubiquinol oxidase from *Paracoccus denitrificans* and resolution into cytochrome *bc*1 and cytochrome *c-aa*<sub>3</sub> complex. *J. Biol. Chem.* 260: 2458-2467.

Branden, M.; Sigurdson, H.; Namslauer, A.; Gennis, R.; Adelroth, P. & Brzezinski, P. (2001) On the role of the K-proton transfer pathway in cytochrome *c* oxidase. *PNAS* 98: 5013-5018.



- Brandner, J.; McEwan, A.; Kaplan, S. & Donohue, T. (1989) Expression of the *Rhodobacter sphaeroides* cytochrome  $c_2$  structure gene. J. Bacteriol. 171: 360-368.
- Bratton, M.; Pressler, M. & Hosler, J. (1999) Suicide inactivation of cytochrome  $c$  oxidase: catalytic turnover in the absence of subunit III alters the active site. Biochemistry 38: 16236-16245.
- Brautigan, D.; Ferguson-Miller, S. & Margoliash, E. (1978) Definition of cytochrome  $c$  binding domains by chemical modification I. J. Biol. Chem. 253: 130-139.
- Brown, S.; Mitchell, R & Richard, P. (1993) Binuclear center structure of terminal protonmotive oxidases. FEBS Lett. 316: 216-223.
- Buse, G.; Soulimane, T.; Dewor, M.; Meyer, H. & Bluggel, M. (1999) Evidence for a copper-coordinated histidine-tyrosine cross-link in the active site of cytochrome oxidase. Protein Sci. 8: 985-990.
- Bushnell, G.; Louie, G.; & Brayer, G. (1990) High-resolution three-dimensional structure of horse heart cytochrome  $c$ . J. Mol. Biol. 214: 585-595.
- Calhoun, M.; Thomas, J. & Gennis, R. (1994) The cytochrome oxidase superfamily of redox-driven proton pumps. TIBS 19: 325-330.
- Cao, J.; Hosler, J.; Shapleigh, J.; Revzin, A. & Ferguson-Miller, S. (1992) Cytochrome  $aa_3$  of *Rhodobacter sphaeroides* as a model for mitochondrial cytochrome  $c$  oxidase. J. Biol. Chem. 267: 24273-24278.
- Capaldi, R. (1990) Structure and function of cytochrome  $c$  oxidase. Ann. Rev. Biochem. 59: 569-596.
- Casey, R.P.; Broger, C.; Thalen, M. & Azzi, A. (1981) Studies on the molecular basis of  $H^+$  translocation by cytochrome  $c$ . J. Bioenerg. Biomembr. 13: 219-228.
- Chan, S. & Li, P. (1990). Cytochrome  $c$  Oxidase: Understanding nature's design of a proton pump. Biochemistry 29: 1-12.
- Chepuri, V. & Gennis, R. (1990) The use of gene fusion to determine the topology of all of the subunits of the cytochrome  $o$  terminal oxidase complex of *Escherichia coli*. J. Biol. Chem. 265: 12978-12986.
- Craig, D. & Wallace, C. (1993) ATP binding to cytochrome  $c$  diminishes electron flow in the mitochondrial respiratory pathway. Protein Sci. 2: 966-976.
- Curry, W.; Grabe, M.; Kurnikov, I.; Skourtis, S.; Beratan, D.; Regan, J.; Aquino, A.; Beroza, P. & Onuchic, J. (1995) Pathways, pathway tubes, pathway docking and propagators in electron transfer proteins. J. Bioenerg. Biomembr. 27: 285-293.

- Cusanovich, M. (1971) Molecular weight of some cytochrome *cc'*. *Biochim. Biophys. Acta.* 236: 238-241.
- Daldal, F.; Mandaci, S.; Winterstein, C.; Myllykallio, H.; Duyck, K. & Zannoni, D. (2001) Mobile cytochrome *c*<sub>2</sub> and membrane-anchored cytochrome *c*<sub>y</sub> are both efficient electron donors to the *cbb*<sub>3</sub>- and *aa*<sub>3</sub>- type cytochrome *c* oxidase during respiratory growth of *Rhodobacetr sphaeroides*. *J. Bacteriol.* 183: 2013-2024.
- Devreese, B.; Brige, A.; Backers, K.; Van Driessche, G.; Meyer, T.; Cusanovich, M. & Van Beeumen, J. (2000) Primary structure characterization of *Rhodocyclus tenuis* diheme cytochrome *c* reveals the existence of two different classes of low-potential diheme cytochrome *c* in purple phototopic bacteria. *Arch. Biochem. Biophys.* 381: 53-62.
- Donohue, T.; Chain, B. & Kaplan, S. (1982) Alteration in the phospholipids composition of *Rhodopseudomonas sphaeroides* and other bacteria induced by Tris. *J. Bacteriol.* 152: 595-606.
- Donohue, T.; McEwan, A.; Van Doren, S.; Crofts, A. & Kaplan, S. (1988) Phenotypic and genetic characterization of cytochrome *c*<sub>2</sub> deficient mutants of *Rhodobacter sphaeroides*. *Biochemistry* 27: 1918-1925.
- Ezzel, C. (1995) *The Journal of NIH Research* 7: 39-43.
- Ferguson-Miller, S. (1999) Physiological uncoupling, intrinsic and extrinsic mechanisms. *Biophysical J. (abstracts)* 76: A1.
- Ferguson-Miller, S. & Babcock, G. (1996). Heme/copper terminal oxidases. *Chemical Reviews* 96: 2889-2907.
- Ferguson-Miller, S.; Brautigan, D. & Margoliash, E. (1978) Definition of cytochrome *c* binding domains by chemical modification. *J. Biol. Chem.* 253: 149-159.
- Ferguson-Miller, S.; Brautigan, D. & Margoliash, E. (1976) Correlation of the kinetics of electron transfer activity of various eukaryotic cytochrome *c* with binding to mitochondrial cytochrome *c* oxidase. *J. Biol. Chem.* 251: 1104-1115.
- Ferguson-Miller, S.; Hochman, J. & Schindler, M. (1986) Aggregation and diffusion in the mitochondrial electron-transfer chain: role in electron flow and energy transfer. *Biochem. Soc. Trans.* 14: 822-824.
- Fetter (1995) Search for residues critical to proton pumping in cytochrome *c* oxidase. Ph.D. Thesis, Michigan State University.
- Fetter, J.; Qian, J.; Shapleigh, J.; Thomas, J; Garcia-Horsman, A.; Schmidt, E.; Hosler, J.; Babcock, G.; Gennis, R. & Ferguson-Miller, S. (1995) Possible proton relay pathways in cytochrome *c* oxidase. *Proc. Natl. Acad. Sci. USA* 92: 1604-1608.

- Florens, L.; Schmidt, B.; McCracken, J.; Hoganson, C.; Fetter, J.; Mills, D.; Babcock, G. & Ferguson-Miller, S. (2001) Fast deuterium access to the buried magnesium/manganese site in cytochrome *c* oxidase. *Biochemistry* 40: 7491-7497.
- Flory, J. & Donohue, T. (1995) Organization and expression of the *Rhodobacter sphaeroides* *cycFG* operon. *J. Bacteriol.* 177: 4311-4320.
- Frank, V. & Kadenbach, B. (1996) Regulation of the  $H^+/e^-$  Stoichiometry of cytochrome *c* oxidase from bovine heart by intramitochondrial ATP/ADP ratio. *FEBS Lett* 382: 121-124.
- Gage, D.; Huang, Z. & Benning, C. (1992) Comparison of sulfoquinovosyl diacylglycerol from spinach and the purple bacterium *Rhodobacter sphaeroides* by fast atom bombardment tandem mass spectrometry. *Lipids* 27: 623-636.
- Garavito, R. & Ferguson-Miller, S. (2001) Detergents as tools in membrane biochemistry. *J. Biol. Chem.* 276: 32403-32406.
- Gennis, R. B. (1988) *Biomembranes*. Springer-Verlag, New York Incorporated, New York.
- Gennis, R. (1998) Cytochrome oxidase: one proton, two mechanisms? *Science* 280: 1712-1713.
- Gennis, R. & Ferguson-Miller, S. (1995) Structure of cytochrome *c* oxidase, energy generator of aerobic life. *Science* 269: 1063-1064.
- Geren, L.; Beasley, J.; Fine, B.; Saunders, A.; Hibdon, S.; Pielak, G.; Durham, B. & Millett, F. (1995) Design of ruthenium-cytochrome *c* derivative to measure electron transfer to the initial acceptor in cytochrome *c* oxidase. *J. Biol. Chem.* 270: 2466- 2472.
- Gray, K.; Grooms, M.; Myllykallio, H.; Moomaw, C.; Slaughter, C. & Daldal, F. (1994) *Rhodobacter capsulatus* contains a novel *cb*-type cytochrome *c* oxidase without a  $Cu_A$  center. *Biochemistry* 33: 3120-3127.
- Gray, H.B. & Winkler, J.R. (1996) Electron transfer in proteins. *Annu. Rev. Biochem.* 65: 537- 561.
- Gregory, L. & Ferguson-Miller, S. (1988) Effect of subunit III removal on control of cytochrome *c* oxidase activity by pH. *Biochemistry* 27: 6307-6314.
- Gupte, S. & Hackenbrock, C. (1988) The role of cytochrome *c* diffusion in mitochondrial electron transport. *J. Biol. Chem.* 263: 5248-5253.
- Haltia, T.; Puustinen, A. & Finel, M. (1988) The *Paracoccus denitrificans* cytochrome *aa<sub>3</sub>* has a third subunit. *Eur. J. Biochem.* 172: 543-546.

Haltia, T.; Saraste, M. & Wikstrom, M. (1991) Subunit III of cytochrome *c* oxidase is not involved in proton translocation: A site-directed mutagenesis study. *EMBO J.* 10: 2015-2021.

Harrenga, A.; Reincke, B.; Ruterjans, H.; Ludwig, B. & Michel, H. (2000) Structure of the soluble domain of cytochrome *c*<sub>552</sub> from *Paracoccus denitrificans* in the oxidized and reduced states. *J. Mol. Biol.* 295: 667-678.

Hill, B. (1991) The reaction of the electrostatic cytochrome *c*-cytochrome oxidase complex with oxygen. *J. Biol. Chem.* 266: 2219-2226.

Hill, B. (1993) The sequence of electron carriers in the reaction of cytochrome *c* oxidase with oxygen. *J. Bioenerg. Biomembr.* 25: 115-120.

Hill, B. (1994) Modeling the sequence of electron transfer reactions in the single turnover of reduced mammalian cytochrome *c* oxidase. *J. Biol. Chem.* 269: 2219-2226.

Hiser, C.; Mills, D.; Schall, M. & Ferguson-Miller, S. (2001). C-terminal truncation and histidine-tagging of cytochrome *c* oxidase subunit II reveals the native processing site, shows involvement of the C-terminus in cytochrome *c* binding, and improves the assay for proton pumping. *Biochemistry* 40: 1606- 1615.

Ho, S.; Hunt, H.; Horton, R.; Pullen, J and Pease, L. (1989) Site-directed mutagenesis by overlap extension using polymerase chain reaction. *Gene* 77: 51- 59.

Hochman, J., Ferguson-Miller, S. & Schindler, M. (1985) Mobility in the mitochondrial electron transport chain. *Biochemistry* 24: 2509-2516.

Hofacker, I. & Schulten, K. (1998) Oxygen and proton pathways in cytochrome *c* oxidase. *Proteins: Structure, Function & Genetics* 30: 100-107.

Hopfeild, J. (1974) Kinetic proofreading: a new mechanism for reducing errors in biosynthetic processes requiring high specificity. *Proc. Natl. Acad. Sci. U S A* 71: 4135-4139.

Hosler, P.; Fetter, J.; Tecklenburg, M.; Espe, M.; Lerma, C. & Ferguson-Miller, S. (1992) Cytochrome *aa*<sub>3</sub> of *Rhodobacter sphaeroides* as a model for mitochondrial cytochrome *c* oxidase. *J. Biol. Chem.* 267: 24264-24272.

Hosler, P.; Ferguson-Miller, S.; Calhoun, M.; Thomas, J.; Hill, J.; Lemieux, L.; Ma, J.; Georgiou, C.; Fetter, J.; Shapleigh, J.; Tecklenburg, M.; Babcock, G. & Gennis, R. (1993) Insight into the active-site structure and function of cytochrome oxidase by analysis of site-directed mutants of bacterial cytochrome *aa*<sub>3</sub> and cytochrome *bo*. *J. Bioenerg. Biomembr.* 25: 121-136.

- Hosler, P.; Shapleigh, J.; Mitchell, D.; Kim, Y.; Pressler, M.; Georgiou, C.; Babcock, G.; Ferguson-Miller, S. & Gennis, R. (1996) Polar residues in helix VIII of subunit I of cytochrome *c* oxidase influence the activity and the structure of the active site. *Biochemistry* 35: 10776-10783.
- Imhoff, J. (1991) Polar lipids and fatty acids in the genus *Rhodobacter*. *System. Appl. Microbiol.* 14: 228-234.
- Iverson, T.; Luna-Chavez, C.; Cecchini, G. & Rees D. (1999) Structure of *Escherichia coli* fumarate reductase respiratory complex. *Science* 284: 1961-1966.
- Iwata, S.; Ostermeier, C.; Brend, L. & Michel, H. (1995) Structure at 2.8Å resolution of cytochrome *c* oxidase from *Paracoccus denitrificans*. *Nature* 376: 660-669.
- Iwata, S.; Lee, J.; Okada, K.; Lee, K.; Iwata, M.; Rasmussen, B.; Link, T.; Ramaswamy, S. & Jap, B. (1998) Complete structure of the 11-subunit bovine mitochondrial cytochrome *bc*<sub>1</sub> complex. *Science* 281: 64-71.
- Jenney, F & Daldal, F. (1993) A novel membrane-associated *c*-type cytochrome, cyt *c*<sub>9</sub> can mediate the photosynthetic growth of *Rhodobacter capsulatus* and *Rhodobacter sphaeroides*. *EMBO J.* 12: 1283- 1292.
- Kadenbach, B.; Frank, V.; Riger, T. & Napiwotzki, J. (1997) Regulation and respiration and energy transduction in cytochrome *c* oxidase isozymes by allosteric effectors. *Mol. Cell Biochem.* 174: 131-135.
- Kadenbach, B.; Jarausch, J.; Hartmann, R. & Merle, P. (1983) Separation of mammalian cytochrome *c* oxidase into 13 polypeptides by sodium dodecyl sulfate gel electrophoresis procedure. *Anal. Biochem.* 129: 517-521.
- Kellin, D. (1925) On cytochrome, a respiratory pigment, common to animals, yeast and higher plants. *Proc. R. Soc. Lond.* B98: 312-339.
- Kennel, S.; Meyer, T.; Kamen, M. & Bartsch, R. (1972) On the monoheme character of cytochrome *c*'. *Proc. Natl. Acad. Sci. U.S.A.* 69: 3432-3435.
- Koppenol, WH.; Vroonland, CA. & Braams, R. (1978) The electric potential field around cytochrome *c* and the effect of ionic strength on reaction rates of horse cytochrome *c*. *Biochim. Biophys. Acta* 503: 499- 508.
- Landau, E. & Rosenbusch, J. (1996) Lipidic cubic phases: A novel concept for the crystallization of membrane proteins. *Proc. Natl. Acad. Sci. USA* 93: 1453-14535.
- Lee, H.; Das, T.; Rousseau, D.; Mills, D.; Ferguson-Miller, S. & Gennis, R. (2000) Mutations in the putative H-channel in the cytochrome *c* oxidase from *Rhodobacter sphaeroides* show that this channel is not important for proton conduction but reveal modulation of properties of heme *a*. *Biochemistry* 39: 2989-2996.

Lee, A.; Kirichenko, A.; Vygodina, T.; Siletsky, S.; Das, T.; Rousseau, D.; Gennis, R. & Konstantinov, A. (2002)  $\text{Ca}^{2+}$ -binding site in *Rhodobacter sphaeroides* cytochrome *c* oxidase. *Biochemistry* 41: 8886- 8898.

Leys, D.; Backers, K.; Meyer, T.; Hagan, W.; Cusanovich, M. & Van Beeumen, J. (2000) Crystal structure of an oxygen-binding cytochrome *c* from *Rhodobacter sphaeroides*. *J. Biol. Chem.* 275: 16050-16056.

Long, J.; Durham, B.; Okamura, M. & Millett, F. (1989) Role of specific lysine residues in binding cytochrome *c*<sub>2</sub> to the *Rhodobacter sphaeroides* reaction center in optimal orientation for rapid electron transfer. *Biochemistry* 28: 6970-6974.

Louie, G. & Brayer, G. (1990) High-resolution refinement of yeast iso-1-cytochrome *c* and comparison with other eukaryotic cytochromes *c*. *J. Mol. Biol.* 214: 527-555.

Louie, G.; Hutcheon, W. & Brayer, G. (1988) Yeast iso-1-cytochrome *c*. A 2.8 Å resolution three-dimensional structure determination. *J. Mol. Biol.* 199: 295-314.

Luecke, H.; Schobert, B.; Richter, H.; Cartailler, J. & Lanyi, J. (1999) Structure of bacteriorhodopsin at 1.55 Å resolution. *J. Mol. Biol.* 291: 899-911.

Ma, J.; Tsatsos, P.; Zaslavsky, D.; Barquera, B.; Thomas, J.; Katsonouri, A.; Puustinen, A.; Wikstrom, M.; Brzezinski, P.; Alben, J. and Gennis, R. (1999) Glutamate-89 in subunit II of cytochrome *bo*<sub>3</sub> from *Escherichia coli* is required for the function of the heme-copper oxidase. *Biochemistry* 38: 15150-15156.

Maltempo, M.; Moss, T. & Cusanovich, M. (1974) Magnetic studies on the changes in the iron environment in Chromatium ferricytochrome *c*'. *Biochim. Biophys. Acta* 342: 290-305.

Marcus, R. (1993) Electron transfer reactions in chemistry: theory and experiment. *Angew. Chem. Int. Ed. Engl.* 32: 1111-1121.

Marcus, R. & Sutin, N. (1985) Electron transfers in chemistry and biology. *Biochim. Biophys. Acta* 811: 265-322.

Matsuura, Y.; Hata, Y.; Yamaguchi, T.; Tanaka, N. & Kakudo, M. (1979) Structure of bonito heart ferricytochrome *c* and some remarks on molecular interaction in its crystalline state. *J. Biochem.* 85: 729-737.

McAuley, K.; Fyfe, P.; Ridge, J.; Isaacs, N.; Cogdell, R. & Jones, M. (1999) Structural details of an interaction between cardiolipin and an integral membrane protein. *PNAS* 96: 14706-14711.

Meyer, T. & Cusanovich, M. (1985) Soluble cytochrome composition of the purple phototrophic bacterium *Rhodospseudomonas sphaeroides* ATCC 17023. *Biochim. Biophys. Acta* 807: 308-391.

Mills, D.A.; Florence, L.; Hiser, C.; Qian, J. & Ferguson-Miller, S. (2000) Where is "outside" in cytochrome *c* oxidase and how and when do protons get there? *Biochim. Biophys. Acta*. 1458: 180-187

Mills, D.A.; Schmidt, B.; Hiser, C.; Westley, E. & Ferguson-Miller, S. (2002) Membrane potential-controlled inhibition of cytochrome *c* oxidase by zinc. *J. of Biol. Chem.* 277: 14894-14901.

Millett, F.; deJong, C.; Paulson, L. & Capaldi, R. (1983) Identification of specific carboxylate groups on cytochrome *c* oxidase that are involved in binding cytochrome *c*. *Biochemistry* 22: 546-552.

Mitchell, D.; Adelroth, P.; Hosler, J.; Fetter, J.; Brzezinski, P.; Pressler, M.; Aasa, R.; Malmstrom, B.; Alben, J.; Babcock, G.; Gennis, R. & Ferguson-Miller, S. (1996) A ligand-exchange mechanism of proton pumping involving tyrosine 422 of subunit I of cytochrome oxidase is ruled out. *Biochemistry* 35: 824-828.

Mitchell, D. & Gennis, R. (1995) Rapid purification of wild type and mutant cytochrome *c* from *Rhodobacter sphaeroides* by  $\text{Ni}^{2+}$ -NTA affinity chromatography. *FEBS Lett.* 368: 148-150.

Moore, G. & Pettigrew, G. (1990) Cytochrome *c*: evolutionary, structural and physiochemical aspects. Springer Verlag, Berlin.

Morgan, J.; Verkhovsky, M. & Wikstrom, M. (1994) The histidine cycle: a new model for proton translocation in the respiratory heme-copper oxidases. *J. Bioenerg. Biomembr.* 26: 599-608.

Moser, C.; Keske, J.; Warncke, K.; Farid, R. & Dutton, P. (1992) Nature of biological electron transfer. *Nature* 355: 796-802.

Moser, C.; Page, C.; Farid, R. & Dutton, P. (1995) Biological electron transfer. *J. Bioenerg. Biomembr.* 27: 263-274.

Myllykallio, H.; Zannoni, D. & Daldal, F. (1999) The membrane-attached electron carrier cytochrome *c<sub>y</sub>* from *Rhodobacter sphaeroides* is functional in respiratory but not in photosynthetic electron transfer. *Proc. Natl. Acad. Sci. USA* 96: 4348-4353.

Ochi, H.; Hata, Y.; Takana, N.; Kakuda, M.; Sakurai, T.; Aihara, S. & Morita, Y. (1983) Structure of rice ferricytochrome *c* at 2.0 Å resolution. *J. Mol. Biol.* 166: 407-418.

Onuchic, J.; Beratan, D.; Winkler, J. & Gray, H. (1992) Pathway analysis of proton-electron transfer reactions. *Annu. Rev. Biophys. Struct.* 21:349-377.

Orlando, J. (1962) *Rhodopseudomonas sphaeroides* cytochrome *c*<sub>553</sub>. *Biochim. Biophys. Acta* 57:373-375.

Orlando, J. & Horio, T. (1961) Observations on a *b*-type cytochrome from *Rhodopseudomonas sphaeroides*. *Biochim. Biophys. Acta* 50: 367-369.

Osheroff, N.; Brautigan, D. & Margoliash, E. (1980) Mapping of anion binding sites on cytochrome *c* by differential chemical modification of lysine residues. *Proc. Natl. Acad. Sci. USA* 77: 4439-4443.

Ostermeier, C.; Herrenga, A.; Ermler, U. & Michel, H. (1997) Structure at 2.7 resolution of *Paracoccus denitrificans* two-subunit cytochrome *c* oxidase complexed with an antibody Fv fragment. *Proc. Natl. Acad. Sci. USA* 94: 10547-10553.

Papa, S.; Capitanio, N.; Capitanio, G.; De Nitto, E. & Minuto, M. (1991) The cytochrome chain of mitochondria exhibits variable H<sup>+</sup>/e<sup>-</sup> stoichiometry. *FEBS Lett.* 288: 183-186.

Patel, C.; Lind, M. & Pielak, G. (2001) Characterization of horse cytochrome *c* expressed in *Escherichia coli*. *Protein Expr. Purif.* 22: 220-224.

Pelletier, H. & Kraut, J. (1992) Crystal structure of a complex between electron transfer partners, cytochrome *c* peroxidase and cytochrome *c*. *Science* 258: 1748-1755.

Pettigrew, G. & Moore, G. (1987). *Cytochrome c: biological aspects*. Springer Verlag, Berlin.

Pfützner, U.; Odenwald, A.; Ostermann, T.; Weingard, L.; Ludwig, B. & Richter, O-M. (1998) Cytochrome *c* oxidase (heme *aa*<sub>3</sub>) from *Paracoccus denitrificans*: analysis of mutations in putative proton channels of subunit I. *J. Bioenerg. Biomemb.* 30: 89-97.

Prince, R.; Cogdell, R. & Crofts, A. (1974) The photo-oxidation of horse heart cytochrome *c* and native cytochrome *c*<sub>2</sub> by reaction centers from *Rhodopseudomonas sphaeroides* R-26. *Biochim. Biophys. Acta.* 347: 1-13

Prince, R. & Dutton, P (1975) A kinetic completion of the cyclic photosynthetic electron pathway of *Rhodopseudomonas sphaeroides*: cytochrome *b*-cytochrome *c*<sub>2</sub> oxidation-reduction. *Biochim. Biophys. Acta* 387: 609-613.

Prochaska, L.; Bisson, R.; Capaldi, R.; Steffens, G. & Buse, G. (1981) Inhibition of cytochrome *c* oxidase function by dicyclohexylcarbodiimide. *Biochem. Biophys. Acta* 637: 360-373.



- Proshlyakov, D.; Pressler, M.; DeMaso, C.; Leykam, J.; DeWitt, D. & Babcock, G. (2000) Oxygen activation and reduction in respiration: involvement of redox-active tyrosine 244. *Science* 290: 1588-1591.
- Ramirez, B.; Malmstrom, B.; Winkler, J. & Gray, H. (1995) The currents of life: The terminal electron-transfer complex of respiration. *Proc. Natl. Acad. Sci. USA* 92: 11949-11951.
- Regan, J.; Di Bilio, A.; Langen, R.; Skov, L.; Winkler, J.; Gray, H. & Onuchic, J. (1995) Electron tunneling in azurin: the coupling across a beta-sheet. *Chem. Biol.* 2: 489-496.
- Riistama, S.; Puustinen, A.; Garcia-Horsman, A.; Iwata, S.; Mitchel, H. & Wikstrom, M. (1996) Channelling of dioxygen into the respiratory enzyme. *Biochim. Biophys. Acta* 1275: 1-4.
- Riistama, S.; Laakkonen, L.; Wikstrom, M.; Verkhovsky, M. & Puustinen, A. (1999) The calcium binding site in cytochrome *aa*<sub>3</sub> from *Paracoccus denitrificans*. *Biochemistry* 38: 10670-10677.
- Rios-Velazquez, C.; Cox, R. & Donohue, T. (2001) Characterization of *Rhodobacter sphaeroides* cytochrome *c*<sub>2</sub> proteins with altered heme attachment sites. *Arch. Biochem. Biophys.* 389: 234-244.
- Roberts, V. & Pique, M. (1999) Definition of the interaction domain for cytochrome *c* on cytochrome *c* oxidase. *J. Biol. Chem.* 274: 38051-38060.
- Robinson, N.; Strey, F. & Talbert, L. (1980) Investigation of the essential boundary layer phospholipids of cytochrome *c* oxidase using Triton x-100 delipidation. *Biochemistry* 19: 3656- 3661.
- Rousseau, D.; Ching, Y. & Wang, J. (1993) Proton translocation in cytochrome oxidase: Redox linkage through proximal ligand exchange on cytochrome *a*<sub>3</sub>. *J. Bioenerg. Biomembr.* 25: 165-176.
- Rott, M. & Donohue, T. (1990) *Rhodobacter sphaeroides spd* Mutations allow cytochrome *c*<sub>2</sub>-independent photosynthetic growth. *J. Bacteriol.* 172: 1954-1961.
- Rumbly, J.; Nickels, E. and Gennis, R. (1997) One-step purification of histidine-tagged cytochrome *bo*<sub>3</sub> from *Escherichia coli* and demonstration that associated that quinone is not required for the structural integrity of the oxidase. *Biochim. Biophys. Acta* 1340: 131-142.
- Saari, H.; Penttila, T. and Wikstrom, M. (1989) interaction of Ca<sup>2+</sup> and H<sup>+</sup> with heme *a* in cytochrome oxidase. *J. Bioenerg. Biomembr.* 12: 325-338.

Sanishvilli, R.; Voltz, K.; Westbrook, E. & Margoliash, E. (1995) The low ionic strength crystal structure of horse cytochrome *c* at 2.1 Å resolution and comparison with its high ionic strength counterpart. *Structure* 3: 707-716.

Saraste, M. (1990) Structural features of cytochrome oxidase. *Q. Rev. Biophys.* 23: 331-366.

Shapleigh, J. & Gennis, R. (1992) Cloning, sequencing and deletion from the chromosome of the gene encoding subunit I of the *aa<sub>3</sub>*-type cytochrome *c* oxidase of *Rhodobacter sphaeroides*. *Mol. Microbiol.* 6: 635-642.

Siegenthaler, P. & Murata, N. (1998) Lipids in photosynthesis: structure, function and genetics. Kluwer Academic Publishers. The Netherlands.

Smirnova, I.; Adelroth, P.; Gennis, R. & Brezeniski, P. (1999) Aspartate-132 in cytochrome *c* oxidase from *Rhodobacter sphaeroides* is involved in two-step proton transfer during oxo-ferryl formation. *Biochemistry* 38: 6826-6833.

Smith, P.; Krohn, R.; Hermanson, G.; Mallia, A.; Gartner, F.; Provenzano, M.; Fujimoto, E.; Goeke, N.; Olson, B. & Klenk, D. (1985) Measurement of protein using bicinchoninic acid. *Analyt. Biochem.* 150: 76- 85.

Smith, H.; Staudenmayer, N. & Millett, F. (1977) Use of specific lysine modifications to locate the reaction site of cytochrome *c* with cytochrome oxidase. *Biochemistry* 16: 4971-4974.

Steinrucke, P.; Steffens, G.; Panskus, G.; Buse, G. & Ludwig, B. (1987) Subunit II of cytochrome *c* oxidase from *Paracoccus denitrificans*, DNA sequence, gene expression and the protein. *Eur. J. Biochem.* 167: 431-439.

Stock, D.; Leslie, A. & Walker, J. (1999) Molecular architecture of the rotary motor in ATP synthase. *Science* 286: 1700-1705.

Stryer, L. *Biochemistry* (1995) Freeman and company, New York.

Stuchebrukhov, A. & Marcus, R. (1995) Theoretical study of electron transfer in ferrocyclochromes. *J. Phys. Chem.* 99: 7581-7590.

Swanson, R.; Trus, B. Mandel, N.; Mandel, G. Kallai, O. & Dickerson, E. (1977) Tuna cytochrome *c* at 2.0 Å resolution. Ferricytochrome structure analysis. *J. Biol. Chem.* 252: 759-775.

Svensson-Ek, M.; Rodgers, L.; Abramson, J.; Tornoth, S.; Brzezeniski, P. & Iwata, S. (2002) The x-ray crystal structures of wild type and EQ (I-286) mutant cytochrome *c* oxidases from *Rhodobacter sphaeroides*. *J. Mol. Biol.* (In press)

- Tahirov, T.; Misaki, S.; Meyer, T.; Cusanovich, M.; Higuchi, Y. & Yasuoka, N. (1996) High-resolution crystal structures of two polymorphs of cytochrome *c*' from the purple phototropic bacterium *Rhodobacter capsulatus*. *J. Mol. Biol.* 259: 467-479.
- Takamiya, S.; Lindorfer, M. & Capaldi, R. (1987) Purification of all thirteen polypeptides of bovine heart cytochrome *c* oxidase from one aliquot of enzyme. Characterization of bovine fetal heart cytochrome *c* oxidase. *FEBS Lett* 218: 277-282.
- Takana, M. & Dickerson, R. (1981) Conformation change of cytochrome *c*: ferricytochrome *c* refinement at 1.8 Å and comparison with the ferrocycytochrome structure. *J. Mol. Biol.* 153: 95-115.
- Tanaka, M.; Yamane, T.; Tsukihara, T.; Ashida, T. & Kakudo, M. (1975) The crystal structure of bonito (katsuo) ferrocycytochrome *c* at 2.3 Å resolution: structure and function. *J. Biochem.* 77: 147-162.
- Thomas, J.; Puustinen, A.; Alben, J.; Gennis, R. & Wikstrom, M. (1993) Substitution of asparagines for aspartate-135 in subunit I of the cytochrome *bo* ubiquinol oxidase of *Escherichia coli* eliminates proton-pumping activity. *Biochemistry* 32: 10923-10928.
- Thony-Meyer, L. (1997) Biogenesis of respiratory cytochromes in bacteria. *Microbiol. Mol. Biol. Rev.* 61: 337-376.
- Toyoshima, C.; Nakasako, M.; Nomura, H. & Ogawa, H. (2000) Crystal structure of calcium pump of sarcoplasmic reticulum at 2.6 Å resolution. *Nature* 405: 647-655.
- Trumpower, B. & Gennis, R. (1994) Energy transduction by cytochrome complexes in mitochondrial and bacterial respiration: the enzymology of coupling electron transfer reactions to transmembrane proton translocation. *Annu.Rev. Biochem* 63: 675-716.
- Tsukihara, T.; Aoyama, H.; Yamashita, E.; Tomizaki, T.; Yamaguchi, H.; Shinzawz-Itoh, K.; Nakashima, R.; Yaono, R. & Yoshikawa, S. (1995) Structure of metal sites of oxidized bovine heart cytochrome *c* oxidase at 2.8 Å. *Science* 269: 1069-1074.
- Tsukihara, T.; Aoyama, H.; Yamashita, E.; Tomizaki, T.; Yamaguchi, H.; Shinzawz-Itoh, K.; Nakashima, R.; Yaono, R. and Yoshikawa, S. (1996) The whole structure of the 13-subunit oxidized cytochrome *c* oxidase at 2.8 Å. *Science* 272: 1136-1144.
- Turba, A.; Jetzek, M. & Ludwig, B. (1995) Purification of *Paracoccus denitrificans* cytochrome *c*<sub>552</sub> and sequences analysis of the gene. *Eur. J. Biochem.* 231: 259-265.
- Van Beeumen, J. (1991) Primary structure diversity of prokaryotic diheme cytochrome *c*. *Biochim. Biophys. Acta* 1058: 56-60.
- Vandenbergh, I.; Leys, D.; Demol, H.; Van Driessche, G.; Meyer, T.; Cusanovich, M. & Van Beeumen, J. (1998) The primary structure of the low redox potential diheme

cytochrome *c* from the phototrophic bacteria *Rhodobacter sphaeroides* and *Rhodobacter adriaticus* reveal a new structural family of *c*-type cytochromes. *Biochemistry* 37: 13075-13081.

Walker, J. & Saraste, M. (1996) Membrane proteins, membrane protein structure. *Current Opinion in Structural Biology* 6: 457-459.

Wang, K.; Geren, L.; Zhen, Y.; Ma, L.; Ferguson-Miller, S.; Durham, B. & Millett, F. (2002) Mutants of the Cu<sub>A</sub> site in cytochrome *c* oxidase of *Rhodobacter sphaeroides*: Rapid kinetics analysis of electron transfer. *Biochemistry* 41: 2298-2304.

Wang, Y. & Margoliash, E. (1995) Enzymic activities of covalent 1:1 complexes of cytochrome *c* and cytochrome *c* peroxidase. *Biochemistry* 34: 1948-1958.

Wang, K.; Zhen, Y.; Sadoski, R.; Grinnell, S.; Geren, L.; Ferguson-Miller, S.; Durham, B. & Millett, F. (1999) Definition of the interaction domain for cytochrome *c* on cytochrome *c* oxidase. *J. Biol. Chem.* 274: 38042-38050.

Weber, P.; Bartsch, R.; Cussanovich, M.; Hamlin, R.; Howard, A.; Jordan, S.; Kamen, M.; Meyer, T.; Weatherford, D. Xuong, D. & Salemme, F. (1980) Structure of cytochrome *c*': a dimeric, high-spin haem protein. *Nature* 286: 302-304.

Wikstrom, M. (1988) Protonic sidedness of binuclear iron-copper center in cytochrome oxidase. *FEBS Lett.* 231: 247-252.

Wikstrom, M.; Bogachev, A.; Finel, M.; Morgan, J.; Puustinen, A.; Raitio, M.; Verkhovskaya, M. & Verkhovsky, M. (1994) Mechanism of proton translocation by the respiratory oxidases: The histidine cycle. *Biochim. Biophys. Acta* 1187: 106-111.

Witt, H. & Ludwig, B. (1997) Isolation, analysis and deletion of gene coding for subunit IV of cytochrome *c* oxidase in *Paracoccus denitrificans*. *J. Biol. Chem.* 272: 5514-5517.

Witt, H.; Zickermann, V. & Ludwig, B. (1995) Site-directed mutagenesis of cytochrome *c* oxidase reveals two acidic residues involved in the binding of cytochrome *c*. *Biochim. Biophys. Acta* 1230: 74-76.

Xu, X.; Bittman, R.; Duportail, G.; Heissler, D.; Vilcheze, C. & London, E. (2001) Effect of the structure of natural sterols and sphingolipids on the formation of ordered sphingolipid/sterol domains (rafts). Comparison of cholesterol to plant, fungal and disease-associated sterols and comparison of sphingomyelin, cerebrosides and ceramide. *J. Biol. Chem.* 276: 33540-33546.

Xu, X. & London, E. (2000) The effect of sterol structure on membrane lipid domains reveals how cholesterol can induce lipid domain formation. *Biochemistry* 39: 843-849.

Yausi, M.; Harada, S.; Kai, Y.; Kasai, N.; Kusunoki, M. & Matsuura, Y. (1992) Three-dimensional structure of ferricytochrome *c'* from *Rhodospirillum rubrum* at 2.8 Å resolution. *J. Biochem.* 111: 317-324.

Yoshikawa, S.; Shinzawa-Itoh, K.; Nakashima, R.; Yaono, R.; Yamashita, E.; Inoue, N.; Yao, M.; Fei, M.; Libeu, C.; Mizushima, T.; Yamaguchi, H.; Tomizaki, T. & Tsukihara, T. (1998) Redox-coupled crystal structural changes in bovine heart cytochrome *c* oxidase. *Science* 280: 1723-1729.

Zeilstra-Ryalls, J. & Kaplan, S. (1995) Aerobic and anaerobic regulation in *Rhodobacter sphaeroides* 2.4.1: the role of the *fnrL* gene. *J. Bacteriol.* 177: 6422-6431.

Zhen, Y.; Schmidt, B.; Kang, U.; Antholine, W. & Ferguson-Miller, S. (2002) Mutants of the Cu<sub>A</sub> site in cytochrome *c* oxidase of *Rodobacter sphaeroides*: Spectral and functional properties. *Biochemistry* 41: 2288-2297.

Zhen, Y.; Hoganson, C.; Babcock, G. & Ferguson-Miller, S. (1999) Definition of the interaction domain for cytochrome *c* on cytochrome *c* oxidase. I. Biochemical, spectral and kinetic characterization of surface mutants in subunit II of *Rhodobacter sphaeroides*. *J. Biol. Chem.* 274: 38032-38041.

Zhen, Y.; Qian, J.; Follmann, K.; Haywary, T.; Nilsson, T.; Dahn, M.; Hilmi, Y.; Hamer, A.; Hosler, J. & Ferguson-Miller, S. (1998) Overexpression and purification of cytochrome *c* oxidase from *Rhodobacter sphaeroides*. *Protein Expr. Purif.* 13: 326-336.